

INVESTIGATING THE GLIAL IMMUNE RESPONSE TO PHOTOTHERMAL AND  
PHOTOMECHANICAL STIMULI

By

John Logan Jenkins

Dissertation

Submitted to the Faculty of the  
Graduate School of Vanderbilt University  
in partial fulfillment of the requirements  
for the degree of

DOCTOR OF PHILOSOPHY

In

Biomedical Engineering

December 17, 2022

Nashville, Tennessee

Approved:

E. Duco Jansen, Ph.D.

Anita Mahadevan-Jansen, Ph.D.

Mark Hutchinson, Ph.D.

Michael Jenkins, Ph.D.

Peter Konrad, M.D., Ph.D.

Copyright © 2022 by John Logan Jenkins

All Rights Reserved

To my wife, Ellen, for her love and support throughout this  
journey.

To my children, James and Lucy, for reminding me to find joy and  
wonder in the newly discovered.

To my parents, Andy and Wendy, and siblings, Brennen, Alex, and  
Chloe, for helping shape the person I have become and strive to be.

## ACKNOWLEDGEMENTS

This dissertation would not be possible without the support of many mentors, friends, and colleagues. I was very fortunate to have my advisor's, Dr. Duco Jansen, direction through the many twist and turns of changing research plans and experiments. I especially would like to thank Dr. Jansen for encouraging my broader education and development through the hundreds of hours I spent on learning business and entrepreneurship fundamentals through Vanderbilt-sponsored courses and projects. During my 7-month research stint at the University of Adelaide, Dr. Mark Hutchinson acted as my temporary advisor and was vital in aiding the research direction of this project, as well as, creating a welcoming environment from where I gained new perspectives on sciences and leadership. I would also like to thank Drs. Anita Mahadevan-Jansen, Michael Jenkins, and Pete Konrad for their guidance in this work as committee members.

I had the pleasure of spending my day-to-day with brilliant scientists, imaginative engineers, and great friends throughout my studies. I would like to thank the Biophotonics Center's neurophotonics group, including Dr. Mohit Ganguly, Dr. Jeremy Ford, Dr. Wilson Adams, and Dr. Graham Throckmorton, all of whom made me a better critical thinker and experimentalist. The many colleagues within Dr. Hutchinson's research group, including Dr. Sam Evans and Dr. Vicky Alexandrou were essential in training this engineer to think and act as a biologist while exploring their beautiful country.

# TABLE OF CONTENTS

DEDICATIONS.....	iii
ACKNOWLEDGEMENTS.....	iv
LIST OF TABLES .....	xii
LIST OF FIGURES .....	xiii
1 Introduction .....	1
1.1 Motivation .....	2
1.2 Specific Aims .....	7
1.3 Dissertation Outline.....	10
2 Background and Significance .....	15
2.1 Central nervous system physiology .....	15
2.1.1 Neurons .....	16
2.1.2 Glia.....	20
2.1.3 Astrocytes .....	21
2.1.4 Microglia.....	22
2.2 Neuropathology .....	27
2.2.1 Chronic Pain.....	27
2.2.2 Inflammation.....	27
2.2.3 Neuromodulation .....	30
2.2.4 Blast-induced traumatic brain injury .....	36
2.2.5 Inflammation.....	39
2.3 Pulsed laser tissue interaction .....	40

2.3.1	Photothermal .....	40
2.3.2	Photomechanical .....	40
2.3.3	Photochemical.....	41
2.4	Measurement Techniques.....	42
2.4.1	Fluorescence Imaging .....	42
2.4.2	Thermal measurements .....	43
3	Pulsed Infrared light modulates inflammatory precursors; reducing pro-inflammatory cytokine release, stimulating intracellular calcium transients, and altering ligand-receptor binding in microglia-like BV2 cells .....	52
3.1	Abstract .....	53
3.2	Introduction .....	54
3.3	Methods.....	57
3.3.1	Cell culture.....	57
3.3.2	<i>in vitro</i> pulsed infrared laser approach and parameters .....	58
3.3.3	ELISA assay.....	58
3.3.4	Fluorescence Imaging .....	59
3.3.5	Thermal Measurements.....	60
3.3.6	Data Analysis .....	61
3.4	Results .....	62
3.4.1	Pulsed infrared light modulates intracellular calcium transients of TLR4-TRPV1 transfected HEK cells to capsaicin stimulus.....	62
3.4.2	Pulsed infrared light induces multiple, distinct intracellular calcium transient phenotypes in BV2 cells .....	63

3.4.3	Temperature rise from pulsed infrared light during fluorescent imaging.....	65
3.4.4	Distinct calcium transients are associated with different temperature rises. ....	66
3.4.5	Pulsed infrared light reduces pro-inflammatory cytokine release <i>in vitro</i> .....	68
3.4.6	Pulsed infrared light does not induce early apoptosis or necrosis at temperature rises needed for intracellular calcium transients .....	70
3.5	Discussion .....	72
3.5.1	Possible mechanisms of action .....	73
3.5.2	Diversity of biological responses in BV2 cell culture .....	74
3.5.3	Temperature rise is a better predictor of biological effect than radiant exposure alone .....	75
3.5.4	Cell viability after pulsed IR exposure .....	76
3.6	Conclusion.....	78
4	The effects of high-amplitude, short-duration pressures transients on intracellular calcium response and inflammatory immune response of neuron, astrocyte, and microglia monocultures.....	84
4.1	Abstract: .....	85
4.2	Introduction .....	86
4.3	Methods and Materials.....	90
4.3.1	Cell Culture.....	90
4.3.2	Fluorescence Imaging .....	92
4.3.3	Multiplex Inflammatory Signaling Analysis .....	94
4.3.4	Pressure Generation and Measurement.....	95
4.3.5	Statistical analysis.....	97

4.4	Results .....	98
4.4.1	High-amplitude, short-duration pressure transients initiate localized spots of intracellular calcium uptake .....	98
4.4.2	Microglia respond to high-amplitude, short-duration pressures via intracellular calcium transients without irreversible damage.....	100
4.4.3	Neurons exhibit a two-phenotype response to high-amplitude, short-duration pressures.....	102
4.4.4	Comparing the responses of astrocytes, microglia, and neurons to high-amplitude, short-duration blast. ....	105
4.4.5	Immune responses of astrocytes and microglia .....	107
4.5	Discussion .....	109
4.5.1	Astrocytes and microglia respond to high-amplitude, short-duration pressure exposures via intracellular calcium transients .....	110
4.5.2	Neuronal intracellular calcium responses to high-amplitude, short-duration pressure exposures.....	112
4.5.3	High-amplitude, short-duration pressure transients can affect cell viability .....	113
4.5.4	Immune signaling responses of microglia and astrocytes to high-amplitude, short-duration pressure transients.....	114
4.5.5	Comparing high-amplitude, short-duration pressure to other blast modalities.....	115
4.6	Conclusion.....	117
5	Summary and Concluding Remarks .....	124
5.1	Summary and Major Conclusions .....	125
5.1.1	Summary .....	125

5.1.2	Major Conclusions .....	128
5.2	Implications .....	130
5.2.1	Directed energies share similarities in microglial response while biophysical mechanisms may be vastly different.....	130
5.2.2	Potential therapeutic target for infrared neural inhibition.....	132
5.2.3	Acute heating in the brain induced by other directed energies .....	133
5.2.4	Mechanism behind pressure-induced calcium transients.....	134
5.2.5	Isolation of initial peak of explosive blast .....	135
5.2.6	Initial pro-inflammatory immune signaling effects from blast are unlikely to drive bTBI pathology .....	136
5.3	Future Directions.....	139
5.3.1	Photothermal effects on Spinal Cord <i>ex vivo</i> .....	139
5.3.2	Photothermal effects on inflammatory response during LITT .....	141
5.3.3	Origin and function of calcium transients in neurons, astrocytes, and microglia after photomechanical exposure in a less rigid environment .....	143
5.3.4	Inflammatory immune signaling from multi-cell model .....	145
5.3.5	Directed energy priming may reduce impact of subsequent insult.....	146
5.4	Contributions and Societal Impact .....	149
5.4.1	Scientific Contributions .....	149
5.4.2	Community and Societal Impact.....	150
A	Intraoperative Neuromonitor using Infrared Neural Stimulation Business Plan .....	156
A.1	Foreword .....	157
A.2	Vanderbeam Technologies Commercialization Plan .....	158

A.2.1	Executive Summary .....	158
A.3	Value, Outcomes, Impact .....	160
A.3.1	Company Overview.....	163
A.3.2	Market, Customer, Competition .....	164
A.3.3	Intellectual Property .....	169
A.3.4	Financial Plan .....	169
A.3.5	Production and Marketing Plan .....	170
A.3.6	Revenue Stream .....	173
A.3.7	Conclusion .....	175
A.4	Vanderbeam Technologies Specific Aims .....	176
B	Neural responses of rat cortical layers due to infrared neural modulation and photoablation of thalamocortical brain slices .....	179
B.1	Abstract .....	180
B.2	Introduction .....	181
B.3	Methods .....	185
B.3.1	Brain Slice .....	185
B.3.2	Electrical Recordings and Stimulation .....	185
B.3.3	Photoablation .....	186
B.3.4	Dead Cell Staining .....	187
B.4	Results .....	188
B.4.1	Photoablation can reduce the necrosis layer of brain slices .....	188
B.4.2	Photoablation protocol does not cause further necrosis in brain slices .....	188
B.5	Discussion .....	191

B.5.1	Light absorption through dead zone .....	191
B.5.2	Brain slice health during ablation .....	192
B.5.3	Brain slice ablation reduces dead zone .....	192
B.5.4	Future Direction .....	193
C	Real-Time Fluorescence Imaging and Pressure Measurements .....	196
C.1	Purpose .....	197
C.2	Methods .....	199
C.3	Results / Discussion .....	201

## LIST OF TABLES

Table 2.1-1. Neuronal ion concentrations.....	17
Table C.2-1. Coefficients needed to calibrate pressure measurements taken from hydrophone B. .....	201

## LIST OF FIGURES

Figure 1.1-1. U.S. overdose deaths per 100,000 population from 1999-2019 by type of opioid. ..	5
Figure 1.1-2. DOD Number of cases of traumatic brain injury from 2000-2020 by severity. ....	6
Figure 2.1-1. Differences in neuron morphologies. ....	18
Figure 2.1-2. Neurons and glia .....	20
Figure 2.1-3. Physiological states of microglia .....	24
Figure 2.2-1. Central Sensitization .....	29
Figure 2.2-2. Classical free-field blast wave at a fixed location.....	36
Figure 2.2-3. Traumatic brain injury response.....	38
Figure 3.4-1. Pulsed infrared light modulates intracellular calcium transients of TLR4 TRPV1 transfected HEK cells to stimulus.....	62
Figure 3.4-2. Pulsed infrared light induces intracellular calcium transients in microglia in vitro. .....	64
Figure 3.4-3. Temperature rise of pulsed infrared light during fluorescent imaging. ....	66
Figure 3.4-4. Distinct calcium transients are associated with different temperature rises. ....	67
Figure 3.4-5. Pulsed infrared light reduces pro-inflammatory cytokine release in vitro.....	69
Figure 3.4-6 Pulsed infrared light does not induce early apoptosis or cell death. ....	71
Figure 4.3-1. Light and pressure delivery system to a custom-built widefield microscope. ....	96
Figure 4.4-1. Calcium images of astrocytes in vitro in response to a high-amplitude, short-duration pressure transient. ....	100
Figure 4.4-2. Response of primary rat cortical astrocytes in vitro to a high-amplitude, short duration pressure wave. ....	102

Figure 4.4-3. Response of primary rat whole brain microglia *in vitro* to a high-amplitude, short duration pressure wave. .... 103

Figure 4.4-4. Response of primary rat cortical neurons *in vitro* to a high-amplitude, short duration pressure wave..... 105

Figure 4.4-5. Comparison of responses of primary astrocytes, microglia, and neurons to high-amplitude, short duration pressure transients..... 106

Figure 4.4-6 Effects of high-amplitude, short duration pressure transients (4.65 MPa) on intracellular protein concentrations and proinflammatory cytokine release. .... 108

Figure B.2-1 Representation of the dead zone associated with brain slicing. .... 184

Figure B.4-1. PI staining before ablation to confirm complete reduction in preexisting dead zone. .... 189

Figure B.4-2. Staining after ablation to shown laser-induced cellular damage. .... 190

Figure C.2-1. Positioning and calibration for real-time pressure measurements. .... 198

# **Chapter I**

## **Introduction**

## 1.1 Motivation

The inflammatory response within the brain and spinal cord is a key biological response to disease, infection, and injury<sup>1</sup>. Chronic pain and traumatic brain injury (TBI) are negatively impacted by the role of inflammation in response to acute injury triggers. In chronic pain, inflammation is critically involved in the central amplification and maintenance of pain that leads to hyperalgesia (increased sensitivity to pain) and allodynia (pain from sources that do not normally cause pain)<sup>2,3</sup>. In TBI, induced-chronic inflammation leads to many of its indicative pathologies, such as increased neuronal cell death, excitotoxicity, weakening of the blood brain barrier, and neurodegeneration<sup>4</sup>.

Central nervous system (CNS) glia, specifically microglia and astrocytes, are key regulators of the immune signaling response that drive beneficial or detrimental cellular adaptations of inflammation<sup>5</sup>. While directed energies, such as induced heat or pressure, are recognized for their roles in modulating the impact of chronic pain<sup>6,7</sup> and TBI<sup>8</sup>, their influence on pro-inflammatory signaling and the primary immune cell, microglia, remains unresolved. Further investigation into glial responses to directed energies is crucial for the identification of relevant treatments for chronic pain and TBI. Laser-based mechanisms for heat and pressure generation<sup>9</sup> allow for a repeatable, highly controllable, and measurement-friendly technique to better understand the impact of directed energies on glia and their inflammatory signaling.

Inflammation in the CNS has potential positive and negative consequences to overall brain and spinal cord health. These consequences of inflammation partially depend on the duration and severity of the immune response<sup>10</sup>. Under certain conditions, inflammation is considered neuroprotective and plays a vital role in tissue repair and enhancing plasticity. Alternatively,

inflammation can be considered neurodegenerative and can cause cognitive impairment, tissue damage, and initiate the onset of neurological disorders. Inflammation during chronic pain and TBI is neurodegenerative and plays a major role in the long-term, detrimental impacts of these disorders. Microglia and astrocytes are key regulators of the inflammatory responses that drive positive or negative outcomes<sup>11</sup>. While both cell types share similar inflammatory pathway machinery, microglia are the first and primary responders to CNS perturbations through surveillance and macrophage-like roles. Microglial activation from distress leads to the increased production and release of inflammatory cytokines and chemokines, which mediate inflammation-induced neurodegenerative mechanisms<sup>5</sup>.

Chronic pain affects 20% of U.S. adults and is responsible for a reduced quality of life, restrictions in mobility, anxiety, and depression<sup>12,13</sup>. Unfortunately, opioids continue to be a primary treatment for chronic pain given the lack of safe and effective alternatives. Long-term opioids were given to 3-4% of the U.S. population to treat pain in the late 2000's<sup>14</sup>. Opioids have a considerable risk of abuse, addiction, and overdose and in 2019 accounted for 50,000 deaths in the U.S. alone<sup>15-17</sup> (Figure 1.1-1). Novel non-addictive treatments for pain are urgently needed to curb this disturbing trend. The chronification of pain, the processes by which an acute pain experience transitions to a chronic pain experience, may largely be due to central sensitization, which is the amplification of neural signals within the CNS that causes pain hypersensitivity<sup>18</sup>. Inflammation is thought to be a main driver of the chronification of pain that leads to its amplification and maintenance. Through the efforts to find non-pharmaceutical treatments for chronic pain, infrared neural inhibition<sup>7,19,20</sup> (INI) emerged as a novel alternative with key advantages in spatial and small-diameter axon selectivities<sup>21</sup>. INI uses pulsed infrared light to cause a non-damaging temperature rise at the neuronal level to block the propagation of pain signals

from being perceived. While the impact of heating on pain-related neural signaling has been established using pulsed infrared light, its impact on pain-related immune response signaling remains unclear.

Blast-induced TBI (bTBI) is a major concern for military personnel as 125,000 cases from U.S. service men and women occurred between 2000-2018<sup>22</sup> (Figure 1.1-2). Unfortunately, no drug-based treatments for TBIs have made it past FDA clinical trials, though over 30 drugs have attempted.<sup>23</sup> Symptoms of bTBI can have devastating impacts on patient physical, cognitive, and emotional health. Acute activation of the inflammatory response is vital to the repair and recovery of the brain in response to injury, while chronic activation of the pro-inflammatory response can lead to secondary injuries<sup>24</sup>. Explosion energy from blasts interact with the body through the propagation of a large overpressure defined by an initial peak after a few microseconds followed by an exponential-like decay for up to milliseconds. The neuronal, glial, and inflammatory responses to the initial peak component of blast onset remains unresolved. This initial peak of overpressure can be simulated experimentally using photomechanical effects to drive the generation of high-amplitude, short-duration pressure transients.

Directed energies, such as heat and pressure, may contribute to the origin and/or treatment of neurological deficits. Understanding the impact of directed energies on glia and their immune response signaling may have wide-ranging ramifications on how we treat neurological disorders. The beneficial or harmful contributions of heat and pressure generation to neurological disorders' severity may impact the development of novel preventative measures, uncover a broader understanding of current technologies' effects on immune signaling, and identify targets of new treatment pathways altogether.

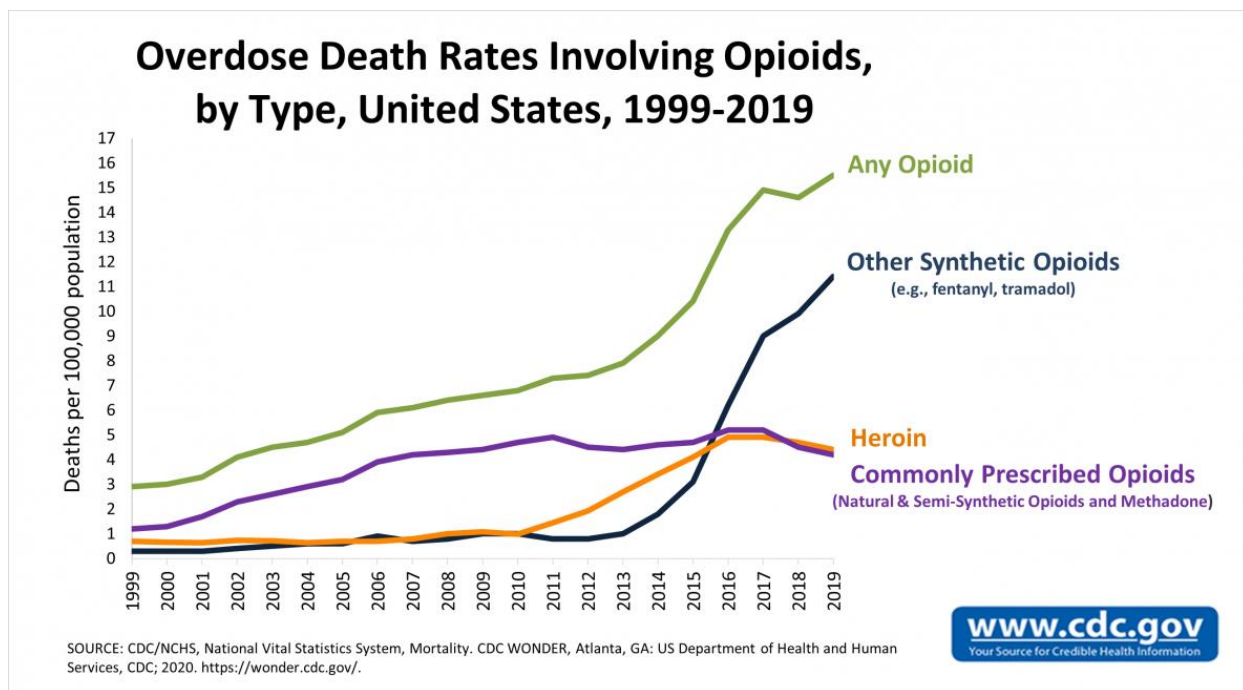


**Figure 1.1-1. U.S. overdose deaths per 100,000 population from 1999-2019 by type of opioid.**

*Reprinted from original source<sup>25</sup>.*

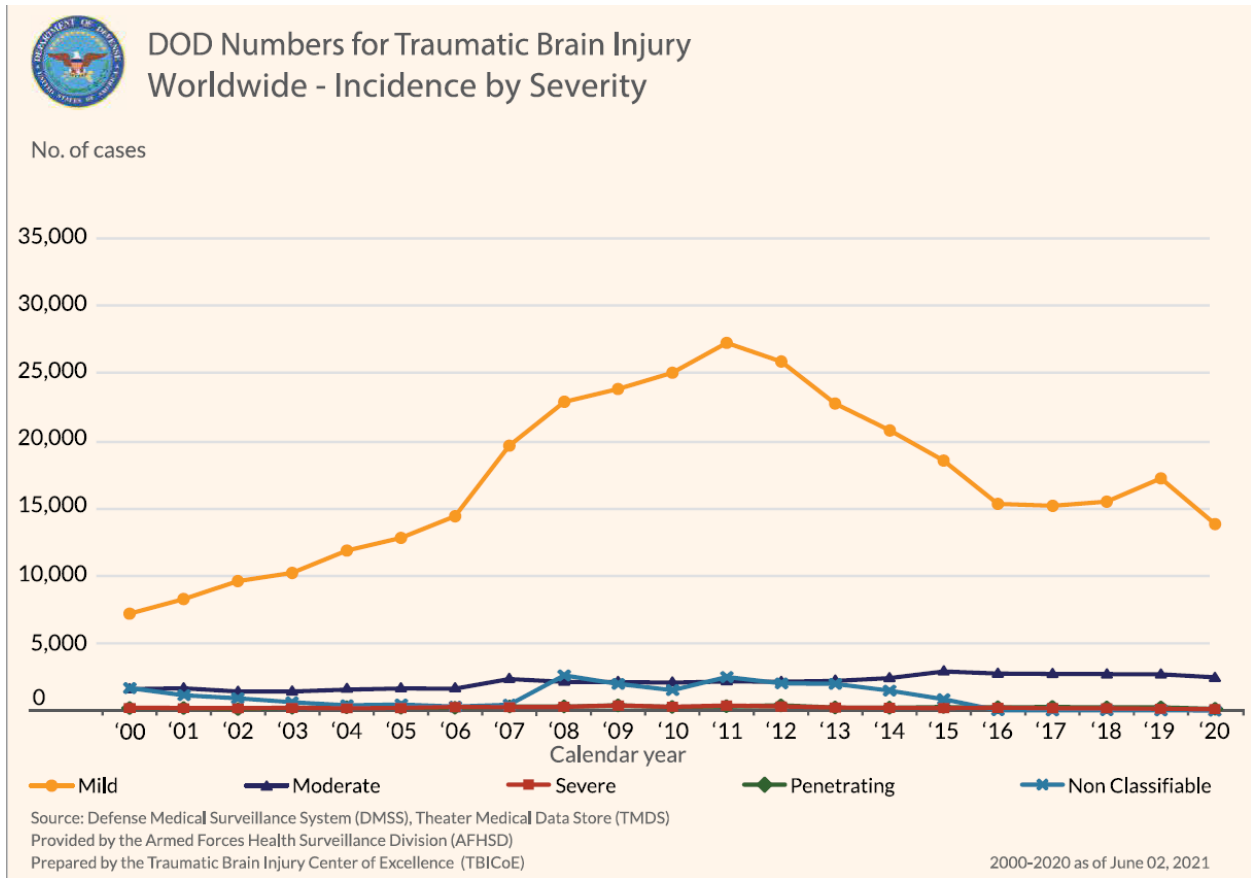


**Figure 1.1-2. DOD Number of cases of traumatic brain injury from 2000-2020 by severity.**

*Reprinted from original source<sup>26</sup>.*

## 1.2 Specific Aims

This dissertation attempts to uncover the impact of photothermal and photomechanical directed energies on glial function and inflammatory precursors. The parameters of each directed energy modality were chosen in the context of heat and pressures experienced during pain treatment and blast-induced traumatic brain injury (bTBI) onset, respectively. While Photothermal and photomechanical effects on neuronal cells have been investigated to some degree, their impacts on glial function and neuro-immune signaling, especially in the context of chronic pain and bTBI, have little to no understanding.

*Specific Aim 1: Characterize the impact of infrared neural inhibition-specific photothermal effects on microglia in vitro.*

Infrared neural inhibition (INI) has been investigated for nearly a decade to determine its impact on pain signal propagation in efforts to eliminate pain perception. The symptomatic targeting of pain-carrying neurons is well established, but the impact of the photothermal stimuli on inflammation, a source of chronic pain, has not been uncovered. Understanding the immune response implications of pulsed infrared light (pulsed IR) exposure is critical to eliminate negative consequences of INI and uncovering new therapeutic targets of the technology. This aim investigates the impact of pulsed IR on microglia *in vitro*. A three-pronged approach was adopted: 1) Examine the impact of pulsed IR priming on immune signaling channel kinetics through calcium imaging of TRPV1-TLR4 activation after photothermal stimuli, 2) probe broad microglial physiological changes due to pulsed IR via single cell calcium imaging of BV2 cells during pulsed IR-heating, 3) explore the impact of heating on subsequent release of pro-inflammatory cytokines

from naive and activated BV2 cells thorough quantification of interleukin-6 concentrations in the cell culture supernatant. Results from this study suggest that pulsed-IR heating does not induce a pro-inflammatory immune response in basal microglia but may prevent the initiation of a pro-inflammatory immune response from innate immune insult. These results provide evidence that INI application may not have negative inflammatory consequences but may have a novel utility in preventing pro-inflammatory immune responses to innate immune insults.

*Specific Aim 2: Identify the impact of blast-like photomechanical effects on neuroimmune function in vitro.*

A typical blast that induces TBI is made up of an initial spike in pressure with a duration on the order of microseconds followed by an exponential-like decay of the pressure with a duration on the order of milliseconds. Most research focuses on the impact of the impulse, or integral of the pressure over time, which is dominated by the long duration component of blast waves. There is a lack of investigation into the impact of the high-amplitude, short duration component of the blast wave, especially on immune signaling responses. Photomechanical effects can simulate the fast gradient of overpressure without having influence from the remaining millisecond of overpressure. The effects of photomechanical exposure on monocultures of primary neurons, astrocytes, and microglia were explored to isolate the responses of each cell type without communication-related effects. Each cell type's sensitivity to photomechanical waves were investigated through the initiation of intracellular calcium transients at varying peak positive pressures. The physiological significance behind the pressure-induced intracellular calcium transients were studied through pharmacology and cell viability means. The impact of photomechanical effects on the inflammatory immune response were probed through quantification of released pro-inflammatory cytokines and intracellular pathway proteins. Results from this aim suggest that glia and neurons

respond to similar high-amplitude, short-duration pressure exposures, though the physiological meaning of the responses may be drastically different. Neurons may negatively impact CNS health after high-amplitude, short duration pressure exposure through death mechanisms, while glia may play an initial neuroprotective role in response to the same pressures. These results suggest that glia may not be the initial deficit to high peak overpressures of blast unlike their neuronal counterparts.

### 1.3 Dissertation Outline

The information comprising this dissertation is organized in the following manner:

Chapter I introduces the motivation for this dissertation and what specific aims are taken to further our scientific understanding of chronic pain and bTBI in response to photothermal and photomechanical stimuli.

Chapter II provides background information for the readers on much of the biology and engineering behind this dissertation. The central nervous system physiology is introduced, as well as pathological states of CNS. Laser-tissue interactions used within this work are described for a clear understanding of heat and pressure generation. Measurement techniques, including imaging, temperature and pressure measurements, and protein quantification, are discussed.

Chapter III uncovers the effects of INI-related heating on microglia and their proinflammatory immune response. This work uncovered the potential for microglial targeting for chronic pain prevention and the potential safety of microglia responses to heat. A manuscript has been written from this work and is currently in submission.

Chapter IV identifies the responses of primary neurons, astrocytes, and microglia to varying high-amplitude, short-duration pressure transients, as well as the initial immune signaling responses of microglia. This work is in preparation for submission to the *Journal of Neurotrauma*.

Chapter V summarizes the results from this dissertation and presents conclusions about how the work may impact the fields of biophotonics, neuroimmunology, and society more broadly. Future directions of this work including continuations within the described fields and new disciplines to explore are described as well.

Appendix A is a small business innovation research (SBIR) grant application's specific aims page and corresponding commercialization plan for a proposed intraoperative neuromonitoring device using infrared neural stimulation (INS).

Appendix B describes a study conducted on rat thalamocortical brain slices to reduce the thickness of damage zones due to slicing via photoablation. This work was published (non-peer reviewed) in SPIE Proceedings.

Appendix C describes a technique to perform real-time pressure measurements during real-time imaging using an off-axis hydrophone. This technique is useful when generated laser-induced pressures create inconsistent pressures from pulse to pulse.

## 1.4 References

1. Gilhus, N. E. & Deuschl, G. Neuroinflammation — a common thread in neurological disorders. *Nature Reviews Neurology* 15:8 **15**, 429–430 (2019).
2. Grace, P. M., Hutchinson, M. R., Maier, S. F. & Watkins, L. R. Pathological pain and the neuroimmune interface. *Nature Review Immunology* **14**, 217–231 (2014).
3. Grace, P. M. *et al.* The Neuroimmunology of Chronic Pain: From Rodents to Humans. *Journal of Neuroscience* **41**, 855–865 (2021).
4. Schimmel, S. J., Acosta, S. & Lozano, D. Neuroinflammation in traumatic brain injury: A chronic response to an acute injury. *Brain Circulation* **3**, 135 (2017).
5. Turner, M. D., Nedjai, B., Hurst, T. & Pennington, D. J. Cytokines and chemokines: At the crossroads of cell signalling and inflammatory disease. *Biochimica et Biophysica Acta (BBA) - Molecular Cell Research* **1843**, 2563–2582 (2014).
6. Won, S. M., Song, E., Reeder, J. T. & Rogers, J. A. Emerging Modalities and Implantable Technologies for Neuromodulation. *Cell* **181**, 115–135 (2020).
7. Duke, A. R. *et al.* Transient and selective suppression of neural activity with infrared light. *Scientific Reports* 2013 3:1 **3**, 1–8 (2013).
8. Bryden, D. W., Tilghman, J. I. & Hinds, S. R. Blast-Related Traumatic Brain Injury: Current Concepts and Research Considerations. *Journal of Experimental Neuroscience* **13**, (2019).

9. Jacques, S. L. Laser-Tissue Interactions: Photochemical, Photothermal, and Photomechanical. *Surgical Clinics of North America* **72**, 531–558 (1992).
10. DiSabato, D. J., Quan, N. & Godbout, J. P. Neuroinflammation: The Devil is in the Details. *J Neurochemistry* **139**, 136 (2016).
11. Li, Q. & Barres, B. A. Microglia and macrophages in brain homeostasis and disease. *Nature Reviews Immunology* 2017 18:4 **18**, 225–242 (2017).
12. Products - Data Briefs - Number 390 - November 2020. <https://www.cdc.gov/nchs/products/databriefs/db390.htm#fig1>. (2020)
13. Dahlhamer, J. *et al.* Prevalence of Chronic Pain and High-Impact Chronic Pain Among Adults — United States, 2016. *MMWR. Morbidity and Mortality Weekly Report* **67**, 1001–1006 (2019).
14. Mills, S. E. E., Nicolson, K. P. & Smith, B. H. Chronic pain: a review of its epidemiology and associated factors in population-based studies. *Br J Anaesthesia* **123**, e273–e283 (2019).
15. Dowell, D., Haegerich, T. M. & Chou, R. CDC Guideline for Prescribing Opioids for Chronic Pain—United States, 2016. *JAMA* **315**, 1624–1645 (2016).
16. Smith, B. H. *et al.* The impact of chronic pain in the community. *Family Practice* **18**, 292–299 (2001).
17. Understanding the Epidemic | Drug Overdose | CDC Injury Center. <https://www.cdc.gov/drugoverdose/epidemic/index.html>. (2022)
18. Ji, R. R., Nackley, A., Huh, Y., Terrando, N. & Maixner, W. Neuroinflammation and central sensitization in chronic and widespread pain. *Anesthesiology* **129**, 343 (2018).

19. Ganguly, M., Jenkins, M. W., Jansen, E. D. & Chiel, H. J. Thermal block of action potentials is primarily due to voltage-dependent potassium currents: a modeling study. *Journal of Neural Engineering* **16**, 036020 (2019).
20. Ford, J. B. *et al.* Optimizing thermal block length during infrared neural inhibition to minimize temperature thresholds. *Journal of Neural Engineering* **18**, 056016 (2021).
21. Lothet, E. H. *et al.* Alternating current and infrared produce an onset-free reversible nerve block. *Neurophotonics* **1**, 011010 (2014).
22. Defense and Veterans Brain Injury Center (DVBIC). DoD worldwide numbers for TBI. [https://dvbic.dcoe.mil/system/files/tbi-numbers/worldwide-totals-2000-2018Q1-total\\_jun-21-2018\\_v1.0\\_2018-07-26\\_0.pdf](https://dvbic.dcoe.mil/system/files/tbi-numbers/worldwide-totals-2000-2018Q1-total_jun-21-2018_v1.0_2018-07-26_0.pdf). (2019).
23. NAE Website - TBI Clinical Trials: Past, Present, and Future. <https://www.nae.edu/152165/TBI-Clinical-Trials-Past-Present-and-Future>.
24. Simon, D. W. *et al.* The far-reaching scope of neuroinflammation after traumatic brain injury. *Nature Reviews Neurology* 2017 13:3 **13**, 171–191 (2017).
25. Health: Overdose Prevention: National Drug Overdose Data. <https://www.in.gov/health/overdose-prevention/data/national/>. (2020)
26. DOD TBI Worldwide Numbers | Health.mil. <https://health.mil/Military-Health-Topics/Centers-of-Excellence/Traumatic-Brain-Injury-Center-of-Excellence/DOD-TBI-Worldwide-Numbers>. (2022)

## **Chapter II**

### **Background and Significance**

#### **2.1 Central nervous system physiology**

The central nervous system (CNS) includes the brain and the spinal cord. The focus of the central nervous system is coordinating incoming and outgoing neural impulses that control thought processes, movement, and organ functioning. The CNS receives sensory input and produces motor responses via nerves. A nerve is composed of a bundle of neurons. Most nerves of the peripheral nervous system contain both sensory and motor neurons. The sensory neurons in the peripheral nerve carry sensory impulses to the CNS. The CNS processes this information and sends the appropriate motor signals back to the nerves via the motor neurons. Neurons are accompanied by vasculature and glial cells. The CNS glial cells, which is described in more detail in section 2.2, include astrocytes, microglia, and oligodendrocytes. Perturbations of the CNS can affect the brain or the spinal cord through trauma, infections, autoimmune disorders, tissue degeneration, strokes, or tumors. In turn, these perturbations can lead to chronic pain, Alzheimer's disease and other forms of dementia, multiple sclerosis, Parkinson's disease, and meningitis.<sup>6</sup> Acute pain, or nociception, results from peripheral nerves transmitting pain signals to the brain via somatosensory neurons through the spinal cord or cranial nerves. Chronic pain differs drastically from acute pain in mechanisms of onset and is characterized by the over activation of these pain pathways. This leads to the symptoms of chronic pain, such as feelings of burning, aching, and electric shock-like sensations. Neurons are not the only cells contributing to pain, but non-neuronal glial cells also can play primary drivers of this pathology.<sup>2</sup>

### 2.1.1 Neurons

Neurons are made up of three main parts: dendrites, soma, and axon. Dendrites receive inputs into the cell from either other neurons or transducers. The soma is the cell body of the neuron where the nucleus and other key features are located. The axon, which is always and only one axon, transmits information out of the cell. Neurons are classified by their morphological characteristics: either unipolar, bipolar, pseudo-unipolar, and multipolar. As the names imply, the polarization of the soma defines the characterization. Unipolar neurons have only one process out of the soma and are often found in the invertebrate nervous system. Bipolar neurons have two processes, the axon and dendrites, which are functionally specialized. Pseudo-unipolar neurons are a variant of bipolar neurons, where the two functionalized processes are fused as they leave the soma. Pseudo-unipolar neurons are usually responsible for transmitting somatosensory information from the periphery to the spinal cord. Multipolar neurons have multiple neurons branching from the soma, though still one axon. Multipolar neurons are diverse in their specific morphology due to the multitude of roles they place in the mammalian nervous system. Figure 2.1-1 illustrates the differences and complexities of neuron morphologies from different species and regions of the brain.<sup>1</sup>

The functionality of neurons is usually described by the action potential that propagates from the dendrites to the axon. To describe an action potential, the environment must first be described. Neurons have a membrane potential due to an electrochemical gradient between the inside and outside of the cell. The gradient is due to different ions being constrained to one side of the membrane at a given time. The main ions that contribute to the electrochemical gradient are potassium ( $K^+$ ), Sodium, ( $Na^+$ ), chloride ( $Cl^-$ ), and organic ions ( $A^-$ ).  $K^+$ ,  $Na^+$ , and  $Cl^-$  can move through the membrane by embedded channels. When the neuron is at rest, the effective transport

of charges is negligible. The resulting gradient contributes to the electrochemical gradient according to their equilibrium potential, or Nernst potential. The Nernst potential,  $E_x$ , is defined by:

$$E_x = \frac{RT}{zF} \ln \frac{[\text{Concentration Outside Cell}]}{[\text{Concentration Inside Cell}]}$$

where R is the ideal gas constant (R=8.314 J/mol/K), T is the temperature in Kelvin, z is the valence of the charge, and F is Faraday's constant (F= 96,485 C/mol).

The concentration of ions in the resting state, as well as the Nernst potential for each ion is shown below.

**Table 2.1-1 Neuronal ion concentrations**

Ion	Intracellular Concentration (mM)	Extracellular Concentration (mM)	Nernst Potential (mV)
K <sup>+</sup>	400	20	-75
Na <sup>+</sup>	50	440	+55
Cl <sup>-</sup>	52	560	-60
A <sup>-</sup>	385	NA	NA

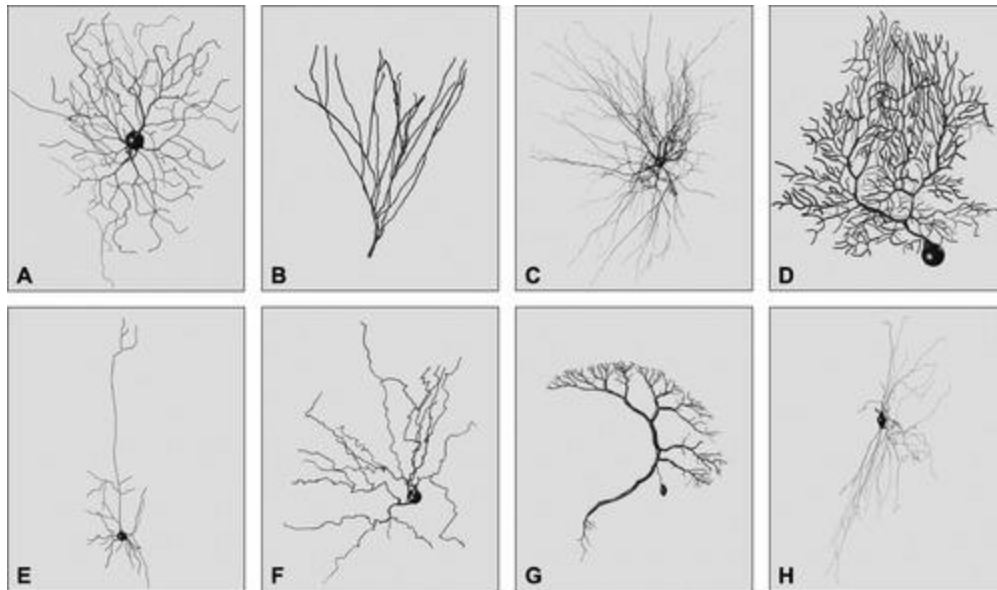


**Figure 2.1-1. Differences in neuron morphologies.**

“Sample neuronal reconstructions selected from the NeuroMorpho.org database based on (principal) cell type: (A) ganglion cell (mouse retina), (B) granule cell (rat hippocampus), (C) motoneuron (cat spinal chord), (D) Purkinje cell (mouse cerebellum), (E) pyramidal cell (rat cerebral cortex), (F) stellate cell (rat cerebral cortex), (G) tangential cell (blowfly visual lobe), (H) relay cell or interneuron (mouse dorsal thalamus).” *Text and figure from source.<sup>1</sup> This is an open-access article distributed under the terms of the Creative Commons Attribution License (CC BY). The use, distribution or reproduction in other forums is permitted, provided the original author(s) or licensor are credited and that the original publication in this journal is cited, in accordance with accepted academic practice. No use, distribution or reproduction is permitted which does not comply with these terms.*

Together, the Nernst potentials of each ion lead to a membrane potential of -70 mV. An action potential is the activation of voltage gated sodium channels (NaV) within the membrane that cause a mass outflux of sodium ions. The channel is called voltage-gated because once the membrane potential reaches a threshold (-50mV), it opens. The initial outflux of Na<sup>+</sup> depolarizes the neuron to +40 mV, at which point the NaV channels close. Similarly, there are voltage-gated potassium channels (KV) that activate when a threshold (-20mV) is reached. The KV channels open to create an influx of extracellular K<sup>+</sup> ions, which hyperpolarizes the neuron. The KV channels close once hyperpolarization has occurred. Lastly, Na/K ATPase sustain the resting potential by transferring Na<sup>+</sup> and K<sup>+</sup> (3 Na<sup>+</sup> out for every 2 K<sup>+</sup> in) against their concentration

gradient. This creates a net hyperpolarizing effect and preserves ion concentrations across the gradient.

Heat can play a role in neuronal function. The movement of Na<sup>+</sup> and K<sup>+</sup> through these channels is a temperature dependent phenomenon. It is hypothesized that KV are more sensitive to temperature changes than sodium channels, and at higher temperatures greater K<sup>+</sup> currents are achieved. At heat block, the term for inhibiting neurons with heat, it is thought that the K<sup>+</sup> current is so high that the membrane cannot depolarize enough to trigger action potentials in that area.<sup>3</sup> As this is an under-researched area of science, further interactions between heat and the CNS are needed.

Changes to neuronal function occur during inflammation and pain. It is well established that inflammatory mediators released locally after tissue injury, including classic mediators, pro-inflammatory cytokines and chemokines, can directly stimulate and cause sensitization of pain-sensing nociceptors located at nerve fibers of primary afferent neurons in peripheral tissues. Therefore, acute inflammation is linked with the development of acute pain.<sup>4</sup> This will be discussed in further detail in Section 2.1.4.

### 2.1.2 Glia

Glia, translating to “glue”, were originally thought to be hold the brain together with little other function. While they arise from the same precursor cells as neurons, they do not share the same function and are not electrically excitable. As more time and resources have been invested in glial research, their importance on the health of the nervous system has been revealed. The human central nervous system has between 2-10 times more glia than neurons. Glial cells are specific to both the central and peripheral nervous system. In the central nervous system, there are astrocytes, microglia, and oligodendrocytes. In the peripheral nervous system, there are satellite glial cells and Schwann cells. Figure 2.1-2 shows the neuron-astrocyte-microglia triad in rat CA1 hippocampus Striatum Pyramidale.<sup>5</sup>

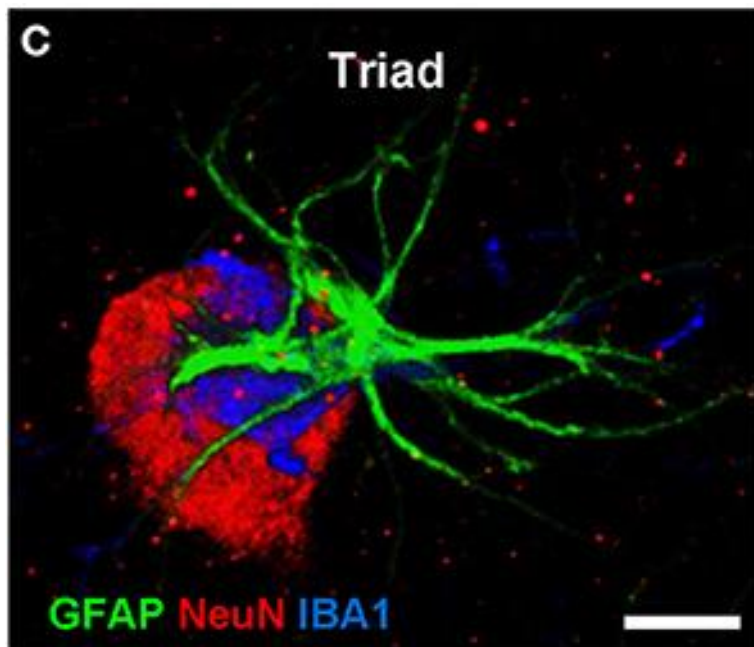


**Figure 2.1-2. Neurons and glia**

“Representation of a triple immunostaining of a neuron-astrocyte-microglia triad. Neuron (NeuN positive, red), astrocyte (GFAP positive, green), microglia (IBA1 positive, blue). Scale bar: 5  $\mu$ m.” *Text and figure from source.<sup>5</sup> This is an open-access article distributed under the terms of the Creative Commons Attribution License (CC BY). The use, distribution or reproduction in other forums is permitted, provided the original author(s) or licensor are credited and that the original publication in this journal is cited, in accordance with accepted academic practice. No use, distribution or reproduction is permitted which does not comply with these terms.*

### 2.1.3 Astrocytes

Astrocytes, like their name implies, are star-shaped cells in the brain and spinal cord that carry out many essential functions in the nervous system. There are two types of astrocyte subtypes, protoplasmic and fibrous, which having carry out different roles. The protoplasmic astrocytes are only found in the grey matter because they encompass the synapses. The fibrous astrocytes, on the other hand, are found only in the white matter because they encompass the nodes of Ranvier. The main *known* functions of astrocytes are separating neurons from one another, regulate the amount of  $K^+$  in the extracellular space, promoting efficient signaling, and nourish surrounding neurons.<sup>6,7</sup>

As mentioned, astrocytes play a significant role in ion homeostasis and signaling. They express potassium, sodium, and calcium channels, though they do not have action potentials like neurons. Intracellular calcium concentration increases are as close to an action potential as it gets in glial cells.<sup>8</sup> The increases in calcium concentrations are a part of astrocyte-astrocyte and astrocyte-neuron signaling that occurs through gap junctions between them. These calcium increase can signify many different events, such as intrinsic oscillations, neurotransmitter release, neurotransmitter uptake, or gap junction calcium signaling.<sup>6,7,9</sup> Other channels, such as potassium, sodium, and aquaporin 4 (AQP4) are common on the astrocyte membrane are important for ion homeostasis. Specifically, astrocytes uptake extracellular potassium as means to prevent neural firing slowing from potassium accumulation. Astrocytes are the direct connection between the blood supply and neurons. They titrate the blood in response to the level of synaptic activity is occurring. i.e., more neuronal firing means more local blood flow.<sup>10</sup> This understanding is now being used in fMRI and optical intrinsic signal imaging as an indirect measure of neuronal activity in the brain.<sup>11,12</sup>

In chronic pain, the transmission of nociceptive signals can be changed to create an exaggerated pain response. For example, projections from astrocytes known as end feet closely monitor synaptic activity for changes in neuronal firing. When the glial cells detect an increase in the extracellular concentrations of neurotransmitters, they begin to uptake greater amounts of the molecules in an attempt to bring the hyperactive synapses under control. Under states of persistent pain, however, there is a significant downregulation of the molecular transporters on astrocytes that are responsible for maintaining excitatory neurotransmitter homeostasis, resulting in less removal of excess excitatory neurotransmitters.<sup>13</sup>

#### 2.1.4 Microglia

Microglia were first discovered by Pio Del Rio-Hortega in 1932.<sup>14</sup> Del Rio-Hortega correctly identified many of the basic functions and morphologies of microglia which will be discussed further. Del Rio-Hortega named the class of cells “microglia” and each individual cell “microgliocyte”, though they are now termed microglial cell. It is widely believed that microglia derive from progenitors that have migrated from the periphery and are of mesodermal/mesenchymal origin.<sup>15</sup> In the first 10 days post-natal, these cells migrate from the blood system as monocytic cells.

Microglia are the resident immune-like cells in the central nervous system and function to present antigens and secrete cytokines and chemokines during inflammation. Microglia have different morphological and function states. In the “resting” or “basal” state, microglia present a ramified morphology with a small soma and fine cellular processes. While in the resting state, if microglia detect a perturbation in the CNS homeostasis, they rapidly change their state to “activated”. In the laboratory, activation is often triggered by the bacterial wall component, lipopolysaccharide (LPS). In the activated state, microglia change their cell shape, gene

expression, and functional behavior.<sup>16-18</sup> In the activated state, microglia lose their fine processes complexity and can change to an amoeboid appearance, which allows them to become increasingly motile. They can move towards the CNS disturbance by following chemotactic gradients. Activated microglia can increase their proliferation to combat invading germs. They can release intracellular enzymes, proinflammatory, and immunoregulatory molecules. Activated microglia are phagocytotic and clear damaged cells, microbes, and tissue debris. The release of chemoattractive factors brings other immune cell types to the CNS and the presentation of antigens to T cells help fight off viral and bacterial infections.<sup>19</sup>

Just like neurons, microglia have a membrane potential dependent on the concentration of ion inside and outside the cell. The membrane potential of microglia *in vivo* has not been recorded, to my knowledge, but it has been recorded in the next best preparation, acute brain slices. In most of these studies the membrane potential of activated microglia were recorded rather than basal microglia, though amount of activation is a gradient and not an all-or-nothing response.<sup>19</sup> They are recording using an electrophysiology technique called whole-cell patch-clamping, which will be discussed in a subsequent chapter. In one study, microglia were found to have a membrane potential of -2 to -40 mV.<sup>20</sup> Another study claims that resting microglia have a membrane potential are -38 mV.<sup>21</sup> Voltage-clamp study of the activated microglia with hyperpolarizing voltage steps showed properties of inward-rectifying K<sup>+</sup> current, which was blocked with the K<sup>+</sup> channel blocker, tetraethylammonium.<sup>22</sup> There are other systems to test microglial resting potentials, such as cultured microglia cells. Human and rodent microglial cells have been shown to have a membrane potential of -50 mV.<sup>23,24</sup>

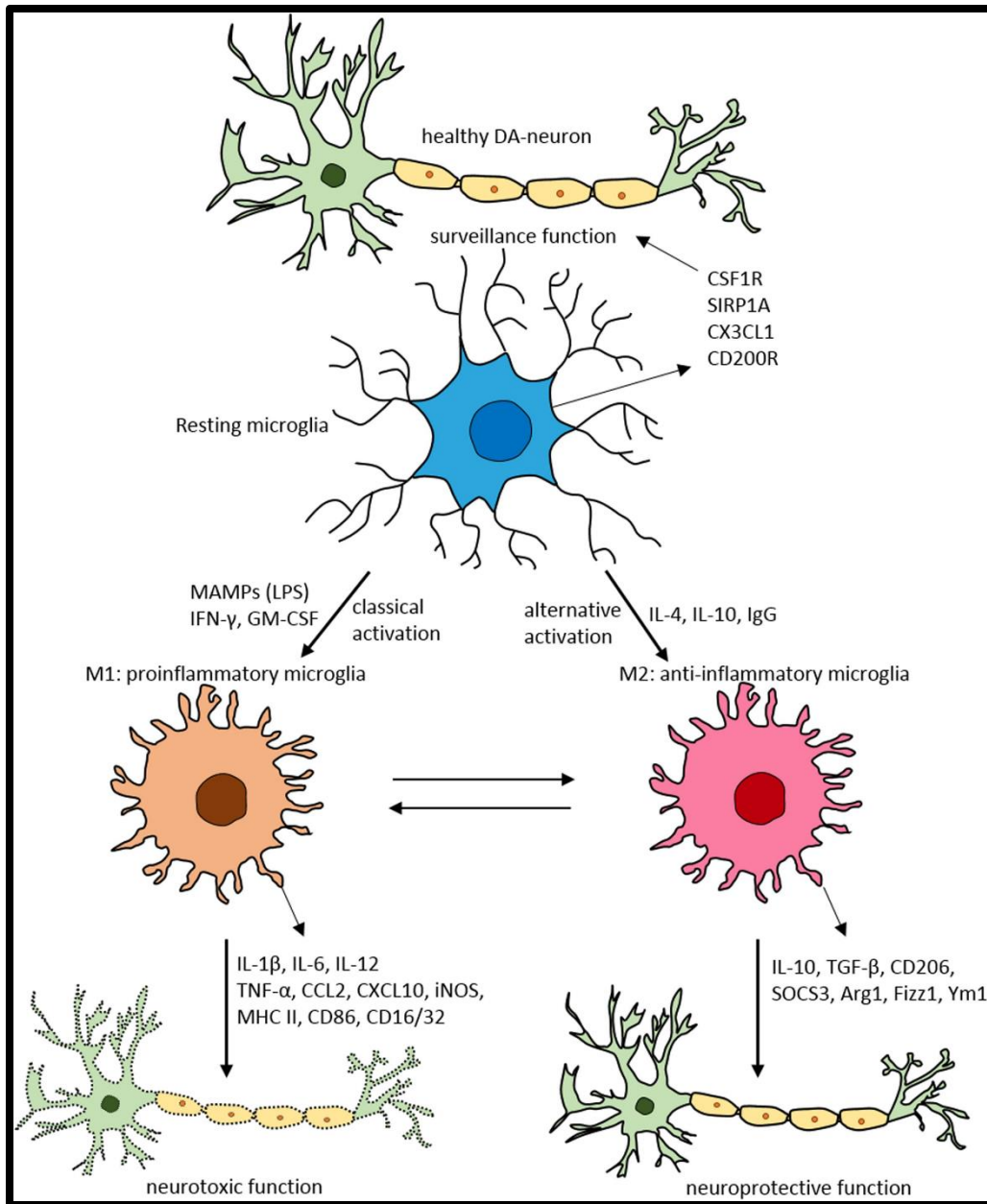


**Figure 2.1-3. Physiological states of microglia**

Microglia can exist in many different physiological states, from homeostatic to responding in neurotoxic or neuroprotective states. *Reprinted from source.<sup>71</sup> This is an open-access article distributed under the terms of the Creative Commons Attribution License (CC BY). The use, distribution or reproduction in other forums is permitted, provided the original author(s) or licensor are credited and that the original publication in this journal is cited, in accordance with accepted academic practice. No use, distribution or reproduction is permitted which does not comply with these terms.*

A major signaling pathway for microglia is through calcium signaling. Intracellular calcium acts as a second messenger in microglia and many microglial responses are thought to be mediated by intracellular calcium signals. Most of information on microglial calcium signaling has been obtained from cultured cells, which only present the activated state. Since cell culture are advantageous for synthetic calcium indicating probe loading, such as Oregon Green 44 BAPTA-1, a number of pathways of microglial calcium signaling have been discovered, including purinergic and complement signaling. Spontaneous microglial calcium transients are infrequent in basal microglia, but inflammatory stimuli significantly elevate the baseline of spontaneous microglial calcium activity.<sup>25</sup>

There are a multitude of neurotransmitter receptors found on microglia, including glutamate receptors, GABA receptors, Purinergic receptors, dopamine receptors, opioid receptors, and a handful of others<sup>26</sup>. It is evident that neurotransmitters instruct microglia to perform distinct types of responses, such as triggering an inflammatory cascade or acquiring a neuroprotective phenotype. Many other receptors are present, such as transient receptor potential vanilloid 4 (TRPV4).<sup>27</sup>

Microglial activation aims to protect the CNS through immunomodulatory messengers. Cytokines compose a large amount of the immunomodulatory and neuromodulatory messengers that can be released by activated microglia. Microglial cytokines and chemokines regulate innate defense mechanisms, help the initiation of immune responses, participate in the recruitment of leukocytes, and support attempts of tissue repair and recovery. Microglia can also sense cytokine and chemokine signals as part of auto- and paracrine communications with astrocytes, neurons, the endothelium, and leukocyte infiltrates.<sup>19,28</sup> Microglial behavior is highly dependent on the cytokine environment and the reactions to an immune challenge may change with the stimulation

context. Failed microglial engagement to perturbations due to excessive activation may significantly contribute to acute and chronic neuropathologies. Dysregulation of microglial cytokine production could promote harmful actions of the defense mechanisms, resulting in direct neurotoxicity, as well as disturb neural cell functions as they are sensitive to cytokine signaling.<sup>28</sup>

## 2.2 Neuropathology

### 2.2.1 Chronic Pain

Chronic pain has become one of the most common diseases with ~25 million people affected in the United States alone <sup>4</sup>. It is estimated that ~4% of the world population is affected by some degree of chronic pain<sup>32</sup>. Chronic pain can be caused by a multitude of possibilities, such as injury, disease, or over-sensitization of neuron that carry pain signals. The treatment for chronic pain is usually prescribed opioids, which in turn, has created what is referred to as the opioid crisis. The opioid crisis is defined as a large increase in the number of opioid abusers. The rate of deaths due to opioid overdose has risen from 3 deaths per 100,000 people in the year 2000 to over 10 deaths per 100,000 people in the United States in 2015. The US government has noticed the alarming increase in the number of opioids prescribed by providers, and Congress has recently added \$3.3 billion to the 2018 spending deal to address the opioid use. \$500 million of which is allocated to the NIH for research into pain management research. A common non-opioid technique to fight chronic pain is neuromodulation.

Acute pain has an adaptive purpose to protect tissue from injury or further injury. Chronic pain is considered mal-adaptive and does not serve a beneficial purpose. Peripheral sensitization and central sensitization are thought to maintain chronic pain conditions. Peripheral sensitization is the increased responsiveness and lessened threshold for spiking by peripheral nociceptive neurons. In contrast, central sensitization is the increased responsiveness of second order nociceptive neurons and high in the CNS. (Figure 2.2-1)<sup>33</sup>

### 2.2.2 Inflammation

Inflammation, either acute or chronic, is triggered by immunogenic stimuli such as tissue injury, pathogens, or lipopolysaccharide. These triggers results in biochemical cascades to

bring the system back to homeostasis. In acute inflammation cases, tissue and damage are enhancing process to healing. In the CNS, the inflammatory process occurs from higher levels of cytokines, microglial activation, infiltration of T cells, and damage to the surrounding tissue. High concentrations of immunologic molecules can cause a state change in microglia to pro-inflammatory.<sup>34</sup>

Microglia survey the synaptic space for local and distant paracrine signals such as cytokines, chemokines, and trophic factors that drive neuronal adaptations at the level of the synapse to refine their likelihood of firing. Some glial cells also release their own proinflammatory cytokines and other mediators, such as reactive oxygen and nitrogen species. Along with additional proinflammatory factors from peripheral immune cells, cytokines can prime the synapse for heightened neuronal firing by increasing the release of excitatory neurotransmitters from neurons.<sup>29</sup> LPS, the cell wall component of gram-negative bacteria, has been used to mimic infection in many animal studies because it initiates a well- characterized immune response via the activation of Toll-like receptor 4 (TLR4). TLR4 is a major receptor functioning to trigger an immune response.<sup>2</sup> Within the immature rat brain, LPS induces a rapid and robust increase in cytokine expression characterized by an increase in the expression of many cytokines and chemokines, including interleukin 1 beta (IL-1 $\beta$ ) and interleukin 6 (IL-6). IL-1 $\beta$  is an important pro-inflammatory mediator, while IL-6 can be either pro-inflammatory or anti-inflammatory.<sup>30</sup> Treatment of neonatal pups with high doses of LPS is linked to white matter damage, decreased oligodendrocyte development, hypo-myelination of neurons and enhanced behavioral pain responses in adulthood. Lower doses of LPS given during the perinatal period also induce a number of long-term changes in the brain, both biochemical and behavioral.<sup>31</sup>

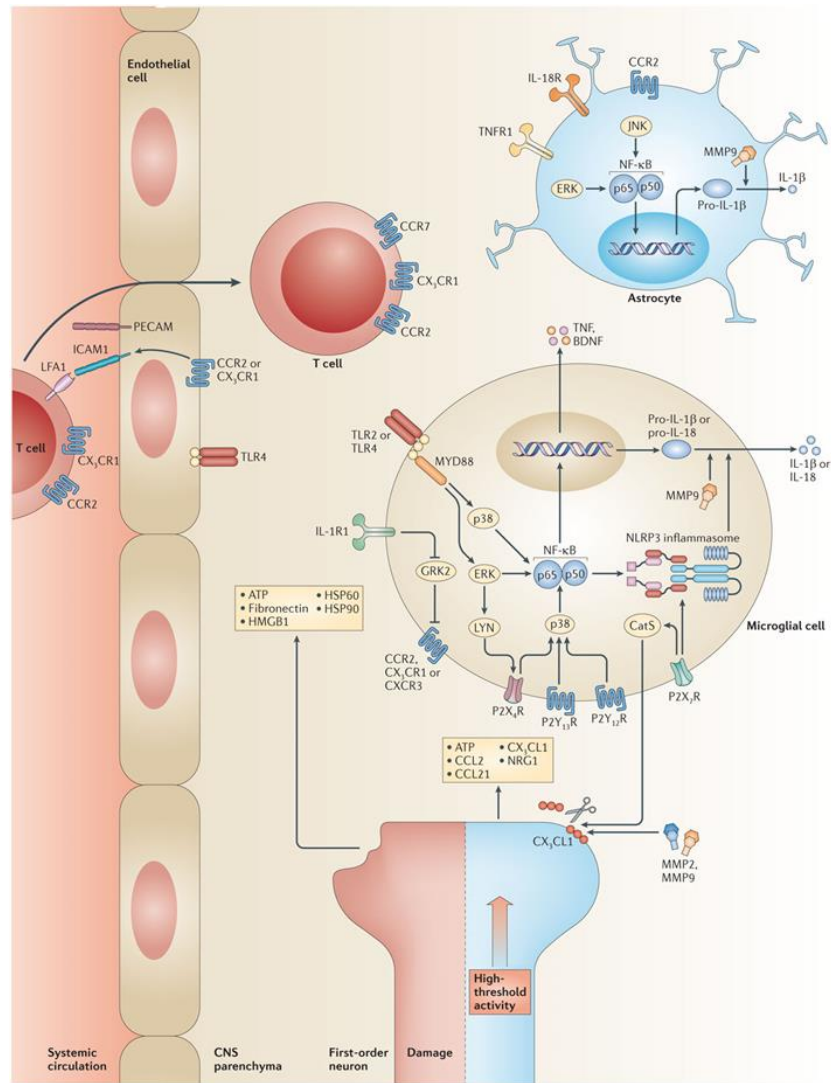


**Figure 2.2-1. Central Sensitization**

“Damage to or high-threshold activation of first-order neurons by noxious stimuli induces the release of ATP, CC-chemokine ligand 2 (CCL2), CCL21 and neuregulin 1 (NRG1), as well as endogenous danger signals to initiate central immune signaling in the dorsal horn of the spinal cord. CCL2 is released and rapidly upregulated by neurons following depolarization, and signals via its cognate receptor CC-chemokine receptor 2 (CCR2) on microglia. CX3C-chemokine ligand 1 (CX3CL1) is liberated from the neuronal membrane by matrix metalloproteinase 9 (MMP9) and MMP2 and by microglial cell-derived cathepsin S (CatS) and signals via CX3C-chemokine receptor 1 (CX3CR1), which is expressed by microglia. CCR2 and CX3CR1 signaling also induces the expression of integrins (such as intercellular adhesion molecule 1 (ICAM1) and platelet endothelial cell adhesion molecule (PECAM1)) by endothelial cells, allowing the transendothelial migration of T cells. Neuronal cell release of CCL21 stimulates local microglia via CCR7, and infiltrating T cells are activated via CXCR3. ATP induces microgliosis via the purinergic receptors P2X<sub>4</sub>R, P2X<sub>7</sub>R, P2Y<sub>12</sub>R and P2Y<sub>13</sub>R. Microglia express Toll-like receptor 2 (TLR2) and TLR4 leading to activation of the MYD88 pathway after detection of endogenous danger signals, such as heat shock protein 60 (HSP60), HSP90, high mobility group box 1 (HMGB1) and fibronectin. Following the detection of such signals, many intracellular pathways are recruited including SRC family kinases (SRC, LYN and FYN), MAPKs (extracellular signal-regulated kinase (ERK), p38 and JUN N-terminal kinase (JNK)) and the inflammasome. This leads to phenotypic changes, increased cell motility and proliferation, altered receptor expression, the activation of transcription factors, such as nuclear factor-κB (NF-κB), and the production of inflammatory mediators (such as interleukin-1β, (IL-1β), IL-18, tumor necrosis factor (TNF) and brain-derived neurotrophic factor (BDNF)). Interleukin-1 receptor (IL-1R1) signaling reduces microglial cell expression of G protein-coupled receptor kinase 2 (GRK2), which is a negative regulator of G protein-coupled receptors (GPCRs), including chemokine receptors. This leads to sustained GPCR signaling, and the exaggerated and prolonged production of pro-inflammatory mediators. The release of soluble mediators also provides a feedback mechanism by which further immune cells are activated.” *Figure and text from source with permission.*<sup>33</sup>

### 2.2.3 Neuromodulation

Neuromodulation is an attractive method to modulate neural activity for the treatment of diseases and impairments. While electrical stimulation remains the gold standard, it still has its drawback. In clinical use, it can have poor spatial specificity, paresthesia, and lead migration<sup>35,36</sup>. The mechanisms of certain technologies, such as spinal cord stimulation, are not fully understood, making the optimization of parameters and predicting unwanted consequences more difficult<sup>37</sup>. High frequency alternating current has been shown to provide block of action potentials in bulk neurons and is used for inhibition treatments.

It is also possible to treat the disease of neuronal function chemically. As described in Section 2, chronic pain can change the ion concentration and the response of neurons to neurotransmitters. Therefore, it is possible to treat chronic pain with chemical additions of neurotransmitters and channel modulators to change channel opening. One example of this is opioids. While chemicals are highly specific on their target to modulate neurons, they usually will do so widespread throughout the body. Another major drawback is the addictive properties of pharmaceuticals and the likelihood of abusing the drugs.<sup>36</sup>

Neuromodulation with optical methods has been shown through a few different techniques. Low-level light therapy (LLLT), or photobiomodulation, has shown to decrease the sensation of pain.<sup>38</sup> Neurotransmitter uncaging, where neurotransmitters (usually glutamate) are inactivated by the addition of a photosensitive area in the vesicles. Optogenetics has become a more potential method for neuromodulation in recent years. While still not clinically relevant, optogenetics has been shown to stimulate and inhibit neurons very specifically.<sup>39</sup> Optogenetic works by transfecting genetic material for the expression of channelrhodopsin, a light sensitive channel, in the neuron membrane. Despite its success in the research setting, its main drawback is requirement that the

genetic code must be changed, which has scientific and ethical barriers. More relevant to this proposal, infrared neural modulation has become a potential treatment of neural problems.

#### 2.2.3.1 Electrical Stimulation

Electrical stimulation has been the gold standard for stimulating neurons for both clinical and basic research applications for decades, if not longer. Neurons are activated by electrical stimulation through the flow of current between a cathode and anode placed on or near the target neural tissue. The injected current depolarizes the cell membrane potential of the neuron reaches its threshold potential voltage-gated ion channels open and generate action potentials that propagate down the axon of the stimulated neuron. Electrical stimulation parameters are well characterized and can be optimized for specific applications. The utility of electrical stimulation can be limited by inherent electrical field spread activation unwanted neural tissue, generation of stimulation artifact that can mask relevant neuronal signals, and electrodes must contact or impale tissue increasing risk for damage.<sup>35,36</sup>

#### 2.2.3.2 Infrared Neural Modulation

Infrared neural modulation (INM) is the use of infrared light to perturb excitable tissues. It had clear advantage over conventional electrical stimulation methods, such as contact-free and spatially precise neuromodulation. INM irradiation may either result in the stimulation or the inhibition of excitable tissue, depending on the irradiation parameters used. A neural signal being generated with a pulse of light is referred to as infrared neural stimulation (INS). Though under a different set of irradiation parameters, infrared light may block neural activity, which is referred to as infrared neural inhibition (INI). In INS and INI, the tissue's absorption of infrared light causes a localized heating. To create this localized heating, wavelengths used for INM usually lie on peaks in the water absorption curve, the main chromophore in tissue at these infrared wavelengths.

Though INS and INI can use the same wavelengths, the spatial and temporal dynamics between them differ drastically.

### 2.2.3.3 Infrared Neural Stimulation

Infrared neural stimulation (INS) is caused by the transient spatiotemporal thermal gradient resulting from each pulse of light<sup>40,41</sup>. Therefore, to elicit a response, heating must be confined within a small enough volume and generated within a short enough time period. Many studies have probed at the underlying mechanisms of INS. The first study by Wells et. al. narrowed the mechanism down to an induced thermal gradient by ruling out other laser-induced mechanisms, such as photochemical, electric field, and photoacoustic effects<sup>41</sup>. Wells et al. found that photochemical effects were unlikely to be the mechanism since infrared light does not have enough energy per photon to drive chemical reactions. They also ruled electrical field effects out by comparing the effects of two different wavelengths with the same induced electrical field. The wavelength not aligned with peaks on the water absorption spectrum was unable to elicit neural activity. Photoacoustic effects were ruled out by experimentally replicating the volumetric expansion of INS laser light with an oscillating piezo-crystal to induce the mechanical perturbations, yet no neural activity resulted. More recently, it has been proposed that mechanical changes to the cell membrane play a role in eliciting a neural response and is still controversial.<sup>42,43</sup>

A photothermal mechanism emerged as the fundamental interaction driving the stimulation of neural tissue. The photothermal mechanism is thought to be due to a thermal gradient instead of a thermal threshold. Since, a steady temperature rise was unable to stimulate frog nerves when temperatures were held at either 0°C and 25°C and irradiated with INS. It is expected that higher radiant exposures would be required for nerves held at 0°C compared to the nerves held at 25°C to be stimulated if a thermal threshold must be reached. It was found that similar radiant exposures

caused stimulation in both cases, ruling out a thermal threshold mechanism<sup>41</sup>. Thus, a transient thermal gradient is hypothesized to moderate INS.

Researchers from other groups have attempted to better understand the biophysical mechanism of INS. Albert et. al. demonstrated that temperature sensitive ion channel transient receptor protein vanilloid family subtype 4 (TRPV4) were important in evoking INS. TRPV4 channels are well known respond to elevated temperatures that are similar to temperatures induced by INS. While this mechanism works for cells with TRPV4 channels, it is not uniformly expressed by all neurons in the nervous system, such as motor axons that were the subject of initial INS works<sup>44</sup>. Shapiro et al. investigated the effect of thermal transients on cell membrane capacitance<sup>42</sup>, which was later expanded upon by Plaksin et al<sup>43</sup>. They showed that temperature transients lead to an increase in capacitance of the cell membrane in excitable and non-excitable cells. The hypothesis is the increased capacitance is a product of lipid bilayers. These results are consistent with the Guoy-Chapman-Stern theory for double layer capacitors. Water was validated as the chromophore needed to evoke INS, by replacing H<sub>2</sub>O with D<sub>2</sub>O. Since D<sub>2</sub>O absorbs infrared light to a much lesser degree, a large enough thermal gradient wasn't produced to evoke INS. While these studies have given a better understand of INS mechanisms, there are likely more mechanisms at work.

INS has been used in a multitude of systems with unique results from each. INS research in the CNS has focused on rat brain slices, *in vivo* rat brain, and *in vivo* non-human primate (NHP) brain experiments to show efficacy, mechanisms, and research applications. INS in the CNS has been shown to have therapeutic, brain mapping, and basic research applications. INS has also been used in a number of PNS applications. INS has shown efficacy in the rat sciatic nerve<sup>45</sup>, human dorsal root nerves<sup>46</sup>, cardiac control of embryotic quail hearts<sup>47</sup>, and cat auditory nerves<sup>48</sup>. There

are some considerations to keep in mind when stimulating with INS. To reduce the chance of damage, stimulation parameters are chosen to mitigate thermal effects from subsequent pulses, thereby avoiding a baseline temperature rise and reducing the thermal load on the tissue. Different wavelengths of light have changed INS safety ratios, the ratio of radiant exposure needed for stimulation to the radiant exposure needed for damage.

#### 2.2.3.4 Infrared Neural Inhibition

Infrared neural inhibition (INI) differs from INS in that it is used to inhibit the generation or propagation of neural signals. Duke et al. first showed the utility of INI in both a vertebrate and an invertebrate model to inhibit action potential generation and propagation<sup>49</sup>. INI has also been shown in the cardiac nerve<sup>50</sup> and the brain<sup>51</sup>. The mechanism of INI is still being explored, however it is believed that a threshold temperature is required<sup>52</sup>. IN 1949, Hodgkin and Katz showed a change in neuron resting potential and action potential kinetics that was dependent upon the temperature of the surrounding media<sup>52</sup>. It is known that temperature plays a role in ion movement and ion channel kinetics, and a hypothesis exists for reduced net membrane currents to a point of action potential failure. It is hypothesized that at higher temperatures, sodium permeability is gradually overtaken by potassium permeability that leads to a block of the onset or propagation of an action potential leading to a heat block<sup>53</sup>.

Temperature may not be the only factor which plays a role in the development of inhibition from heat block. Mou et. al. investigated how the diameter of axons affects the temperature at inhibition threshold by simulating increased temperatures along axons in a frog sciatic nerve geometry.<sup>54</sup> Simulations demonstrated that larger diameter axons require a higher temperature for global conduction block as compared to smaller diameter axons. It was also found that the threshold temperature required for achieving a block of action potential propagation was greater

than that required to produce a block of action potential generation. Lothet et. al. experimentally showed that small diameters fibers can be selectively altered by INI<sup>55</sup>. Ganguly et. al. have shown that potassium channels are more heavily affected by heat and may cause an accumulation of potassium in the extracellular space.<sup>56</sup>

#### 2.2.4 Blast-induced traumatic brain injury

Traumatic brain injury (TBI) is a brain dysfunction caused by an external force that may have short- and long-term effects on Service members and their families. Statistics from the Defense and Veterans Brain Injury Center (DVBIC) state nearly 400K individuals from the department of defense sustained a TBI from 2001 to 2018. A third of whom were exposed to blast events.<sup>57</sup> There are currently no treatments specific to bTBI, and treatments for TBI usually treat the symptoms rather than any underlying origin. For mild TBI, the usual treatment is rest and symptomatic treatment.

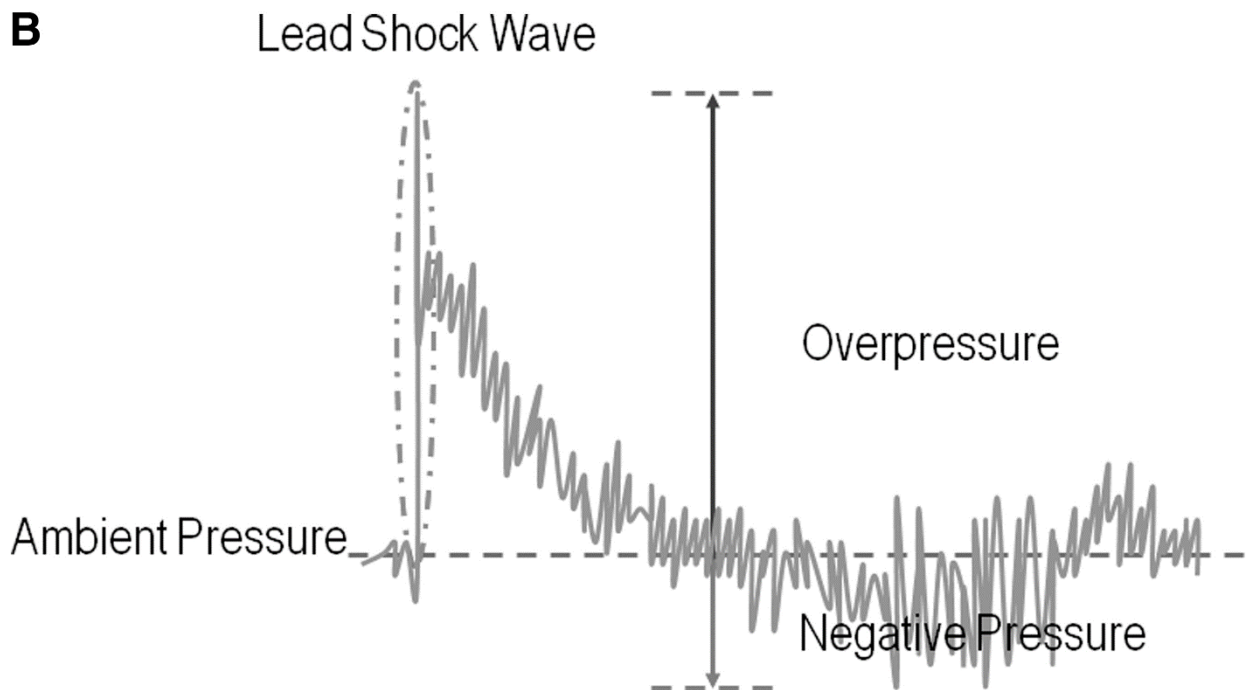


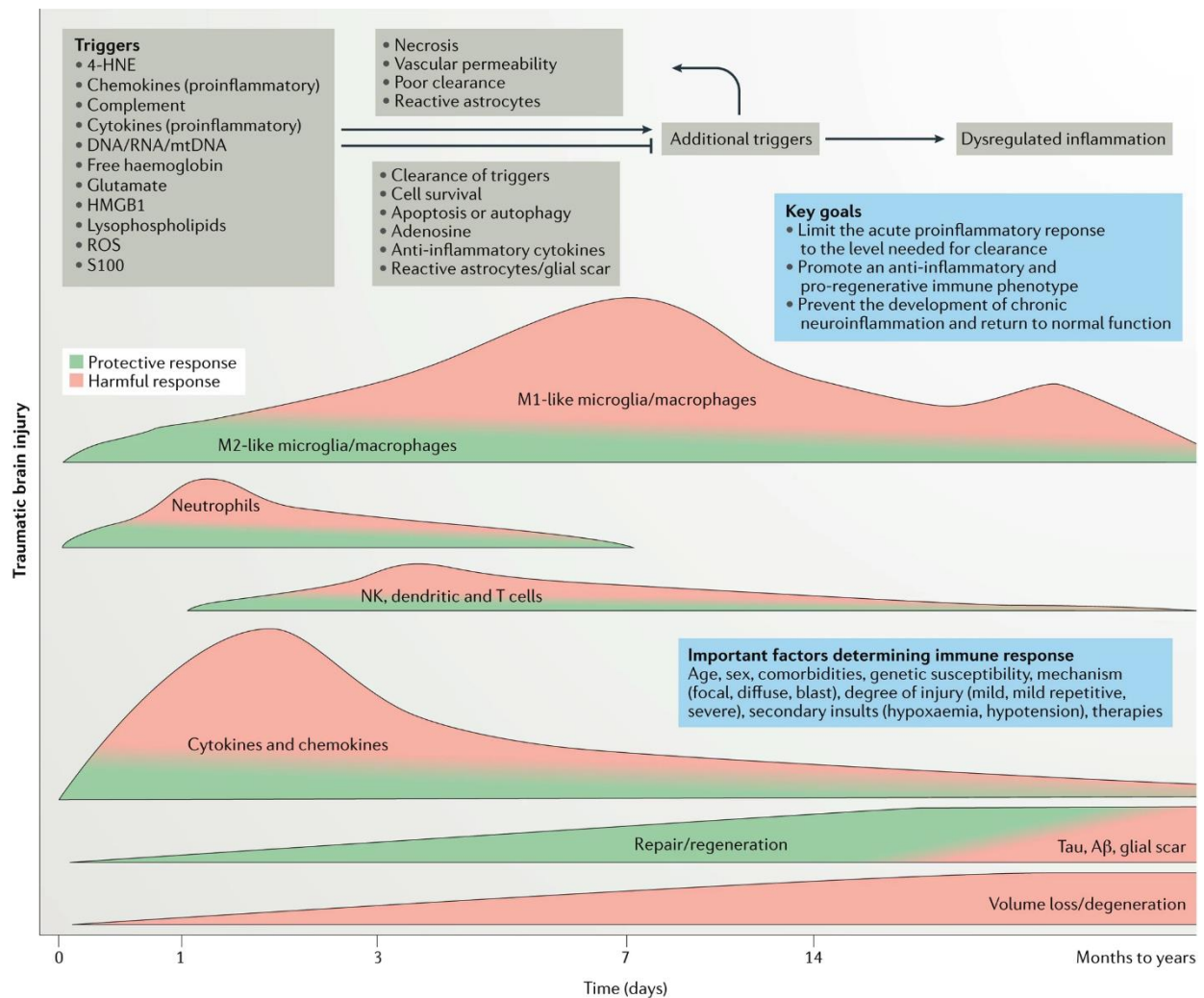
**Figure 2.2-2. Classical free-field blast wave at a fixed location.**

*Preprinted and modified from source with permission<sup>69</sup>*

A detonation of an explosive device can elicit a primary blast wave. The blast consists of a high positive pressure wave that expands radially from the source, followed by a longer but less intense negative pressure (Figure 2.2-2). The idealized pressure pattern is known as the Friedlander<sup>58</sup> curve and can be characterized by the peak overpressure, the duration, and impulse,

or the integrative of a pressure-time plot. These characteristics can vary depending on the explosive material and how long the measurement radius is. Often in the context of a battlefield, there are reflections and beam shaping from the environment that is not shown from the Friedlander curve.<sup>59</sup> Head trauma due to blast overpressure is incompletely understood and will require multidisciplinary methods to better understand the impact of bTBIs. It is currently thought that there is no singular mechanism governing the effects of blast on the brain, but rather multiple mechanisms that depend on the complexity of the blast.<sup>60</sup>

TBI is not just an acute injury. Neuroinflammation associated with the acute and chronic symptoms of TBI may be a main driver of symptoms. Following TBI, there are many detrimental processes that cascade throughout the brain. The primary injury is the mechanical damage to the neurons, glia, and blood vessels, which can vary in intensity depending on the nature of the TBI. There is usually direct neural cell loss and necrotic death due to the primary injury. The primary injury triggers many biochemical cascades that often cause secondary cell death, which prolong the time of injury. There are many secondary death processes, including excitotoxicity, oxidative stress, mitochondrial impairment, damage to the blood brain barrier, and inflammation.<sup>61</sup>



Nature Reviews | Neurology

**Figure 2.2-3. Traumatic brain injury response**

“Primary mechanical injury to the CNS may cause cell membrane disruption, vascular rupture and blood–brain barrier (BBB) damage followed by secondary reactions involving ionic imbalance, release of excitatory amino acids, calcium overload, and mitochondrial dysfunction, culminating in cell death pathways. Primary and secondary injury lead to release of damage-associated molecular patterns, cytokines, chemokines, activation of microglia and astrocytes, and recruitment of circulating immune cells. Temporally, these immune responses largely overlap. The inflammatory response is crucial to clearance of debris, repair, and regeneration after traumatic brain injury. However, dysregulated inflammation can lead to additional acute and chronic brain injury. 4-HNE, 4-hydroxynonenol; HMGB1, high mobility group protein B1; mtDNA, mitochondrial DNA; ROS, reactive oxygen species.” *Reprinted and text from source with permission.*<sup>70</sup>

### 2.2.5 Inflammation

The major cause of secondary cell death in TBI is inflammation. Neuroinflammation increases neural cell death through CNS immune cells, such as microglia and their inflammatory immune response. Released cytokine, chemokines, and other inflammatory molecules can interrupt the normal repair process. Following immune activation to repair damaged cells, there is an infiltration of neutrophils, monocytes, and lymphocytes that cross the blood brain barrier to release inflammation regulators, such as prostaglandins, pro-inflammatory cytokines and other inflammatory molecules.<sup>62</sup> When the inflammation outlasts the usual time for repair, it becomes chronic with negative consequences. In the context of TBI, microglia are not thought to become activated in response to damage until days later, though pro-inflammatory cytokine and chemokines are released within days of an injury. The timeline of immune response to TBI is shown in Figure 2.2-3.

## 2.3 Pulsed laser tissue interaction

### 2.3.1 Photothermal

A single pulse of light can generate heat depending on the absorption coefficient of the material, the radiant exposure used, the density of tissue, and the specific heat.<sup>72</sup> In the cases where the laser pulse is sufficiently short, thermal diffusion is negligible and the heat rise is predictable. After heat is generated, it is no longer a photothermal phenomenon but solely a thermal event. Photothermal interactions can cause permanent changes in tissue including coagulation, vaporization, and carbonization. Coagulation is the process of a liquid changing to a solid, such as blood. Vaporization is the process of water vaporizing from phase change, often resulting thermal decomposition of tissue fragments. Carbonization is the process of carbon atoms being released when all water molecules are vaporized. The generated heat can dissipate through 3 possible means: conduction, convection, and radiation. Conduction is the transfer of thermal energy from one solid or fluid media to another, convection is the transfer of thermal energy through a fluid due to bulk motion, and radiation is thermal energy transferred via electromagnetic waves. Photothermal interactions are especially important for this dissertation as it is the way in which heat is generated during infrared neural modulation.

### 2.3.2 Photomechanical

Mechanical waves can be also generated during laser irradiation. These photomechanical interactions include the generation of pressure waves, photoablation, explosive vaporization, and plasma induced ablation. This work will focus on pressure waves which can be generated by thermoelastic expansion, ablative recoil, and cavitation collapse.<sup>72</sup> Thermoelastic expansion entail heating tissue with a pulse laser that is stress confined, meaning that pressure is generated faster than it can dissipate. When stress confined, the pressure from generative from heating cannot

escape the zone fast enough and a build-up occurs. Ablative recoil entails the recoil caused by the ejection of an ablative material. Ablation is caused by the vaporization of water and photothermal disruption of tissue. Cavitation collapse occurs after vaporization in an aqueous environment that grows a bubble that can collapse to a single point and generate a pressure wave. The pressure waves that are generated from these methods can travel at the speed of sound for the medium or faster than it in certain circumstances.

### 2.3.3 Photochemical

The 3<sup>rd</sup> type of laser-tissue interaction is photochemical, or light inducing chemical reactions. A well-known use of this interaction is in photodynamic therapy in which a photosensitizer creates reactive oxygen species after low irradiance. Often, the duration of laser exposure is many magnitudes higher than those necessary to cause photothermal or photomechanical interactions. Photochemical interactions are not thought to be driving the cellular responses reported in this dissertation and therefore it will not be discussed in greater detail.

## 2.4 Measurement Techniques

### 2.4.1 Fluorescence Imaging

Monitoring intracellular ion change is necessary to the understanding of signaling and functional pathways in neuronal systems. Ion changes are central to many fundamental processes such as muscle contraction as well as synaptic nerve signal transmission. Homeostatic regulation of these ionic gradients is critical for most cellular functions. Therefore, measuring ionic concentrations with both spatial and temporal resolution has become critical in research ranging from drug discovery to neuronal function studies<sup>63,64</sup>. Measuring ion concentration changes can be done ion sensitive dyes and voltage sensitive dyes.

Fluorescent dyes change their fluorescence due to changes in the specified biological marker, such as ion concentration or membrane potential, and represent a direct measure of neural activity. The spatial resolution of these responses is constrained to the wavelength of light. The temporal resolution is on the order of milliseconds, the same timescale as action potentials, making it possible to study neural activity. The two main types of fluorescent dyes used for neuronal quantification are ion sensitive dyes and voltage sensitive dyes. Fluorescence imaging with ion sensitive dyes is used to visualize both neural and glial activity<sup>64,65</sup>. Fluorescent dye molecules can be loaded directly into cells or via passive diffusion, and they report on the intracellular concentrations through changes in fluorescence. Fluorescent dyes for detecting ion concentration gradients have been demonstrated for potassium, sodium, and chloride. While calcium sensitive dyes were once the most reliable, new ion dyes have been shown to be just as reliable. Asante Potassium Green is a fluorescent indicator for measuring cytosolic K<sup>+</sup> concentration. It loads readily into neurons and is excited by visible light. Its large fluorescence dynamic range allows sensing of even small changes in K<sup>+</sup> concentration. Asante Potassium Green works well with 2-

photon excitation at near-infrared wavelengths and although not fully resistant to photobleaching it is more robust than other dyes. It is useful for confocal microscopy, flow cytometry, and screening.

## 2.4.2 Thermal measurements

### 2.4.2.1 Thermal imaging

Thermal imaging is used to measure samples that need high spatial resolution ( $\mu\text{m}$ ), large field of view, moderate temporal resolutions (10's ms), and moderate thermal resolution (0.1  $^{\circ}\text{C}$ ). It also does not need to be in contact with the measured sample. It has difficulty measuring samples through water, such as biological tissue due to the high absorption of sensed wavelengths.<sup>66</sup> Thermal cameras are able to quantify temperature by measuring radiant energy that all matter gives off above zero Kelvin.<sup>67</sup> The intensity of the irradiate power emitted by a blackbody is related to temperature. In this work, a thermal camera was used to map temperature increases from a photothermal stimuli at the border of water and glass.

### 2.4.2.2 Thermocouple

A point measurement-based device with high spatial (10's  $\mu\text{m}$ ), temporal (ms), and thermal (0.01  $^{\circ}\text{C}$ ) resolution is a thermocouple. A thermocouple utilizes the Seebeck effect to measure temperature, which entails a potential difference created by a junction of two metals. The voltage difference is linear with temperature making it ideal for thermal measurements. The main drawbacks are its point source nature, making spatial variations in temperature difficult to measure and it must be in contact with sample, potentially altering the thermal dynamics. In this work, thermocouples were used to measure temperatures in small, confined areas in complex instrumental setups.

## 2.5 Reference

1. Meijering E. Neuron tracing in perspective. *Journal of Quantitative Cell Science* **77A**, 693-2010 (2014).
2. Buchanan, M. M., Hutchinson, M., Watkins, L. R. & Yin, H. Toll-like receptor 4 in CNS pathologies. *J Neurochem* **114**, (2010).
3. Ganguly, M., Jenkins, M. W., Chiel, H. J. & Jansen, E. D. Modeling the effects of elevated temperatures on action potential propagation in unmyelinated axons. in *Proc. SPIE 9690, Clinical and Translational Neurophotonics 96901O1-96901O7* (2016)
4. Nahin, R. L. Estimates of Pain Prevalence and Severity in Adults: United States, 2012. *J Pain* **16**, 769–780 (2015).
5. Lana D et. al. The neuron-astrocyte-microglia triad in rat model of chronic cerebral hypoperfusion: protective effect of dipyridamole. *Front. Aging Neurosci.* **6** (2014)
6. Halassa, M. M., Fellin, T. & Haydon, P. G. The tripartite synapse: roles for gliotransmission in health and disease. *Trends Mol Med* **13**, 54–63 (2007).
7. Nedergaard, M., Ransom, B. & Goldman, S. A. New roles for astrocytes: Redefining the functional architecture of the brain. *Trends Neurosci* **26**, 523–530 (2003).
8. Charles, A. C., Merrill, J. E., Dirksen, E. R. & Sandersont, M. J. Intercellular signaling in glial cells: Calcium waves and oscillations in response to mechanical stimulation and glutamate. *Neuron* **6**, 983–992 (1991).
9. Volterra, A. & Meldolesi, J. Astrocytes, from brain glue to communication elements: the revolution continues. *Nat Rev Neurosci* **6**, 626–640 (2005).

10. Koehler, R. C., Roman, R. J. & Harder, D. R. Astrocytes and the regulation of cerebral blood flow. *Trends Neurosci* **32**, 160–169 (2009).
11. Cornell-Bell, A., Finkbeiner, S., Cooper, M. & Smith, S. Glutamate induces calcium waves in cultured astrocytes: long-range glial signaling. *Science (1979)* **247**, 470–473 (1990).
12. Cayce, J. M. *et al.* Infrared neural stimulation of primary visual cortex in non-human primates. *Neuroimage* **84**, 181–190 (2014).
13. Sofroniew, M. V & Vinters, H. V. Astrocytes: biology and pathology. *Acta Neuropathol* **119**, 7–35 (2010).
14. Del Rio-Hortega, P. & Penfield, W. *Cytology & Cellular Pathology of the Nervous System*. (1932).
15. Chan, W. Y., Kohsaka, S. & Rezaie, P. The origin and cell lineage of microglia—New concepts. *Brain Res Rev* **53**, 344–354 (2007).
16. Block, M. L., Zecca, L. & Hong, J.-S. Microglia-mediated neurotoxicity: uncovering the molecular mechanisms. *Nat Rev Neurosci* **8**, 57–69 (2007).
17. Davoust, N., Vuillat, C., Androdias, G. & Nataf, S. From bone marrow to microglia: barriers and avenues. *Trends Immunol* **29**, 227–234 (2008).
18. Graeber, M. B. & Streit, W. J. Microglia: biology and pathology. *Acta Neuropathol* **119**, 89–105 (2010).
19. Hanisch, U.-K. & Kettenmann, H. Microglia: active sensor and versatile effector cells in the normal and pathologic brain. *Nat Neurosci* **10**, 1387–1394 (2007).

20. Boucsein, C., Kettenmann, H. & Nolte, C. Electrophysiological properties of microglial cells in normal and pathologic rat brain slices. *European Journal of Neuroscience* **12**, 2049–2058 (2000).
21. Schilling, T. & Eder, C. Ion channel expression in resting and activated microglia of hippocampal slices from juvenile mice. *Brain Res* **1186**, 21–28 (2007).
22. Brockhaus, J., Ilchner, S., Banati, R. B. & Kettenmann, H. Membrane properties of amoeboid microglial cells in the corpus callosum slice from early postnatal mice. *J Neurosci* **13**, 4412–21 (1993).
23. Kettenmann, H., Hoppe, D., Gottmann, K., Banati, R. & Kreutzberg, G. Cultured microglial cells have a distinct pattern of membrane channels different from peritoneal macrophages. *J Neurosci Res* **26**, 278–287 (1990).
24. Nöurenberg, W., Illes, P. & Gebicke-Haerter, P. J. Sodium channel in isolated human brain macrophages (microglia). *Glia* **10**, 165–172 (1994).
25. Tvrdik, P. & Kalani, M. Y. S. In Vivo Imaging of Microglial Calcium Signaling in Brain Inflammation and Injury. *Int J Mol Sci* **18**, (2017).
26. Pocock, J. M. & Kettenmann, H. Neurotransmitter receptors on microglia. *Trends Neurosci* **30**, 527–535 (2007).
27. Konno, M. *et al.* Stimulation of transient receptor potential vanilloid 4 channel suppresses abnormal activation of microglia induced by lipopolysaccharide. *Glia* **60**, 761–770 (2012).
28. Hanisch, U.-K. Microglia as a source and target of cytokines. *Glia* **40**, 140–155 (2002).

29. Ji, R.-R., Chamesian, A. & Zhang, Y.-Q. Pain regulation by non-neuronal cells and inflammation. *Science* **354**, 572–577 (2016).
30. Souza, K. L. A., Gurgul-Convey, E., Elsner, M. & Lenzen, S. Interaction between pro-inflammatory and anti-inflammatory cytokines in insulin-producing cells. *Journal of Endocrinology* **197**, 139–150 (2008).
31. Bilbo, S. D. & Schwarz, J. M. The immune system and developmental programming of brain and behavior. *Front Neuroendocrinol* **33**, 267–86 (2012).
32. PRWeb. *Global Pain Management Market to Reach US\$60 Billion by 2015, According to a New Report by Global Industry Analysts, Inc.* (2012).
33. Grace, P. M., Hutchinson, M. R., Maier, S. F. & Watkins, L. R. Pathological pain and the neuroimmune interface. *Nat Rev Immunol* **14**, 217–231 (2014).
34. Woodburn, S. C., Bollinger, J. L. & Wohleb, E. S. The semantics of microglia activation: neuroinflammation, homeostasis, and stress. *J Neuroinflammation* **18**, 258 (2021).
35. Grider, J. S. *et al.* Effectiveness of Spinal Cord Stimulation in Chronic Spinal Pain: A Systematic Review. *Pain Physician* **19**, E33-54 (2016).
36. Liebano, R. E., Rakel, B., Vance, C. G. T., Walsh, D. M. & Sluka, K. A. An investigation of the development of analgesic tolerance to TENS in humans. *Pain* **152**, 335–342 (2011).
37. Mazzullo, J. M. The gate control theory of pain. *Br Med J* **2**, 586–7 (1978).
38. Sushko, B. S., Lymans'kyĭ, I. P. & Huliar, S. O. [Action of the red and infrared electromagnetic waves of light-emitting diodes on the behavioral manifestation of somatic pain]. *Fiziol Zh* **53**, 51–60 (2007).

39. Boyden, E. S., Zhang, F., Bamberg, E., Nagel, G. & Deisseroth, K. Millisecond-timescale, genetically targeted optical control of neural activity. **8**, 1263–1268 (2005).
40. Wells, J. *et al.* Optical stimulation of neural tissue in vivo. *Opt Lett* **30**, 504–506 (2005).
41. Wells, J. *et al.* Biophysical Mechanisms of Transient Optical Stimulation of Peripheral Nerve. *Biophys J* **93**, 2567–2580 (2007).
42. Shapiro, M. G., Homma, K., Villarreal, S., Richter, C. & Bezanilla, F. Infrared light excites cells by changing their electrical capacitance. *Nat Commun* **3**, 310–376 (2012).
43. Plaksin, M., Shapira, E., Kimmel, E. & Shoham, S. Thermal Transients Excite Neurons through Universal Intramembrane Mechanoelectrical Effects. *Phys Rev X* **8**, 011043 (2018).
44. Albert, E. S. *et al.* TRPV4 channels mediate the infrared laser-evoked response in sensory neurons. *J Neurophysiol* **107**, 3227–3234 (2012).
45. Wells, J., Konrad, P., Kao, C., Duco Jansen, E. & Mahadevan-Jansen, A. Pulsed laser versus electrical energy for peripheral nerve stimulation. *J Neurosci Methods* **163**, 326–337 (2007).
46. Cayce, J. M. *et al.* Infrared neural stimulation of human spinal nerve roots *in vivo*. *Neurophotonics* **2**, 015007 (2015).
47. Jenkins, M. W. *et al.* Optical pacing of the embryonic heart. *Nat Photonics* **4**, 623–626 (2010).
48. Izzo, A., Richter, C., Jansen, E. D. & Walsh, J. Laser stimulation of the auditory nerve. *Lasers Surg Med* **38**, 745–753 (2006).
49. Duke, A. R. *et al.* Transient and selective suppression of neural activity with infrared light. *Sci Rep* **3**, 2600 (2013).

50. Jenkins, M. W. *et al.* Optical pacing of the adult rabbit heart. *Biomed Opt Express* **4**, 1626–1635 (2013).
51. Mahadevan-Jansen, A. *et al.* Imaging optically induced neural activity in the brain. *Conf Proc IEEE Eng Med Biol Soc* **2010**, 3379–3381 (2010).
52. Hodgkin, A. L. & Katz, B. the Effect of Temperature on the Electrical Activity of the Giant Axon of the Squid. *J. Physiol. (1949) Lucas Gasser Schoepfle & Erlanger Cardot & Arvanitaki* **09**, 240–249 (1949).
53. Huxley, A. Ion Movements During Nerve Activity. *Ann N Y Acad Sci* **81**, 221–246 (1959).
54. Zongxia Mou, Z., Triantis, I. F., Woods, V. M., Toumazou, C. & Nikolic, K. A Simulation Study of the Combined Thermoelectric Extracellular Stimulation of the Sciatic Nerve of the *Xenopus Laevis*: The Localized Transient Heat Block. *IEEE Trans Biomed Eng* **59**, 1758–1769 (2012).
55. Lothet, E. H. *et al.* Selective inhibition of small-diameter axons using infrared light. *Sci Rep* **7**, (2017).
56. Ganguly, M., Jenkins, M. W., Chiel, H. J. & Jansen, E. D. Modeling the effects of elevated temperatures on action potential propagation in unmyelinated axons. in *Proc. SPIE 9690, Clinical and Translational Neurophotonics 96901O1-96901O7* (2016).
57. Regasa, L., Agimi, Y., Trauma, K. S.-T. J. of H. Traumatic brain injury following military deployment: evaluation of diagnosis and cause of injury. (2019)
58. Kerr, A. G., Byrne, J. E. T., Concussive effects of bomb blast on the ear. *J Laryngol Oto.* (1975)
59. Bandak, F., *et al.* Injury biomechanics, neuropathology, and simplified physics of explosive blast and impact mild traumatic brain injury. *Handb. Clin. Neurol.* (2015)

60. Bryden, D. W., Tilghman, J. I. & Hinds, S. R. Blast-Related Traumatic Brain Injury: Current Concepts and Research Considerations. *J Exp Neurosci* **13**, (2019).
61. Schimmel, S. J., Acosta, S. & Lozano, D. Neuroinflammation in traumatic brain injury: A chronic response to an acute injury. *Brain Circ* **3**, 135 (2017).
62. Hernandez-Ontiveros, D. G. *et al.* Microglia activation as a biomarker for traumatic brain injury. *Front Neurol* **4**, (2013).
63. Bazzigaluppi, P., Dufour, S. & Carlen, P. L. Wide field fluorescent imaging of extracellular spatiotemporal potassium dynamics in vivo. *NeuroImage* (2015)
64. Rimmele, T. S. & Chatton, J.-Y. A Novel Optical Intracellular Imaging Approach for Potassium Dynamics in Astrocytes. *PLoS One* **9**, e109243 (2014).
65. Cayce, J. M. *et al.* Calcium imaging of infrared-stimulated activity in rodent brain. *Cell Calcium* **55**, 183–190 (2014).
66. Hale, G. M. & Querry, M. R. Optical Constants of Water in the 200-nm to 200- $\mu$ m Wavelength Region. *Applied Optics, Vol. 12, Issue 3, pp. 555-563* **12**, 555–563 (1973).
67. Welch, A. & Gemert, M. van. *Optical-thermal response of laser-irradiated tissue*. (2011).
68. Biomarkers of Neuroinflammation: Proceedings of a Workshop. *Biomarkers of Neuroinflammation* (2017)
69. Nakagawa, A. *et al.* Mechanisms of primary blast-induced traumatic brain injury: Insights from shock-wave research. *J Neurotrauma* **28**, 1101–1119 (2011).
70. Simon, D. W. *et al.* The far-reaching scope of neuroinflammation after traumatic brain injury. *Nature Reviews Neurology* 2017 13:3 **13**, 171–191 (2017).

71. Sabramaniam S. T. & Federoff H. J. Targeting Microglia activation States as a Therapeutic Avenue in Parkinson's Disease. *Frontiers in Aging Neuroscience* **9**, (2017).
72. Van Gemert M. J. & Welch A.J. *Clinical Use of Laser-Tissue Interactions* **10**, (1989).

## Chapter III

### **Pulsed Infrared light modulates inflammatory precursors; reducing pro-inflammatory cytokine release, stimulating intracellular calcium transients, and altering ligand-receptor binding in microglia-like BV2 cells**

J. Logan Jenkins<sup>1,2,3,4</sup>, Sam Evans<sup>3,4</sup>, Wilson Adams<sup>1,2</sup>, Anita Mahadevan-Jansen<sup>1,2</sup>, Mark R. Hutchinson<sup>3,4</sup>, E. Duco Jansen<sup>1,2</sup>

<sup>1</sup>Department of Biomedical Engineering, Vanderbilt University, Nashville, TN, USA

<sup>2</sup>Vanderbilt Biophotonics Center, Vanderbilt University, Nashville, TN, USA

<sup>3</sup>Neuroimmunopharmacology Laboratory, School of Biomedicine, University of Adelaide, Adelaide, SA, AUS

<sup>4</sup>ARC Centre of Excellence for Nanoscale BioPhotonics, Adelaide, SA, AUS

### 3.1 Abstract

The prevalence of chronic pain has led to the opioid pandemic, in which 3-4% of the adult US population has been treated with long-term opioid therapy. In search of non-addictive, non-pharmacological treatments of chronic pain, infrared neural inhibition uses pulsed infrared light to block the propagation of neuronal pain signals and has emerged as a promising neurotechnology, yet its impact on non-neuronal cells in the central nervous system has not been explored. This study uses calcium imaging, thermal imaging, and pro-inflammatory cytokine ELISA assays to determine the effects of pulsed infrared light exposure on BV2 cells, an immortalized microglia-like cell line. Pulsed infrared light and its induced temperature rise were found to modulate ligand-receptor activation, induces multiple, unique intracellular calcium transient phenotypes, and reduce the release of a pro-inflammatory cytokine in response to an innate immune danger signal. This work reveals the potential utility of pulsed infrared light to intervene in the molecular origins of chronic pain while also providing disease modification through targeting pro-inflammatory immune signaling.

### 3.2 Introduction

About 20% of US adults suffer from chronic pain and 8% have high-impact chronic pain; defined as chronic pain that frequently limits life or work activities. It is associated with dependence on opioids, anxiety and depression, restrictions in mobility, and reduced quality of life.<sup>1,2</sup> In the U.S., A deeper look into chronic pain unveils a higher prevalence among women, older adults, rural residents, and adults with public health insurance.<sup>3</sup> Approximately 3% to 4% of the adult US population was treated with long-term opioid therapy for pain in the late 2000's.<sup>4</sup> The abuse, addiction, and overdose risks of opioids have been well documented<sup>5-7</sup> and there is a need for non-addictive treatments for pain.<sup>8</sup>

Non-pharmacological treatments for chronic pain are currently available with the most well-known medical device technologies being electrical stimulation (REF). Transcutaneous or implanted electrical stimulation, such as spinal cord stimulation, can provide temporary pain relief, but suffers from poor spatial specificity often resulting in undesirable side effects on the autonomic nervous system<sup>9</sup> and lead migration<sup>10</sup>. Infrared neural inhibition (INI) has emerged as a promising technique that overcomes some of the shortcomings of electrical stimulation for pain relief indications.<sup>11-13</sup> INI uses pulsed infrared light (IR) to cause a non-damaging, temperature increase at the neuronal level to block the propagation of pain signals from being perceived. INI has advantages in inhibitory selectivity, both spatial due to the tight confinement of light and to the inherent nature of INI to preferentially block small diameter axons, such as c-fibers; critical nociceptive neurons.<sup>14</sup> These techniques, along with most other neuromodulation approaches, are only known to target the symptoms of pain and do not affect the potential underlying causes of pain. Importantly, molecular targets for INI have been identified, such as the transient receptor

potential cation channel subfamily V member 1 (TRPV1) channel<sup>15</sup>, which is also mechanistically linked to the chronification of pain.<sup>16,17</sup>

The process by which the acute pain experience, whether through nociceptive, neuropathic, or via other central origins, becomes a chronic pain experience, can involve complex structural cellular and molecular adaptations associated with central sensitization.<sup>18,19</sup> Pro-inflammatory immune signaling and its associated cellular adaptations are thought to be a critical driver of the chronification of pain that leads to its amplification and maintenance.<sup>20</sup> Classical inflammation is beneficial in acute injury and acute pain experience can engage critical healing events in the periphery. However, if these events persist or drive maladaptive processes then central sensitization can lead to long lived and unwanted hyperalgesia and allodynia. It is important to distinguish these pro-inflammatory immune signaling events associated with the persistence of pain as distinct from states where neuroinflammation abounds. Whilst the glial immune signaling associated with the persistence of pain may include changes in vascular permeability, enhanced reactivity of glial cells, and production of inflammatory mediators like cytokines and chemokines, these events do not occur to the extremes seen in neurodegenerative conditions, and as such have been recently referred to as parainflammation.<sup>21</sup> Therefore, intervention strategies that are capable of curbing the production of inflammatory mediators like cytokines and chemokines implicated in chronic pain is seen as a promising method to modify the chronic pain disease trajectory.

Microglia, the innate immune cell of the central nervous system, are the first responders to many neuronally-derived mediators, such as chemokines, ATP, and endogenous danger signals. Microglia transition from a basal state to a state of reactive gliosis once such signals are detected, which triggers the release of cytokines, chemokines, damage-associated molecular patterns (DAMPs), and inflammatory mediators.<sup>22,23</sup> This process can be initiated by the binding of

endogenous factors, like damaged neuronal components, to Toll-like receptors (TLRs). Of specific relevance to chronic pain, TLR4 has been associated with microglial reactivity and mechanistically implicated in the nociceptive hypersensitivity after peripheral nerve injury.<sup>24,25</sup> Activation of TLR4 signaling through the formation of the functional heterodimer complex, initiates a wide range of intracellular signaling pathways, including MAPK, p38, JNK, and activation of transcription factors, like Nuclear Factor- $\kappa$ B (NF- $\kappa$ B).<sup>26</sup> NF- $\kappa$ B is a critical transcription factor for pro-inflammatory cytokine transcription and the subsequent translation and release of pro-inflammatory mediators such as the cytokines interleukin-1 $\beta$  (IL-1 $\beta$ ) and interleukin-6 (IL-6). Intracellular calcium transients are directly involved in TLR4-based signaling pathways as calcium entry is necessary for NF- $\kappa$ B activation and initiates the release of intracellular calcium stores from the endoplasmic reticulum.<sup>27,28</sup> Of note, several other ion channel classes are involved in the creation and propagation of a glial reactivity state, including the heat and pain sensors like the TRPV1 channel.

Given the importance of glial signals in chronic pain and the mechanistically common molecular targets of INI it is critical to determine the wider non-neuronal actions of INI. Therefore, the aim of this study is to better understand the effects of pulsed infrared light on microglial function in order to explore how infrared neural inhibition might act on the diversity of cell types within the central nervous system. Since the innate immune driven pro-inflammatory signaling response of microglia is a driver of chronic pain states, this study sought to quantify the effects of pulsed IR on the pro-inflammatory cytokine production pathway. This will be accomplished through a probing of the complete pathway from 1) ligand-binding immune response initiation, 2) to the induced calcium transients that signals for physiological changes, and 3) the release of pro-inflammatory cytokines.

### 3.3 Methods

#### 3.3.1 Cell culture

##### 3.3.1.1 Innate immune receptor level signaling experiments

HEK293 (HEK) cell lines were maintained in Dulbecco's modified Eagle's medium (Gibco, Waltham, MA, USA) supplemented with 10% (v/v) fetal bovine serum and 2 mM l-glutamine, 50 U/ml penicillin, 50 µg/ml streptomycin. Cells were grown in a humidified incubator of 95% /5% Air/CO<sub>2</sub> at 37°C. Cells were transfected with TLR4 and TRPV1 transmembrane channels. The cells were plated in black-walled, clear-bottomed, half-area 96-well plates (Corning, Corning, NY, USA) at 20,000 cells/well. TRPV1 agonist 500 nM capsaicin (Cap) was added to the sample media during plate-reader calcium imaging to stimulate an intracellular calcium response, of relevance to both pain and the thermal INI stimulus. TRPV1 antagonist capsazepine (CPZ) was added 5 minutes prior to pulsed IR exposure to block the impact of pulsed IR and Cap exposures on TRPV1 calcium signaling.

##### 3.3.1.2 Microglia-like BV2 cellular responses

An immortalized, microglia-like cell line, BV2, was maintained in Dulbecco's modified Eagle's medium supplemented with 10% (v/v) fetal bovine serum and 2 mM l-glutamine, 50 U/ml penicillin, 50 µg/ml streptomycin, and 100 µg/ml Normocin. Cells were grown in a humidified incubator of 95% air/5% CO<sub>2</sub> at 37°C. The cells were plated in black-walled, clear-bottomed, half-area 96-well plates at 20,000 cells/well for ELISA assay experiments to quantify released pro-inflammatory cytokine interleukin-6. In a subset of ELISA assay experiments, lipopolysaccharide (LPS, 100ng/mL) was used to stimulate an immune response. For single cell analysis using calcium imaging, BV2 cells were plated in poly-D-lysine coated 35mm dishes with a 14mm glass bottom (Mattek, Ashland, MA) 24 hours prior to imaging.

### 3.3.2 in vitro pulsed infrared laser approach and parameters

Pulsed infrared laser light at 1875 nm from a pulsed diode laser (Capella, Lockheed Martin Aculight, Bothell, WA, USA) was delivered to BV2 during live calcium imaging via a 400  $\mu\text{m}$  optical fiber. A micromanipulator (Sutter Instruments, Novato, CA, USA) was used for precise positioning of the optical fiber to the layers of cells. The optical fiber face was at a 45° angle to the cell-coverslip plane and the center of the optical fiber was about 230  $\mu\text{m}$  away from the cell surface. Monte Carlo modelling suggests that the spot size of the light doubles from the fiber face to the coverslip at these distances, therefore reducing the radiant exposure by 50%. A further 30% reduction in the radiant exposure is due to water absorption prior to light reaching the cells. For experiments using 35mm imaging dishes (Figures 3.4-2, 3.4-3, 3.4-4, and 3.4-6), pulse trains at 250  $\mu\text{s}$  pulse widths, 200 Hz, and 60 s train length were used at radiant exposures up to 1500 J/cm<sup>2</sup> over the entire pulse train. In experiments where half-area 96 well plates were used (Figures 3.4-1 and 3.4-5) pulsed IR was delivered from a 600  $\mu\text{m}$  fiber from below the HEK or BV2 samples through clear-bottoms of the wells. The fiber was positioned at a distance of 1.4 cm away to expose the entire surface of the well to pulsed IR. Laser pulse parameters used in these experiments differed from the imaging experiments. IR light was delivered at 1.1 W/cm<sup>2</sup> for 20 to 80 seconds resulting in radiant exposures from 22 to 88 J/cm<sup>2</sup>.

### 3.3.3 ELISA assay

The black-walled, clear-bottomed, half-area 96-well ELISA microplates (BD Bioscience, San Jose, CA, USA) were coated with 1  $\mu\text{g}/\text{mL}$  poly-D-lysine prior to BV2 seeding. BV2 cells were taken out of the incubator and exposed to pulsed IR one well at a time. Immediately after exposure, media was added to wells with or without lipopolysaccharide (LPS), a component of bacteria cell walls that initiate the immune response. The cells were then incubated for 4 hours

before supernatant was collected and frozen. Mouse interleukin-6 ELISA assays (GIBCO, Waltham, MA, USA) were used to measure IL-6 concentration. The ELISA protocol used was provided by the company with the following alterations: standard curve IL-6 concentrations range from 1000 pg/mL to 7.8 pg/mL and dilution factor of ½ was used.

### 3.3.4 Fluorescence Imaging

#### 3.3.4.1 HEK Calcium Fluorescence Imaging

HEK cells were loaded with fluorescent calcium indicator, Fluo 4-AM (5µM), for 45 minutes at 37°C prior to imaging. Pulsed IR light was delivered from below the half-area, 96 well plates to expose all the cells within the well 5-15 minutes prior to imaging. Loaded HEK cells were imaged for 35 seconds per well using a heated plate reader to determine intracellular calcium changes due to pulsed IR.

#### 3.3.4.2 BV2 Calcium Fluorescence Imaging

Changes in intracellular calcium concentration of BV2 cells were monitored by calcium imaging using the single-wavelength calcium indicator Fluo-4-AM (Life Technologies, Carlsbad, CA, USA). Experiments were performed 24 hours after BV2 seeding. BV2 cells were incubated at 37 °C for 30 minutes to 1 hour with Fluo-4-AM (3 µM) dissolved in flurobrite solution (GIBCO, Waltham, MA, USA). Measurements of intracellular calcium were performed by using an epifluorescence micro-scope (Nikon Eclipse Ti-S) equipped with long-distance dry objective (20x, 0.4NA) and standard filters for GFP fluorescence. The excitation wavelength was 470 nm, filtered from a broadband LED light source. Data acquisition was controlled by NIS Elements (Nikon Imaging Systems, Toyko, Japan).

### 3.3.4.3 Cell Viability Fluorescence Imaging

Necrosis and apoptosis stains were used to determine the viability of the cell cultures during calcium imaging. Two fluorescent probes were used to better understand the impact of temperature rise on the BV2s in the 35mm imaging dish setup of Figure 3.4-2. 1  $\mu$ M Propidium Iodide (Invitrogen, Waltham, MA, USA) and 5 $\mu$ M Biotracker NucView 405 blue Caspase-3 dye (Biotium, Fremont, CA, USA) were added to the imaging solution prior to pulsed IR exposure. Cells were imaged immediately before laser exposure and 40 minutes after exposure to track changes in necrosis and apoptosis.

After collection of the supernatant from half-area, 96 well plates for cytokine quantification via ELISA assay, an MTT assay was used to determine cellular metabolic activity, and therefore cell viability. Cells were incubated with the dye at 37°C for 4 hours prior to solubilization and collection. The solution was then imaged with a microplate reader to determine absorbance.

### 3.3.5 Thermal Measurements

A FLIR SC8300-series high-speed indium-antimonide CCD camera equipped with a 4X germanium imaging objective (FLIR Systems Inc., Nashua, NH, USA) was used for all thermal imaging. Thermal emissivity was empirically derived for the optical path through the bottom a glass bottom dish. Imaging through aqueous liquid gives a penetration depth of about 10 $\mu$ m, making top imaging of imaging dish impractical in the aqueous environment. Thermal images matching the BV2 calcium imaging setup with 35mm imaging dishes were collected at 30 frames per second during pulsed IR exposure to create temperature maps over time.

Thermocouple measurements were taken with a fine wire type K thermocouple (Omega Engineering, Norwalk, CT, USA) connected to a DI-245 acquisition system (Dataq Instruments, Akron, OH, USA). The thermocouple was attached to a micromanipulator for precise placement

in the center of a half-area 96 well plate. Thermal measurements were collected at a frequency of 2000 Hz.

### 3.3.6 Data Analysis

Each calcium imaging recording was considered as n. Each experimental condition had a minimum of 5 different cell culture dishes from which calcium imaging recording were taken. A custom-written FIJI script was used, similar to Borrachero-Conejo and Adams et. al.<sup>15</sup>, to accelerate data extraction and analysis. MATLAB (Mathworks, Natick, MA, USA) was used for further analysis. Raw calcium imaging recording characteristics were extracted, including spatial position, spatial position relative to the delivery fiber, relative maximum change in fluorescence ( $\Delta F/F$ ), time to peak fluorescence, full-width half-maximum (FWHM). An imaging artifact due to defocusing of the imaging plane from the gradient heat was disregarded in the analysis. Calcium imaging recording consisted of 30 seconds of baseline activity before delivery of pulsed infrared light for 60 seconds and at least 3 minutes of post-exposure recordings. Each cell's raw fluorescence intensity was normalized with respect to the mean raw intensity of the 10 frames prior to pulsed IR exposure. Statistical comparison of metrics is performed with a 2-sided student's t test unless otherwise noted. Error bars reported are standard error of the mean (SEM) response between cells unless otherwise denoted.

### 3.4 Results

#### 3.4.1 Pulsed infrared light modulates intracellular calcium transients of TLR4-TRPV1 transfected HEK cells to capsaicin stimulus

To determine the effects of infrared light on subsequent stimulation of the TLR4-TRPV1 complex, TLR4 TRPV1 transfected HEK cells were exposed to pulsed IR prior to stimulation with TRPV1 agonist capsaicin while measuring intracellular calcium transients. TLR4 TRPV1 transfected HEK cells were pre-exposed with 0-88 J/cm<sup>2</sup> of pulsed infrared light from five to fifteen minutes prior to administration of 500 nM capsaicin at t=4.5 seconds (Figure 3.4-1).

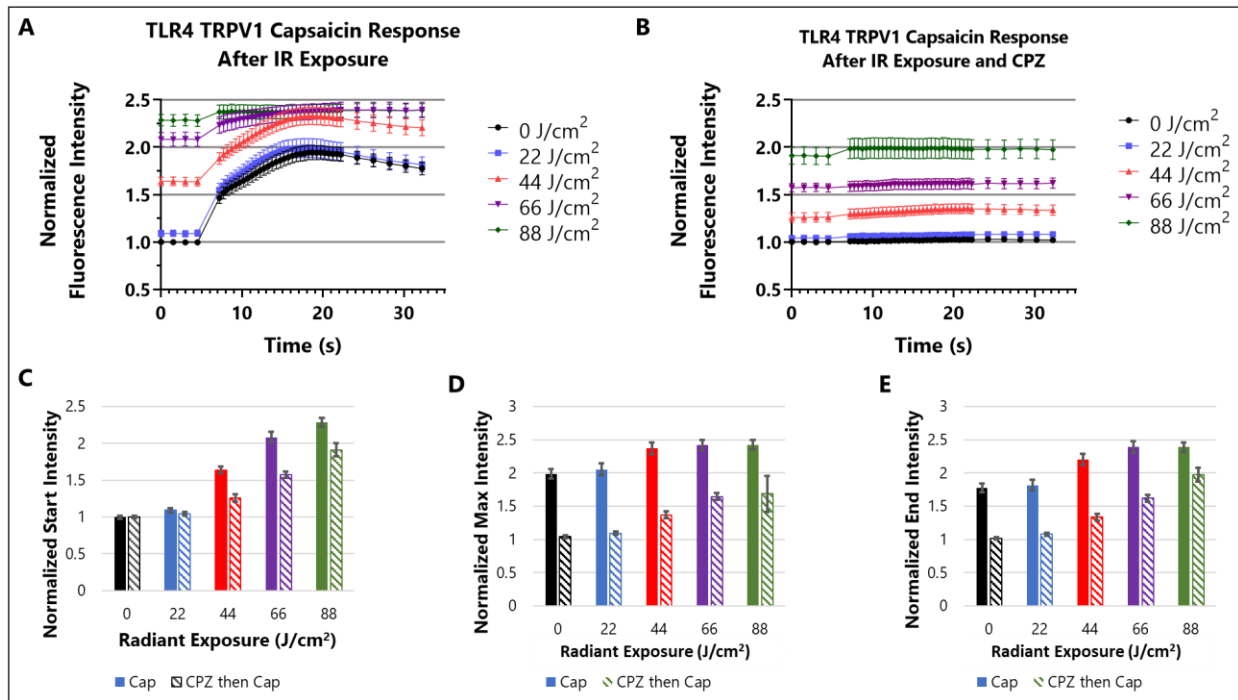


**Figure 3.4-1. Pulsed infrared light modulates intracellular calcium transients of TLR4 TRPV1 transfected HEK cells to stimulus.**

(A) TLR4-TRPV1 transfected HEK cells in half-area 96 well plates were pre-exposed with pulsed infrared light at varying radiant exposures 5-15 minutes prior to an injection of TRPV1 agonist, 500nM capsaicin (Cap) at t=4.5s to induce intracellular calcium transients (n=15). (B) TRPV1 antagonist, 10µM capsazepine (CPZ), was introduced before laser and Cap exposures (n=9). (C-E) Normalized fluorescent intensities from subfigures A (solid) and B (striped) of varying radiant exposures (C) before Cap, (D) at maximum intensity, (E) and at the end of the experiment.

Changes in the fluorescence intensity, normalized to the pre-capsaicin intensities of the 0 J/cm<sup>2</sup> control, were monitored over the course of 30 seconds post-exposure (Figure 3.4-1A). In the no

pulsed IR control, the addition of capsaicin increases the intracellular calcium signal by 100% within 15 seconds. The fluorescence signal then gradually declines for the remaining 20 seconds of the experiment. Increasing the radiant exposure increases the initial baseline of the calcium signal. Higher radiant exposures only slightly increase the maximum total intracellular calcium intensity after capsaicin stimulation. At radiant exposures at and above  $66 \text{ J/cm}^2$ , the fluorescence signal does not reduce throughout the experiment. When adding TRPV1 antagonist capsazepine (CPZ) prior to pulsed IR exposure, the addition of capsaicin does not increase the fluorescence intensity in all laser exposures used (Figure 3.4-1B). The initial baseline shift due to the pre-exposure of pulsed IR remains elevated in the presence of CPZ, but at lower totals than without CPZ (Figure 3.4-1C). The maximum intensity of calcium signal is lower when exposed to capsaicin in the presence of CPZ as compared to only Cap (Figure 3.4-1D). Lastly, the normalized end calcium intensities are lower in the presence of CPZ than only Cap (Figure 3.4-1E). Overall, TLR4-antagonist CPZ decreases but does not eliminate the baseline shift of calcium fluorescence due to prior pulsed IR exposure.

### 3.4.2 Pulsed infrared light induces multiple, distinct intracellular calcium transient phenotypes in BV2 cells

To understand how pulsed IR can alter microglial physiology and the pro-inflammatory cytokine production pathway, we employed calcium imaging of BV2 cells using an inverted widefield microscope (Figure 3.4-2A). As discussed, intracellular calcium transients are a broad indicator of physiological changes occurring within the cell. One pathway that is critical for pro-inflammatory cytokine production associated with chronic pain is via TLR4 signaling activation. During pulse IR exposure, a thermal lensing imaging artifact is present that makes interpretations difficult during this time, overlaid with red (Figure 3.4-2C).

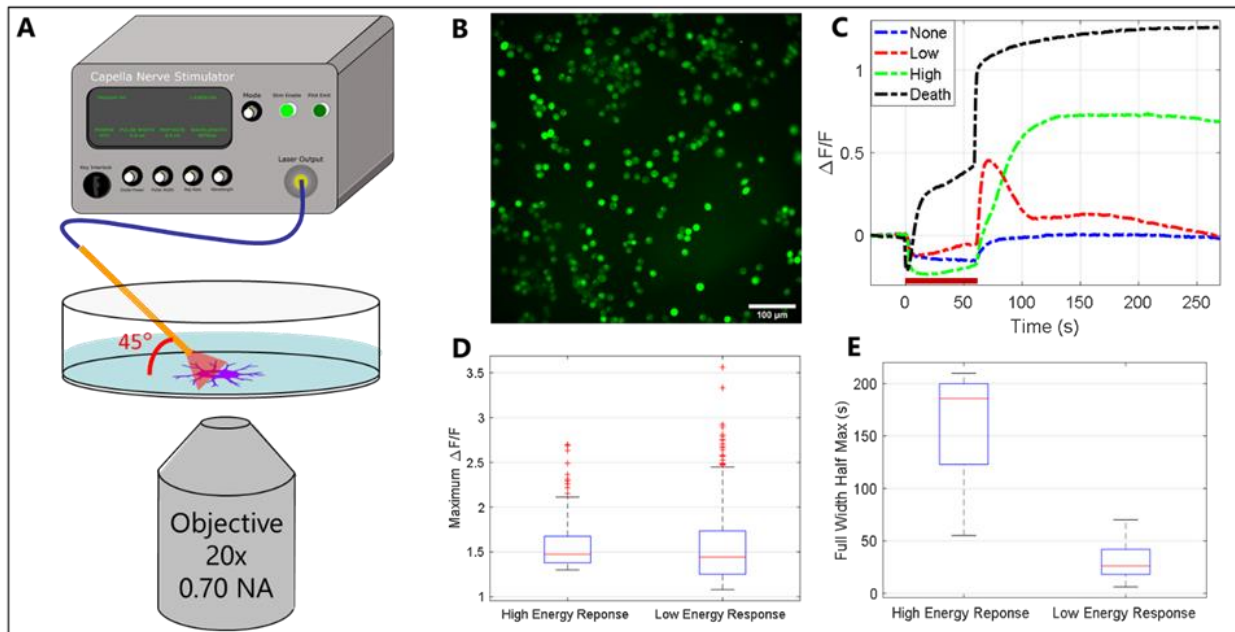


**Figure 3.4-2. Pulsed infrared light induces intracellular calcium transients in microglia in vitro.**

(A) Illustration of imaging setup used to measure intracellular calcium transients in microglia. A 400µm optical fiber delivered the infrared light at 45° angle to the bottom of the imaging dish. (B) Maximum intensity projection of microglia stained with calcium indicator, Fluo-4 AM, and exposed to pulsed infrared light. (C) Representative calcium transient characteristics induced during varying radiant exposures of 180 J/cm<sup>2</sup> to 1410 J/cm<sup>2</sup> for 60 seconds (dark red bar). The calcium transient phenotypes are defined by less than a 10% change in fluorescence intensity over initial fluorescence intensity ( $\Delta F/F$ ) after the laser exposure compared to before laser exposure (“None” response, blue), a greater than 10%  $\Delta F/F$  immediately after laser exposure and the fluorescence intensity reducing to baseline within 80 seconds (“low energy” response, red), a greater than 30%  $\Delta F/F$  that remains elevated for at least 200 seconds (“high energy” response, green), and a sharp increase in  $\Delta F/F$  before total laser exposure is delivered and remains elevated for over 200 seconds (“Death” response, black). (D) Box and whisker plot of the maximum  $\Delta F/F$  of cells categorized as “high energy” response or “low energy” response. (E) Box and whisker plot of the calcium increase duration via the full width half max of cells categorized as “high energy” response or “low energy” response.

Images of BV2 cells were taken at one frame per second (Figure 3.4-2B). BV2 cells presented unique calcium transient phenotypes, defined as “none”, “low energy”, “high energy”, and “death”, as determined by the percent change in fluorescence over time. (Figure 3.4-2C) To better characterize the responses of BV2 cells to pulsed infrared light, BV2 calcium responses, both amplitude and full-width half-max duration, were quantified (Figures 3.4-2D-E). While both the “low energy” and “high energy” calcium transient phenotypes have a similar maximum increase in  $\Delta F/F$ , the full-width half-max duration is the main differentiator of the signal subtypes. For the “high energy” exposure, the response remaining elevated for the entirety of the experiment in most cases, while for the “low energy” exposures, the response remained elevated for an average of 30

seconds. Also shown in Figure 3.4-2C, are the “no response” and “death response” of BV2 cells. In the “no response” calcium transient phenotype, there is a decrease in signal during the duration of the IR light pulse train. This decrease has been determined to be an artifact due the gradient heating of the environment (thermal lensing), which in turn defocuses the imaging system off the cells. This area of the response-time curve is more qualitative than quantitative due the imaging artifact. The “death” calcium transient phenotype is unique to the “high energy” and “low energy” responses in that the calcium transient initiates very early in the pulse train and stays elevated for the duration of the experiment.

### 3.4.3 Temperature rise from pulsed infrared light during fluorescent imaging

The current understanding is that infrared neural inhibition is due to the photothermal effects of pulsed infrared light.<sup>12</sup> To understand how pulsed IR is converted into heat, a full characterization of the spatial, temporal temperature increase was performed under calcium imaging conditions. Using thermal imaging, the thermal field was characterized at multiple radiant exposures. The 400  $\mu\text{m}$  optical fiber was delivered at a 45° angle from the x-y plane into a 35 mm imaging dish, as demonstrated in Figure 3.4-2A.

Due to the incident angle of the optical fiber, the thermal map is nonconcentric. The maximum temperature rise map is instead ellipsoidal with an elongated heat gradient on the far side of the optical fiber (Figure 3.4-3A). A cross section through the hottest point and parallel to the y axis shows a symmetrical temperature gradient on either side of the maximum. (Figure 3.4-3B) A cross-section through hottest point and parallel to the x axis shows a sharper gradient nearer the optical fiber and an elongated temperature gradient opposite the fiber. (Figure 3.4-3C) The large field of view during calcium imaging allows for a nonuniform thermal map at the cell level. The temperature rise over the duration of the pulse train shows a quick rise in temperature followed by

a steady state temperature for vast majority of the pulse train. This is followed by a sharp decrease after the pulse train ends at the hottest point. Different radiant exposures produce different maximum temperature rises. With the highest radiant exposure of  $714 \text{ J/cm}^2$  producing a maximum temperature rise of approximately  $30 \text{ }^\circ\text{C}$  from a starting temperature of  $20 \text{ }^\circ\text{C}$ . (Figure 3.4-3D)

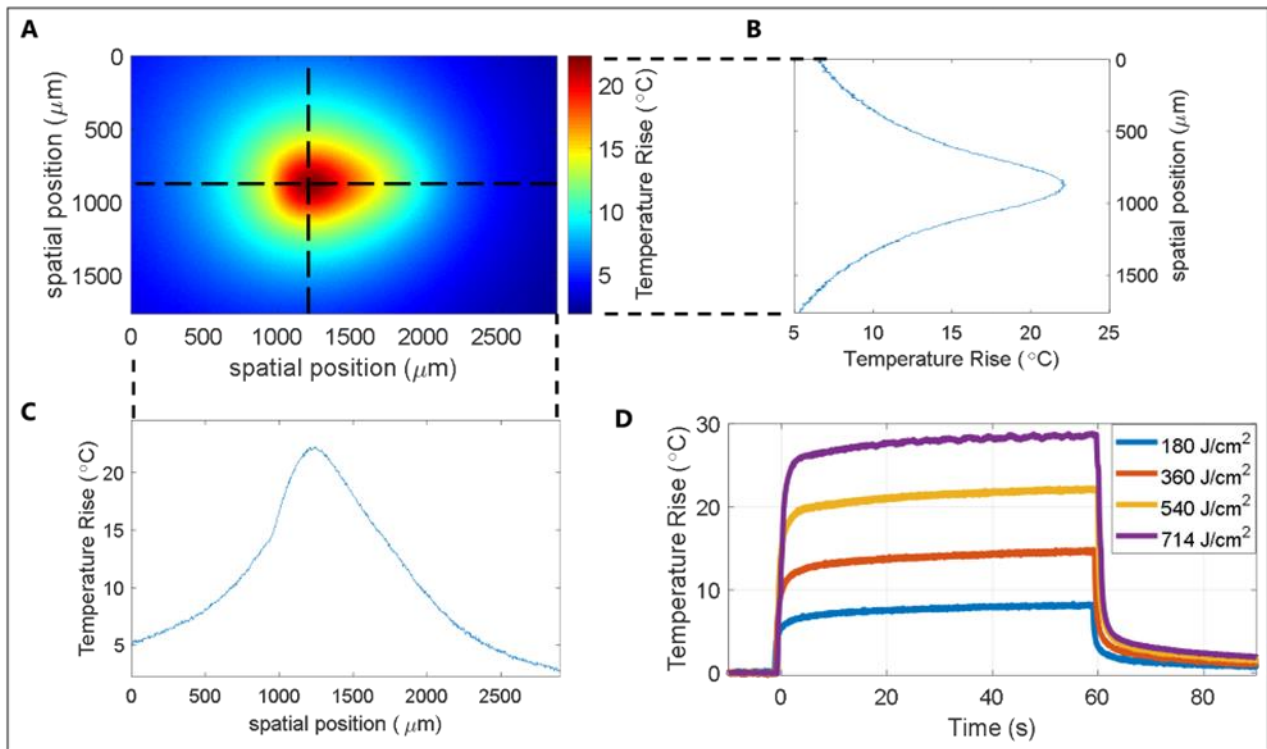


**Figure 3.4-3. Temperature rise of pulsed infrared light during fluorescent imaging.**

(A) Thermal image of the temperature rise in imaging dishes due to  $540 \text{ J/cm}^2$  over 60 seconds delivered via a  $400\mu\text{m}$  fiber at a  $45^\circ$  angle. (B) Temperature rise along a vertical line through the maximum temperature rise point in sub-figure A. (C) Temperature rise along a horizontal line through the maximum temperature rise point in sub-figure A. (D) Temperature rise through the hottest point during the 60 second light exposure at varying radiant exposures.

### 3.4.4 Distinct calcium transients are associated with different temperature rises.

As shown in Figure 3.4-2, multiple, distinct calcium transient phenotypes are initiated at varying radiant exposures. A spatial patterning of the calcium transients emerged in the images where cells more central to the optical fiber would produce a “high energy” calcium transient, while peripheral cells would produce a “low energy” response. To determine the differences in temperature rises between these subtypes of calcium responses, the empirically derived

temperature maps shown in Figure 3.4-3 were overlaid onto each calcium image described in Figure 3.4-2. This method was used to correlate the maximum temperature each cell experienced to the associated calcium transients (Figure 3.4-4A). Fiducial markers within the field of view of both thermal and calcium images were used for image registration.

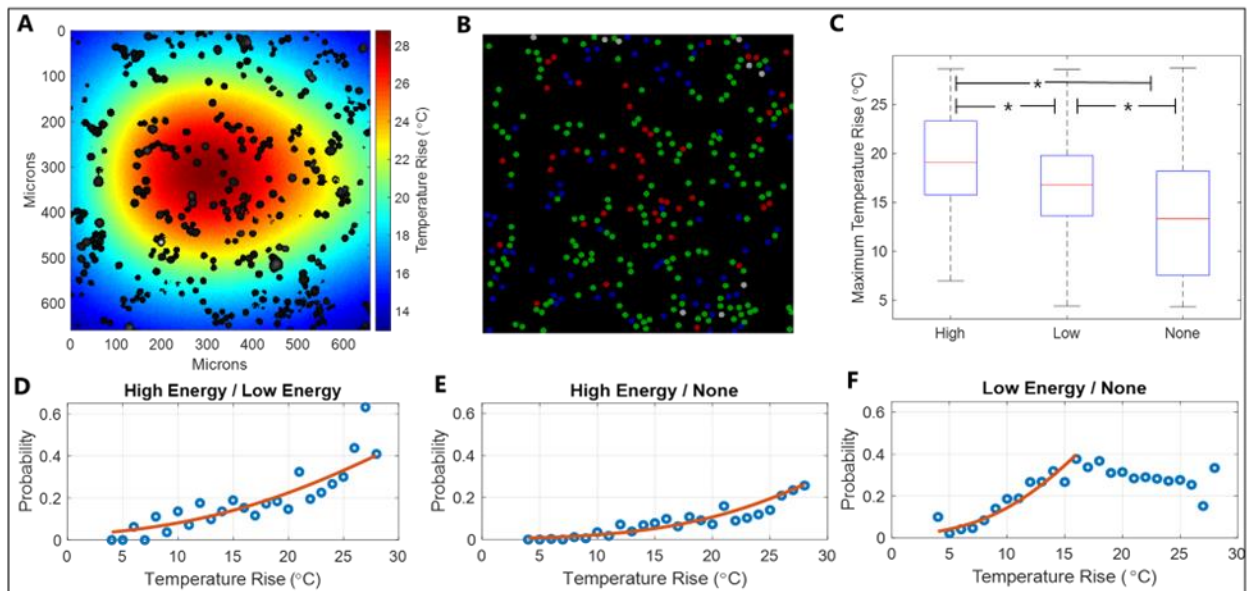


**Figure 3.4-4. Distinct calcium transients are associated with different temperature rises.**

(A) Overlay of BV2 (black) on the temperature rise map (color) after co-registration. (B) Map of calcium transient responses of microglia in sub-figure 4A (red: high energy response, blue: low energy response, green: no response). (C) Box and whisker plot of the maximum temperature rise of each BV2 cell and their associated intracellular calcium responses (Wilcox rank sum,  $p < 0.001$ , high: average temperature rise =  $19.4^{\circ}\text{C}$ ,  $n = 300$  cells, low: average temperature rise =  $16.7^{\circ}\text{C}$ ,  $n = 1200$  cells, none: average temperature rise =  $13.1^{\circ}\text{C}$ ,  $n = 3000$  cells). (D-F) PROBIT analysis of the probability a cell will respond as (D) high energy response instead of low energy response, (E) high energy response instead of no response, or (F) low response instead of no response given a maximum temperature rise over 60 seconds. Best fit lines in red.

After image registration, representative calcium images with cells overlaid using different colors corresponding to different cell response phenotypes (green: no response, blue: low response, red: high response, Figure 3.4-4B). The average temperature rise needed to induce a response for each cell was extracted using the above method. BV2 cells required a temperature rise of  $19.4^{\circ}\text{C}$  to generate a “high energy response”,  $16.7^{\circ}\text{C}$  to generate a “low energy response”, and cells with an average temperature rise  $13.1^{\circ}\text{C}$  did not exhibit a calcium response. (Figure 3.4-4C) To better

understand the relationship between these different responses, PROBIT analyses were used between two groups from each response giving the predictability of having a cell exhibit a certain response at a certain temperature rise. This analysis was performed for each “high energy” vs “low energy”, “high energy” vs “none”, and “low energy” vs “none” (Figure 3.4-4 D, E, F). Notably, neither the “low energy response” nor “high energy response” are present in over 50% of the total cells.

#### 3.4.5 Pulsed infrared light reduces pro-inflammatory cytokine release *in vitro*.

A major role of microglia in the chronification of pain is the initiation of glial reactivity and the release of pro-inflammatory cytokines. Interleukin-6 (IL-6) is a pro-inflammatory cytokine that is produced in both humans and rodent models. It can be dysregulated and/or continually synthesized in response to danger signals that leads to a cycle of neuroinflammation.<sup>29</sup>. To better understand the direct impact of IR light on the release of a pro-inflammatory cytokine, IL-6 concentrations were measured using ELISA assays after exposure to pulsed IR light.

In the basal state BV2 cells with only vehicle (no LPS) and pulsed IR light, there is no significant change in normalized IL-6 concentrations as radiant exposure is increased up to 88 J/cm<sup>2</sup>. When LPS is added immediately post-exposure, the normalized concentration of IL-6 is gradually reduced starting at 44 J/cm<sup>2</sup> to 80% and to just 5% at 88 J/cm<sup>2</sup>. (Figure 3.4-5A) All experiments were normalized to the non-irradiated control in each microplate. The temperature rise is substantially different in the 100 µL of half-area, 96 well plates in comparison to the 2 mL of media in 35 mm imaging dishes. For this reason, the thermal characteristics are very different between the two setups. The maximum temperature rise is as low as 9 °C using 5 J/cm<sup>2</sup> and as high as 27 °C using 88 J/cm<sup>2</sup>. (Figure 3.4-5B) The maximum temperature rise is measured at the center of the well. Using a MTT assay, cell viability was measured for each radiant exposure used

on the same batch of cells from Figure 3.4-5A. Cell viability reduces slightly beginning at 66 J/cm<sup>2</sup> to 93% and continues to decline to 79% at the 88 J/cm<sup>2</sup>. The cells that were unable to metabolize MTT were concentrated at the center of the wells which corresponds with the hottest points within the well due to the Gaussian distribution of light out of the fiber. (Figure 3.4-5C)

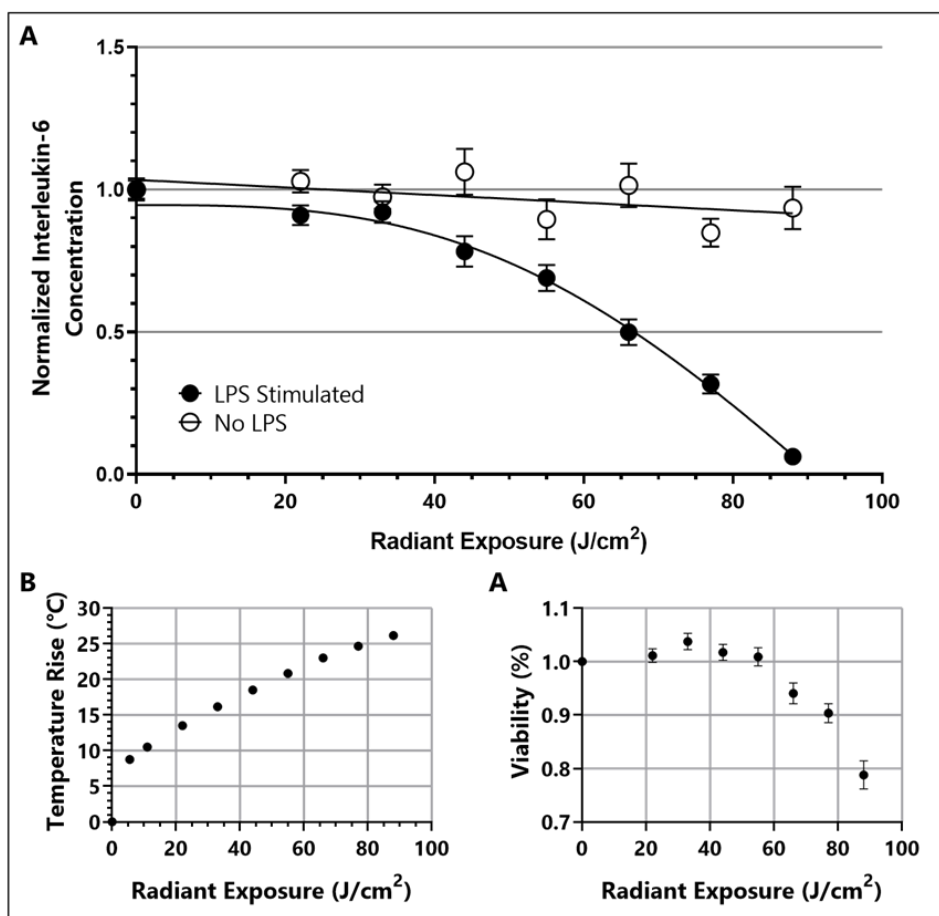


**Figure 3.4-5. Pulsed infrared light reduces pro-inflammatory cytokine release in vitro.**

(A) ELISA assays measured released concentrations of pro-inflammatory cytokine, interleukin-6 (IL-6) in BV2 cell culture after exposure to varying radiant exposures and subsequent injection of 100 ng/mL lipopolysaccharide (LPS, solid circle) or vehicle (hollow circle) and incubated for 4 hours. (LPS experiments: n=21 wells, No LPS experiments: n=15 wells). (B) Maximum temperature rise within the half-area 96 well plate wells at varying radiant exposure. (C) Viability of BV2 cell cultures after infrared light exposure and incubation as measured by colorimetric MTT assay (n=36 wells).

### 3.4.6 Pulsed infrared light does not induce early apoptosis or necrosis at temperature rises needed for intracellular calcium transients

Temperature rise above a few degrees Celsius will carry a concern about negative effects to cell health. Therefore, necrosis and apoptosis were measured to understand the effects that pulsed IR and the associated temperature rise have on BV2 cells within the calcium imaging setup.

Experiments were performed to collect calcium, PI, and Caspase-3 data within the same cell population to correlate immediate calcium transients to later cell death events. The necrosis and apoptosis indicators were only up taken at radiant exposures twice as high as radiant exposures needed to induce intracellular calcium transients. Radiant exposures needed to induce cell death of  $1410 \text{ J/cm}^2$  correlated to a maximum temperature rises of  $35 \text{ }^\circ\text{C}$  to  $42 \text{ }^\circ\text{C}$ . In this high radiant exposure case, the calcium dye (Figure 3.4-6A), caspase-3 dye (Figure 3.4-6B), and propidium iodine (Figure 3.4-6C) are shown. The caspase-3 and PI dyes were taken up around the hottest point of temperature rise near the point of maximum temperature rise. A PROBIT analysis of the probability of cell death, either necrosis or apoptosis at a given temperature and the resulting s-curve shows a 50% chance of cell death and apoptosis at maximum temperature rises of  $38 \text{ }^\circ\text{C}$  (Figure 3.4-6D).

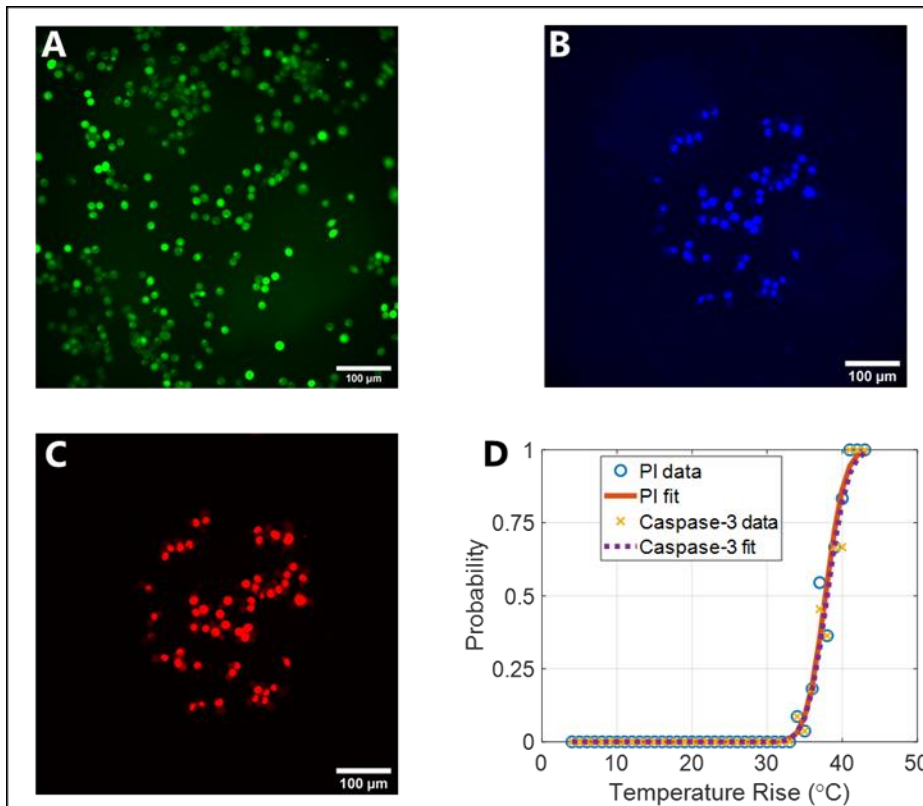


**Figure 3.4-6. Pulsed infrared light does not induce early apoptosis or cell death.**

(A) Fluorescence image of microglia with calcium indicator, Fluo-4 AM. (B) Image of microglia stained with early apoptosis maker, caspase-3, 40 minutes after exposure to  $1410 \text{ J/cm}^2$  of pulsed infrared light over 60 seconds. (C) Image of microglia stained with cell death marker, propidium iodide, 40 minutes after exposure to  $1410 \text{ J/cm}^2$  of pulsed infrared light over 60 seconds. (D). PROBIT analysis of the probability a cell will uptake early apoptosis or cell death markers at a given temperature rise.

### 3.5 Discussion

The purpose of this study was to uncover how the innate immune receptor signaling pathway from initiation to cytokine release was impacted by pulsed infrared light parameters similar to those used in infrared neural inhibition. The results showed that pulsed IR modulates the calcium response from subsequent capsaicin-TRPV1 binding in HEK cells and the antagonist CPZ partially reduces the initial baseline shift from IR exposure. Real-time calcium imaging of BV2 cells uncovered multiple, distinct calcium transient phenotypes induced by pulsed IR that vary in  $\Delta F/F$  and duration of calcium changes. Importantly, the heating profile from nonuniform laser exposure was fully characterized to map single cell calcium responses to temperature changes. This uncovered significant differences in temperature rise associated with each distinct calcium transient phenotype, creating a within-dish controlled variable. PROBIT analyses indicated that only a subset of the BV2 population respond to pulsed IR exposure. Basal BV2 cell IL-6 cytokine release was not impacted by IR. However, BV2 cell LPS-stimulated IL-6 cytokine release was significantly reduced by pulsed IR exposure. The BV2 cell viability was reduced 10% at 77 J/cm<sup>2</sup>, while the reduction in IL-6 cytokine release was ~70% at the same radiant exposure. Further cell health testing suggests that nearly twice the radiant exposure and temperature rise was needed to induce necrosis or apoptosis than to induce intracellular calcium transients. Therefore, it is sufficient to conclude that the effects on BV2 cell LPS-induced IL-6 release are not due to cell toxicity and may be linked to the pulsed IR heating effect, or other photo-bioeffects yet to be determined. Moreover, the necrosis and apoptosis pathways induced a specific calcium transient phenotype that is different than the “low energy” and “high energy” responses.

### 3.5.1 Possible mechanisms of action

The mechanism by which pulsed IR light causes a reduction in release of pro-inflammatory cytokines in stimulated microglial-like BV2 cells is not completely clear, but evidence shown in this work has highlighted the roles of altered agonist-receptor binding, induced intracellular calcium transients, and laser-induced temperature rises. Chronologically, it is possible that the temperature increase created by pulsed IR causes an increase in intracellular calcium from extracellular and/or intracellular sources. This reduces the effects of innate immune receptor targeted danger signals on receptors such as TLR4, which can be modulated by heat sensitive TRPV1 activation.<sup>30</sup> The TLR4 signal reduction could be due to a direct modulation of the ligand-receptor binding at TLR4, a modulation of a mechanistically linked channels, like TRPV1, or indirectly through a reduction of available intracellular calcium necessary for TLR4-dependent intracellular signaling, thereby creating a state of TLR4 tachyphylaxis. Finally, the impact of pulsed IR on the production of pro-inflammatory cytokine, IL-6, may be due to these upstream signaling events or due to the downstream modulation of transcription and translation of the cytokines. In the context of chronic pain, if reactive microglial cells were successfully targeted using pulsed IR then this pulsed IR dependent reduction of released pro-inflammatory cytokines would beneficially impact the chronic pain state. Higher order model systems are needed to confirm that this hypothesized reduction of released pro-inflammatory cytokines can translate to a reduction of pro-inflammatory signaling *in vivo*. Importantly, there was no unwanted pro-inflammatory cytokine release in non-LPS stimulated cells at any radiant exposure and temperature tested. This is an important first step in the further exploration of therapeutic applications of INM and other temperature-based modalities and demonstrates the potential utility of using such techniques to combat chronic pain and other neurological deficits.

### 3.5.2 Diversity of biological responses in BV2 cell culture

The diversity of calcium responses of BV2 cells to pulsed IR can be categorized, broadly, into four different groups: no response, low energy response, high energy response, and death response. The BV2 cells that do not change calcium levels after irradiation are classified as no response. As shown in Figure 3.4-4, cells below a certain temperature rise do not respond to the laser-induced stimulus. This is an expected phenomenon as the stimulus is not intense enough to activate the cell. There is another group of no response cells that do not respond regardless of the stimulus intensity. The lack of response may be due to the heterogeneity of BV2 cells within the culture as having differences in growth cycle, expressed membrane proteins, overall health, etc. Notably, the heterogeneity in cell responses would not be observed in bulk measurement techniques such as the ELISA assay but requires single cell recording methods.

Two distinct intracellular calcium transients from non-dying cells were initiated by pulsed IR light: “low energy” response and “high energy” responses. The responses differ in the duration of calcium increase and the temperature increase that is required for activation. Intracellular calcium transients are involved in many known pathways like cytokine production, phagocytosis, apoptosis, and state changes.<sup>31</sup> Therefore, calcium is a highly sensitive marker of physiological changes but with low specificity. The difference in the IR-induced calcium transients suggest that different physiological pathways may be activated depending on the temperature rise of the cell. Further investigation is needed to uncover the exact pathways that are involved.

Lastly, the cells that die due to the pulsed IR light exhibit a unique calcium transient compared to the transients discussed earlier. The main difference between “death” response and the “high energy” response is the onset of the calcium transients. During the death response, intracellular calcium responses are initiated within seconds of the pulsed IR train being initiated. The low and

high energy responses were only initiated after the full dose of pulsed IR was delivered. The calcium signal measured during the pulsed IR exposure is unreliable due to the thermal lensing effect changing the focal plane of the imaging system. The death response is unique in that the fluorescent signal is strong enough to overcome the focal plane shift and begin before the pulsed IR train is completed. For the same reason, the low and high energy responses may begin earlier than measured in this study.

### 3.5.3 Temperature rise is a better predictor of biological effect than radiant exposure alone

The radiant exposure needed to induce a physiological change differed between the imaging and ELISA setups greatly, with the imaging setup needed 540 to 714 J/cm<sup>2</sup> to induce calcium transients while the ELISA assays needed only 66 J/cm<sup>2</sup> to impact cytokine release. The magnitude difference in radiant exposure thresholds may suggest different biological mechanism of action if it is purely the light dose-dependent phenomena. As described previously, the wavelength of light, 1875 nm, is highly absorbed by water and converted into to heat. Previous studies on pulsed IR light and its effect on the nervous system have concluded that temperature gradients and thresholds are an important underlying mechanism to change physiology rather than the laser-induced chemical or mechanical effects.<sup>15,32</sup> The volumes of media surrounding the cells are vastly different between the two setups, with 2 mL used during widefield imaging experiments and 100 μL used during ELISA assay and plate-reader calcium imaging experiments, which will create vastly different heating environments. In both setups, experiments were performed at room temperature and cells would cool to 20 °C before experimentation. As shown in Figures 3.4-3D and 3.4-5B, the temperature rise required for calcium transients was 15-20 °C and the temperature rise required for disruption in cytokine release was 20-25 °C. If the “high energy” response calcium transient is involved in the cytokine production pathway, the temperature rise required is likely

overlapping and may indicate a connection. It should be noted that in the temperature rise measured for cytokine release disruption is at the hottest point and would be lower near the edges of the wells for this bulk measurement. The temperature rises required for physiological changes are in much better agreement than the necessary radiant exposures, suggesting that these responses are driven by temperature changes and may be driven by a singular mechanism of action.

#### 3.5.4 Cell viability after pulsed IR exposure

Cell death and damage are main concerns when discussing temperature rises over a few degrees Celsius. As discussed previously, the temperature rise is from experiments performed under room temperature conditions and not incubation temperatures, for which high temperature rises would likely be lethal. The Arrhenius model predicts damage is a function of the maximum temperature and duration of increased temperature. The heating characteristics used in this study include maximum temperatures below 50 °C and duration in the tens of seconds, which is likely why there is limited impact on cell viability. Cells have innate defenses against temperature-related damage as well. Specifically, heat shock proteins inhibit cell death and promote survivability.<sup>33,34</sup> The death markers used in this study, PI and Caspase-3, show early necrosis and apoptosis at temperatures much higher than the low and high energy response thresholds; 38 °C compared to 20 °C, respectively. MTT assays were used in the cytokine experiments in Figure 3.4-5, which measure the ability of cells to metabolize. The temperature rise needed to reduce cytokine release by 50% is 23°C. The temperature needed to reduce viability by 50% was not measured, but can be assumed to be larger than the highest measured temperature rise of 26 °C. It should be noted that the temperature shown in Figure 3.4-5 is the maximum temperature rise in the dish from a non-uniform laser beam. This resulted in losing cell viability in the center of the wells before peripheral cells. While the temperature rises needed to modulate cell physiology in the two setups can easily

be compared, the cell viability measurements cannot. A limitation in this work is that cell death and apoptosis were measured 40 minutes after pulsed IR exposure and certain cell death pathways may need more time to initiate.

### 3.6 Conclusion

In conclusion, we have demonstrated the first evidence that acute temperature increases from pulsed infrared light impacts a source of chronic pain; pro-inflammatory cytokine release. This is in addition to the known utility of pulsed infrared light to block the propagation of pain signals in the nervous system. Specifically, we have laid out a pathway by which the temperature rise from pulsed infrared light 1) reduces the response of subsequent ligand-membrane channel activation after exposure to pulsed IR, 2) induces multiple, unique intracellular calcium transient phenotypes that are not related to apoptosis and necrosis, and 3) reduces the release of pro-inflammatory cytokine IL-6 in activated BV2 cells, while not impacting IL-6 release in immunologically resting BV2 cells. In cell culture, the temperature rise necessary to impact BV2 physiology is 15-25 °C from room temperature (20 °C). With this new discovery, pulsed infrared light has the potential to intervene, not only in the symptomatic experience of chronic pain, but also provide disease modification through targeting pro-inflammatory immune signaling.

### 3.7 References

1. Products - Data Briefs - Number 390 - November 2020. Accessed February 27, 2022. <https://www.cdc.gov/nchs/products/databriefs/db390.htm#fig1> (2020).
2. Dahlhamer J, Lucas J, Zelaya, C, et al. Prevalence of Chronic Pain and High-Impact Chronic Pain Among Adults — United States, 2016. *MMWR Morbidity and Mortality Weekly Report*. (2019).
3. Mills SEE, Nicolson KP, Smith BH. Chronic pain: a review of its epidemiology and associated factors in population-based studies. *Br J Anaesth*. **123**(2):e273-e283 (2019).
4. Boudreau D, von Korff M, Rutter CM, et al. Trends in long-term opioid therapy for chronic non-cancer pain. *Pharmacoepidemiol Drug Saf*. **18**(12):1166-1175 (2009).
5. Dowell D, Haegerich TM, Chou R. CDC Guideline for Prescribing Opioids for Chronic Pain—United States, 2016. *JAMA*. **315**(15):1624-1645 (2016).
6. Smith BH, Elliott AM, Alastair Chambers W, Smith WC, Hannaford PC, Penny K. The impact of chronic pain in the community. *Fam Pract*. **18**(3):292-299 (2001).
7. Understanding the Epidemic | Drug Overdose | CDC Injury Center. Accessed February 27, 2022. <https://www.cdc.gov/drugoverdose/epidemic/index.html> (2022)
8. NIH HEAL Initiative Research Plan | NIH HEAL Initiative. Accessed February 27, 2022. <https://heal.nih.gov/about/research-plan> (2022)
9. Paff M, Loh A, Sarica C, Lozano AM, Fasano A. Update on Current Technologies for Deep Brain Stimulation in Parkinson’s Disease. *Journal of Movement Disorders*. **13**(3):185 (2020).

10. Mekhail NA, Mathews M, Nageeb F, Guirguis M, Mekhail MN, Cheng J. Retrospective Review of 707 Cases of Spinal Cord Stimulation: Indications and Complications. *Pain Practice*. **11**(2):148-153 (2011).
11. Duke AR, Jenkins MW, Lu H, McManus JM, Chiel HJ, Jansen ED. Transient and selective suppression of neural activity with infrared light. *Scientific Reports 2013* **3**(1):1-8 (2013).
12. Ganguly M, Jenkins MW, Jansen ED, Chiel HJ. Thermal block of action potentials is primarily due to voltage-dependent potassium currents: a modeling study. *Journal of Neural Engineering*. **16**(3):036020 (2019).
13. Ford JB, Ganguly M, Zhuo J, et al. Optimizing thermal block length during infrared neural inhibition to minimize temperature thresholds. *Journal of Neural Engineering*. **18**(5):056016 (2021).
14. Lothet EH, Shaw KM, Lu H, et al. Selective inhibition of small-diameter axons using infrared light. *Scientific Reports 2017* **7**(1):1-8 (2017).
15. Borrachero-Conejo AI, Adams WR, Saracino E, et al. Stimulation of water and calcium dynamics in astrocytes with pulsed infrared light. *FASEB Journal*. **34**(5):6539-6553 (2020).
16. Choi SI, Lim JY, Yoo S, Kim H, Hwang SW. Emerging Role of Spinal Cord TRPV1 in Pain Exacerbation. *Neural Plasticity*. (2016).
17. Jara-Oseguera A, Simon SA, Rosenbaum T. TRPV1: ON THE ROAD TO PAIN RELIEF. *Curr Mol Pharmacol*. **1**(3):255 (2008).
18. Crofford LJ, Casey KL. Central modulation of pain perception. *Rheum Dis Clin North Am*. **25**(1):1-13 (1999).

19. Napadow V, Harris RE. What has functional connectivity and chemical neuroimaging in fibromyalgia taught us about the mechanisms and management of “centralized” pain? *Arthritis Res Ther.* **16**(5) (2014).
20. Grace PM, Hutchinson MR, Maier SF, Watkins LR. Pathological pain and the neuroimmune interface. *Nature Reviews Immunology* 2014 14:4. **14**(4):217-231 (2014).
21. Ji RR, Xu ZZ, Gao YJ. Emerging targets in neuroinflammation-driven chronic pain. *Nat Rev Drug Discov.* **13**(7):533-548 (2014).
22. Calvo M, Zhu N, Tsantoulas C, et al. Neuregulin-ErbB signaling promotes microglial proliferation and chemotaxis contributing to microgliosis and pain after peripheral nerve injury. *J Neurosci.* **30**(15):5437-5450 (2010).
23. Kawasaki Y, Xu ZZ, Wang X, et al. Distinct roles of matrix metalloproteases in the early- and late-phase development of neuropathic pain. *Nature Med.* **14**(3):331-336 (2008).
24. Lewis SS, Loram LC, Hutchinson MR, et al. (+)-Naloxone, an opioid-inactive toll-like receptor 4 signaling inhibitor, reverses multiple models of chronic neuropathic pain in rats. *Journal of Pain.* **13**(5):498-506 (2012).
25. Hutchinson MR, Ramos KM, Loram LC, et al. Evidence for a role of heat shock protein-90 in toll like receptor 4 mediated pain enhancement in rats. *Neuroscience.* **164**(4):1821-1832 (2009).
26. Ji RR, Berta T, Nedergaard M. Glia and pain: Is chronic pain a gliopathy? *Pain.* **154**(Suppl. 1):10-28 (2013).
27. Lilienbaum A, Israël A. From Calcium to NF- $\kappa$ B Signaling Pathways in Neurons. *Molecular and Cellular Biology.* **23**(8):2680 (2003).

28. Dresselhaus EC, Meffert MK. Cellular Specificity of NF- $\kappa$ B Function in the Nervous System. *Frontiers in Immunology*. **10** (2019).
29. Tanaka T, Narazaki M, Kishimoto T. IL-6 in Inflammation, Immunity, and Disease. *Cold Spring Harbor Perspectives in Biology*. **6**(10):16295-16296 (2014).
30. Assas BM, Miyan JA, Pennock JL. Cross-talk between neural and immune receptors provides a potential mechanism of homeostatic regulation in the gut mucosa. *Mucosal Immunol*. **7**(6):1283-1289 (2014).
31. Mizoguchi Y, Monji A. Microglial intracellular Ca<sup>2+</sup> signaling in synaptic development and its alterations in neurodevelopmental disorders. *Frontiers in Cellular Neuroscience*. **11**:69 (2017).
32. Wells JD, M.D. CK, Jansen ED, M.D. PEK, Mahadevan-Jansen A. Application of infrared light for in vivo neural stimulation. *Journal of Biomedical Optics* **10**(6):064003 (2005).
33. Wilmlink GJ, Opalenik SR, Beckham JT, et al. Molecular Imaging-Assisted Optimization of Hsp70 Expression during Laser-Induced Thermal Preconditioning for Wound Repair Enhancement. *Journal of Investigative Dermatology*. **129**(1):205-216 (2009).
34. Beere HM. "The stress of dying": the role of heat shock proteins in the regulation of apoptosis. *J Cell Sci*. **117**:2641-2651 (2004).
35. Cayce JM, Friedman RM, Chen G, Jansen ED, Mahadevan-Jansen A, Roe AW. Infrared neural stimulation of primary visual cortex in non-human primates. *NeuroImage* **84**: 181-190 (2014).
36. Kilgore K, Bhadra N. Nerve conduction block utilising high-frequency alternating current. *Medical and Biological Engineering and Computing*. **42**(3):394-406 (2004).

37. Cayce JM, Wells JD, Malphrus JD, Kao C, Thomsen S, Tulipan NB, Konrad PE, Jansen ED, Mahadevan-Jansen A. Infrared neural stimulation of human spinal nerve roots in vivo. *Neurophotonics* 2(1):015007 (2015).

## Chapter IV

### **The effects of high-amplitude, short-duration pressures transients on intracellular calcium response and inflammatory immune response of neuron, astrocyte, and microglia monocultures.**

J. Logan Jenkins<sup>1,2</sup>, Pratheepa Kumari<sup>1,2</sup>, Jacob Hardenburger<sup>1,2</sup>, Wilson Adams<sup>1,2</sup>, Anita Mahadevan-Jansen<sup>1,2,3</sup>, Bryan Millis<sup>1,2</sup>, E. Duco Jansen<sup>1,2,3</sup>

<sup>1</sup>Department of Biomedical Engineering, Vanderbilt University, Nashville, TN, USA

<sup>2</sup>Vanderbilt Biophotonics Center, Vanderbilt University, Nashville, TN, USA

<sup>3</sup>Department of Neurological Surgery, Vanderbilt University Medical Center

#### **4.1 Abstract:**

Blast-induced traumatic brain injury (bTBI) was reported in 125,000 U.S. service men and women from 2000-2018. With no prophylactic treatments having been granted FDA approval, there is a clear need for further understanding of the impact of blast on the central nervous system. The biological response of brain cells due to the near instantaneous overpressure of blast onset remains unresolved. Laser-induced pressures allow for an isolation of high-amplitude, short-duration pressure transients, similar to the initial peak of blast pressures. In this study, we uncover the effects of high-amplitude, short-duration pressure transients on monocultures of astrocytes, microglia, and neurons through intracellular calcium imaging, cell viability assays, and quantification of intracellular and extracellular immune signaling proteins. The results indicate that while all three cell types follow a similar activation curve for induced intracellular calcium transients, the downstream impact of high-amplitude, short-duration pressures on neurons and glia diverge. Neurons are especially susceptible to non-reversible damage, while glia may activate neuroprotective pathways rather than neurodegenerative pathways in response to high-amplitude, short-duration pressures. This work has important implications for the development of countermeasures for bTBI with either the high frequency component of a blast wave or the effects of that component being potential targets for prevention.

## 4.2 Introduction

While traumatic brain injuries (TBI) are a concern for a large, diverse group of individuals, especially adolescents and the elderly<sup>1</sup>, military personnel are uniquely at-risk of blast-induced traumatic brain injury (bTBI). Blasts from improvised explosive devices (IEDs) and improvised rocket assisted mortars (IRAMS) are a particular threat in combat<sup>2</sup>. Symptoms of bTBI can have devastating impacts on the physical, cognitive, and emotional health of patients. From 2000-2018, there were over 380,000 cases of TBI from U.S. service men and women ranging from mild to severe, of which a third were exposed to blast events<sup>3</sup>. Currently, no drug-based treatments for TBIs have made it past FDA clinical trials<sup>4</sup>. Therefore, bTBIs remain a main focus in research endeavors to better understand the mechanisms of damage and develop potential treatments.

Explosion energy from blasts interact with the body through the propagation of a large overpressure (a positive pressure transient), sometimes referred to as a ‘shockwave’, although strictly speaking only pressure transients that travel at supersonic speed can be classified as true shockwaves. The physiological effects due to this overpressure are characterized as primary, secondary, tertiary, and quaternary blast injuries. Primary blast injury is caused solely by the blast wave interacting with the body. Secondary through quaternary blast injuries are due to later effects of blast like injury from projectiles or physical displacement of the body. The mechanisms by which the primary blast injury from direct pressure exposure affects the brain at a cellular level remains unclear. There are a number of methods to replicate blast waves in a research setting, including micro explosions, shock tube, ultrasound, and laser<sup>5</sup>. Laser-based methods have advantages in creating ultrashort pressure waves that mimic the initial spike of field blasts, allowing for precise spatial targeting of samples, and small fiber-based form factors for implementation with detection methods. Laser-induced pressure waves can be generated through

several mechanisms of action: cavitation bubble expansion and collapse, plasma formation, thermoelastic expansion, or ablative recoil.<sup>6</sup>

The mammalian brain consists of a complex interweaving and interaction between neurons, astrocytes, microglia, and vasculature that respond to blast in a multifaceted manner. From a tissue perspective, blast-damaged portions of the brain can undergo inflammation, ischemia, edema, and vasoconstriction<sup>7</sup>. On the cellular level, the response of neurons to blasts have been extensively studied. Known effects of blasts on neurons include diffuse axonal injury, swollen cell bodies, and neurotransmission loss<sup>8</sup>. The role of glia in bTBIs remains much less clear than their neuronal counterparts. Astrocytes, the main support cell to neurons, respond to TBIs by maintaining neuronal environments via modulating extracellular osmolarity and ion concentrations, buffering neurotransmitters, and calibrating neurovascular coupling.<sup>9</sup> Microglia, the resident immune cell in the brain, respond to TBIs in either a neuroprotective or neurodegenerative manner. An acute activation of the inflammatory response is vital to the repair and recovery of the brain, while a chronic activation can lead to secondary injury and be detrimental<sup>10</sup>

A ubiquitous indicator of cellular activation across neurons, astrocytes, and microglia is intracellular calcium transients. Intracellular calcium transients drive many physiological functions for neurons, astrocytes, and microglia<sup>11</sup>. In neurons, calcium is a main indicator of excitability, neurotransmission, and metabolism<sup>12</sup>. In astrocytes, calcium transients are linked to synaptic transmission, neurodegeneration, immune response, brain energy metabolism, and inflammation<sup>13</sup>. In microglia, intracellular calcium transients play a role in state changes, cytokine production and release, and phagocytosis<sup>14</sup>. Intracellular calcium transient can initiate through multiple sites of origination, broadly extracellular or intracellular. Transient receptor potential (TRP) channels are one of the main families of calcium channels that allow an influx of

extracellular calcium. Several subtypes of TRP channels are known to be heat and/or pressure sensitive<sup>15</sup>. Major intracellular calcium stores include the endoplasmic reticulum, the mitochondria, and the lysosomes and are largely regulated by inositol 1,4,5-triphosphate (IP<sub>3</sub>) receptors<sup>16</sup>.

The calcium transients in glia can modulate several different paths including cytokine production through via intracellular protein nuclear factor kappa B (NF- $\kappa$ B)<sup>11,17</sup>. Proinflammatory cytokines, such as interleukin (IL)-1 $\alpha$ , IL-1 $\beta$ , IL-6, and TNF- $\alpha$ , can initiate acute and chronic inflammation with potential beneficial and damaging effects within neurological response to danger stimuli<sup>18</sup>. Other intracellular pathway proteins play major roles in the immune response of microglia and astrocytes. The three others that are relevant to this work are CREB, Akt, and STAT3. cAMP response element-binding protein (CREB) impacts the immune response by inhibiting NF- $\kappa$ B activation, inducing macrophage survival, and promoting the proliferation, survival, and regulation of T and B lymphocytes<sup>19</sup>. Protein kinase B (Akt) prevents cell injury, inhibits microglia activation pathway and proliferation, and inhibits apoptotic pathway caspase-3<sup>20</sup>. The function of Signal Transducer And Activator Of Transcription 3 (STAT3) is more complex with disagreement of its function to promote pro-inflammatory or anti-inflammatory responses through microglial polarization<sup>21</sup>.

In this study, primary neurons, astrocytes, and microglia are separately subjected to the initial peak of blast-induced pressure waves through pulsed laser-induced pressure generation to better understand the direct impact of fast rise overpressures on each cell type at multiple peak positive pressures. Cellular responses are assessed through induced intracellular calcium transients, cell death by the uptake of necrosis and apoptosis markers, and immune activation

through changes in released proinflammatory cytokine concentrations and intracellular pathway messenger protein concentrations.

## 4.3 Methods and Materials

### 4.3.1 Cell Culture

Primary astrocytes, microglia, and neuron cultures were prepared in accordance with animal use protocols approved by the Vanderbilt University Institute for Animal Care and Use Committee (VU-IACUC, Protocol M1600084).

#### 4.3.1.1 Primary Rat Cortical Astrocytes

Primary astrocytes were isolated from day 0-2 postnatal Sprague-Dawley rat pups (Envigo/Harlan, Indianapolis, IN, USA). The neural cortices were mechanically dissected and placed in 1 mL of Dulbecco's Modified Eagle Medium (DMEM) supplemented with 5 mM L-glutamine, 15% (v/v) fetal bovine serum (FBS), and penicillin/streptomycin (100 U/mL and 100 µg/mL, respectively). Tissues were mechanically dissociated and strained through a 40 µm cell strainer (Falcon, BD Bioscience, Bedford, MA). Strained cells in suspension were plated on culture flasks containing the previously described DMEM. Cells were frozen in liquid nitrogen and thawed for experimentation. Cells were maintained in incubation at 37 °C with 5% CO<sub>2</sub> and 95% relative humidity levels for at least three weeks prior to experimentation. After 14 days *in vitro*, medium concentrations of FBS were reduced to 10% (v/v). Cells were used between days 21 and 35 *in vitro* for experiments upon re-plating. Primary astrocytes were detached using a 0.025% trypsin/EDTA solution for 5 minutes at 37°C and 5% CO<sub>2</sub> to plate cells for live imaging experiments. Cells were reseeded on glass-bottom 35mm cell culture dishes (#0 coverglass, 7 mm diameter, Mattek, Waltham, MA, USA) coated with Poly-D-lysine (PDL) at a concentration of about 30,000 cells/cm<sup>2</sup>. Imaging experiments were performed between 48-96 hours after re-plating.

#### 4.3.1.2 Primary Rat Whole Brain Microglia

P2 dissociated rat whole brain microglia were purchased after isolation from Sprague Dawley rat pups (Transnetyx, Memphis, TN, USA). Microglia were shipped in vials of Hibernate A (ThermoFisher Scientific, Waltham, MA, USA) on dry ice. Vials of microglia were placed in a 4°C refrigerator prior to use for up to 48 hours. The Transnetyx protocol was used for microglia plating. In brief, vials of microglia were placed in a 30°C water bath for 1 minute prior to centrifuging 2 mL of microglia in Hibernate A at 200G. Supernatant was discarded, and cell were resuspended in 1 mL NbActiv1 (Transnetyx, Memphis, TN, USA) with 1x Glutamax and penicillin/streptomycin (100 U/mL and 100 µg/mL, respectively). Cells were counted using an image-based hemocytometer and Trypan blue in a 1:1 ratio. Cells were plated on a glass 35mm cell culture dish (#0 glass, 7mm, Mattek, Waltham, MA, USA) coated with PDL at a concentration of about 50,000 cells/cm<sup>2</sup>. Cells were maintained in incubation at 37 °C with 5% CO<sub>2</sub> and 95% relative humidity levels for 3-7 days until experimentation. Every 3 days, fresh NbActiv1 was added to the dishes in a 1:1 ratio with existing media.

#### 4.3.1.3 Primary Rat Cortical Neurons

E18 dissociated rat cortical neurons were purchased after isolation from Sprague Dawley rat pups (Transnetyx, Memphis, TN, USA). Neurons were shipped in vials of Hibernate A (ThermoFisher Scientific, Waltham, MA, USA) on dry ice. Vials of neurons were placed in an icebox within a 4°C refrigerator prior to use for up to 48 hours. The Transnetyx protocol was used for neuron plating. In brief, vials and were placed in a 30°C water bath for 1 minute prior to centrifuging 2 mL of neurons in Hibernate A at 200G. Supernatant was discarded, and cell were resuspended in 1 mL NbActiv1 (Transnetyx, Memphis, TN, USA). Cells were counted using an image-based hemocytometer and Trypan blue in a 1:1 ratio. Cells were plated on a glass 35mm

cell culture dish (#0 glass, 7mm, Mattek, Waltham, MA, USA) coated with PDL at a concentration of about 16,000 cells/cm<sup>2</sup>. Cells were maintained in incubation at 37 °C with 5% CO<sub>2</sub> and 95% relative humidity levels for 12-16 days until experimentation. Every 3-4 days, astrocyte-incubated NbActiv1 was added to the dishes in a 1:1 ratio with existing media.

#### 4.3.2 Fluorescence Imaging

##### 4.3.2.1 Imaging Solutions

Fresh standard imaging solution was composed of the following salts in deionized water (in mM): 140 NaCl, 4 KCl, 2 MgCl<sub>2</sub>, 2 CaCl<sub>2</sub>, 10 HEPES, 5 glucose, pH 7.4 with NaOH, and osmolarity adjusted to ~318 mOsm with mannitol. Ca<sup>2+</sup>-free extracellular solution was formulated with deionized water containing the following salt concentrations (mM): 140 NaCl, 4 KCl, 4 MgCl<sub>2</sub>, 10 HEPES, 5 glucose, 0.5 EGTA, pH 7.4 with NaOH and osmolarity adjusted to ~318 mOsm with mannitol. Stock solutions of pharmacological agents were prepared from vendors by solubilizing them in their appropriate diluent solutions for pharmacological studies. Stock aliquots of Ruthenium red (RR, 10mM) and 2-Aminoethoxydiphenylborane (2- APB, 100mM) were prepared in water and stored at -20 °C. Working concentrations of pharmacological agents for imaging experiments were as follows: RR 10 μM, 2-APB 100 μM, in physiological saline solution.

##### 4.3.2.2 Calcium Imaging

To image intracellular calcium dynamics of primary rat astrocytes, microglia, and neurons, cells seeded on #0 glass-bottom imaging dishes were rinsed and incubated with physiological saline solution containing 3 μM of Calbryte 520 AM (AAT Bioquest, Sunnyvale, CA, USA) and for 45-75 minutes. After dye loading, cells were rinsed with and maintained in a standard bath solution for the duration of imaging sessions (<15 minutes). Imaging dishes were placed in a 32 °C heated water bath integrated into a custom-built widefield microscope with 10x, 0.3 NA water-

immersion objective (UMPLFLN, Olympus, Shinjuku City, Tokyo, JP) and ultrafast CMOS camera (ORCA, Hamamatsu, Hamamtsu City, JP) (Figure 4.3-1A). Fluorescence excitation was provided by a broadband light source (Lumencore Sola) bandpass filtered to a wavelength range centered around 488 nm. Camera sensor exposure times were held constant at 7 ms for microglia and neuron experiments, and 30 ms for astrocyte experiments.

During an imaging experiment, fluorescence images of dye-loaded microglia and neurons were acquired at a 2 Hz framerate for 30 seconds, then 89 Hz frame rate for 0.5 seconds prior to pressure exposure and 1 second after exposure, and 2 Hz for the last 180 seconds. Astrocytes were imaged at a 2 Hz framerate for 30 seconds, then 30 Hz framerate for 0.5 seconds before pressure exposure and 1 second after pressure exposure, and 2 Hz framerate for the last 180 seconds. Approximately 30 seconds into the recording period, cells were exposed to high-amplitude, short-duration pressure as described in the High-amplitude, short-duration pressure methods. Bath application of pharmacological agents was used to study the influence of molecular signaling pathways involved in high-amplitude, short-duration pressure calcium transients. All images were acquired in NIS Elements (Nikon Imaging Systems, Melville, NY, USA) and analyzed using custom processing and analysis workflows with Fiji.

#### 4.3.2.3 Cell Viability Fluorescence Imaging

Necrosis and apoptosis stains were used to determine the viability of the cell cultures during calcium imaging. Two fluorescent probes were used to better understand the impact of high-amplitude, short duration pressures transients on primary CNS cells in the 35mm imaging dish. Necrosis stain 1  $\mu$ M Propidium Iodide (Invitrogen, Waltham, MA, USA) and apoptosis stain 5 $\mu$ M Biotracker NucView 488 Caspase-3 dye (Biotium, Fremont, CA, USA) were added to the imaging solution for 10 minutes and 40 minutes prior to pressure exposure, respectively. Fields of

views were imaged immediately before laser exposure and 10 and 40 minutes after exposure to determine signs of cellular necrosis and apoptosis, respectively.

#### 4.3.2.4 Data Processing

Raw fluorescence traces were extracted using similar methods as Boracherro-Conejo *et al.*<sup>22</sup>. The raw fluorescence traces were temporally aligned via a laser light emission artifact during the pulse, intensity normalized, and processed to extract multiple calcium response metrics. Each cell's raw fluorescence intensity was normalized to the mean raw intensity of the 20 frames preceding pressure exposure, then reported and analyzed as fractions ( $\Delta F/F$ ). Quantitative metrics extracted from each cell's calcium time series trace included maximum change in relative fluorescence (peak  $\Delta F/F$ ), elapsed time-to-peak fluorescence intensity (time-to-peak, in seconds), the full-width half-maximum of each cell's response (duration, in seconds). A cell was deemed activated if a 10% increase in relative calcium fluorescence within 30 seconds of pressure exposure was measured. The percentage of activated cells relative to the total number of cells observed is reported as "percentage of responding cells" on a per-imaging-experiment basis.

#### 4.3.3 Multiplex Inflammatory Signaling Analysis

The quantification of pro-inflammatory cytokine concentrations and intracellular pathway protein concentrations were made via multiplex analysis. Pro-inflammatory cytokine quantification used Milliplex Panel RECYTMAG-65K (Millipore Sigma, Burlington, MA, USA) and measured by Vanderbilt Hormone Assay & Analytical Services Core using the manufacturer's protocol. Microglia and astrocytes plated on #0 glass bottomed 35mm dishes were exposed to vehicle, 100 ng/mL lipopolysaccharide (LPS), or 4.65 MPa pressure transients. After exposures, cells were aspirated and given just enough volume of media (vehicle for vehicle and pressure groups, LPS media for LPS group) to cover the inner glass well (100  $\mu$ L). Samples were incubated

in normal incubation parameters for 24 hours. Dishes of sterile water surrounded the wells during incubation to reduce volume loss due to evaporation. After 24 hours of incubation, the entire remaining volume of media (30-40  $\mu\text{L}$ ) was collected. Vehicle media was added to the collected samples to bring the volume to 60  $\mu\text{L}$  for each sample. Samples were immediately frozen at  $-80^{\circ}\text{C}$  and delivered to the core for analysis. Concentration raw data was normalized to the vehicle group for each of the pro-inflammatory cytokines.

The quantification of intracellular pathway proteins was made using Milliplex Panel 48-681MAG and measured by Vanderbilt Hormone Assay & Analytical services using the manufacturer's protocol. Microglia and astrocytes plated in #0 glass-bottomed 35mm dishes were exposed to vehicle and 4.65 MPa of high-amplitude, short-duration pressure transient. 2.5 hours after exposures, samples were aspirated of all media, washed with ice-cold PBS once, and added 50  $\mu\text{L}$  Milliplex lysis buffer with protease inhibitor (Millipore Sigma, Burlington, MA, USA). Cells were scraped of using the tip of a 50  $\mu\text{L}$  pipette tip and cell suspensions were collected in a microcentrifuge tube and shaken at  $4^{\circ}\text{C}$  for 15 minutes. Cells were spun at 1000G using a tabletop centrifuge. Supernatant was collected ( $\sim 30$   $\mu\text{L}$ ) and brought to 65  $\mu\text{L}$  with Milliplex lysis buffer. Samples were then frozen at  $-80^{\circ}\text{C}$  until transferred to the core. Raw intracellular protein concentrations were normalized by the cell type to the vehicle group for each protein analyzed.

#### 4.3.4 Pressure Generation and Measurement

Pressure transients were generated using 6 ns pulse from a 355 nm Q-switched laser (Minilite II, Amplitude Laser Inc., Milpitas, CA, USA). The output of the laser at maximum voltage was  $9.0 \pm 0.2$  mJ per pulse. The 3 mm beam diameter leaving the laser was expanded using a telescope lens system before being brought to the base of the pressure delivery system (Figure 4.3-3B). The pressure delivery system consists of an objective on a z translation stage, a heated,

aluminum water bath, and an aluminum sample holder for imaging dish placement. The light is delivered to a 20x ReflX objective (Edmund optics, Barrington, NJ, USA) and transmitted through the water bath onto the bottom surface of the glass-bottomed imaging dish in the sample holder. For pressure generation via thermoelastic expansion or ablative recoil, a strong light absorber must be present. Black permanent marker (Sharpie PRO Permanent Marker XL, Chisel Tip, Sharpie, Atlanta, GA, USA) was brushed back and forth 5 times on the bottom of glass-bottom imaging dishes (Figure 4.3 4D). The subsequent layer of black absorber was dried for 1 minute in a biosafety cabinet prior to incubation. The black absorption layer reduced the light energy transmission by 99% when compared to no black layer. The spot of laser illumination on the black-painted glass imaging dish was 2 mm in diameter for a peak positive pressure measurement of 4.65 MPa. Lower pressures resulted changing the objective focus location using the z translation stage and lowering the energy density at the glass surface.

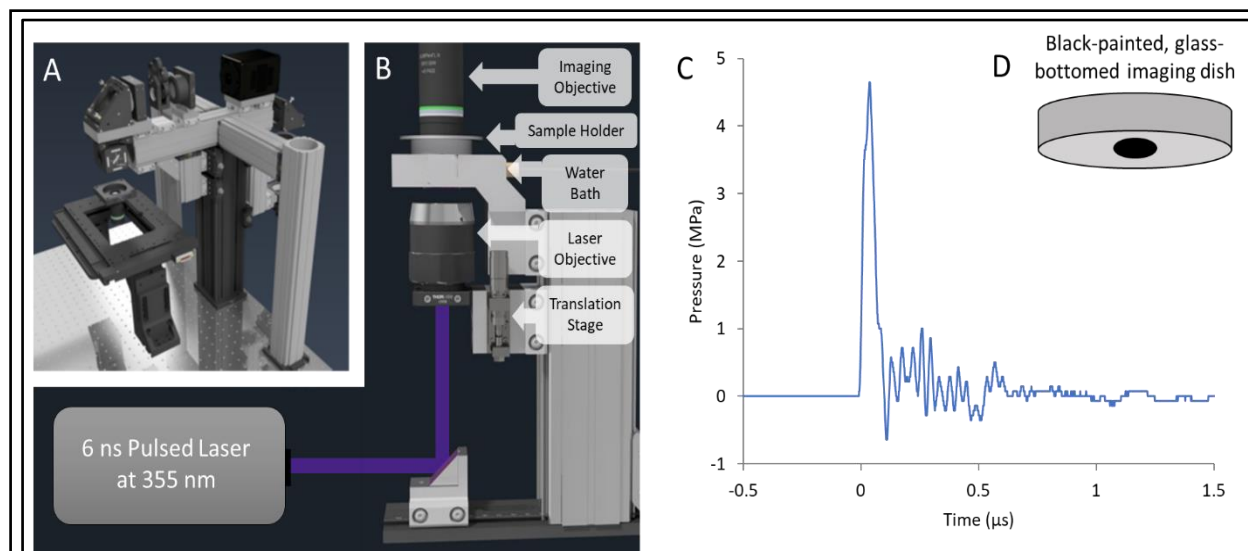


**Figure 4.3-1. Light and pressure delivery system to a custom-built widefield microscope.**

(A) Schematic of the custom-built upright microscope with 10x dipping (water immersion) objective and automated stage. (B) Pressure Delivery System. 6 ns pulsed laser light (355nm) is delivered via 20x objective on a z-translation stage. Light is transmitted inside a heated, degassed water bath to the bottom of an imaging dish with cell samples. Cell Samples are placed in the stage holder and submerged in the water bath for fluorescence imaging. (C) Representative pressure transient at the cell surface from a single 6 ns laser pulse at  $t=0 \mu\text{s}$ . (D) Illustration of the 35 mm glass-bottomed dish with 7 mm inner well. Bottom of inner well was brushed with a permanent marker to create a highly absorbed layer below the cells.

Pressure measurements were taken using a high angle acceptance needle hydrophone with frequency range 1-20 MHz (HNC-200, Onda Corp., Sunnyvale, CA, USA) connected to a hydrophone pre-amplifier (AH-2010-100, Onda Corp). The voltage signal was transmitted to a Picoscope 3000 series oscilloscope for data collection and converted to pressure in Pascals using Onda calibration data. For high-amplitude, short-duration pressure calibration, the hydrophone was placed inside a 35mm imaging dish without cells and brought directly above (<1 mm away) the glass of the imaging dish in the same spot used for fluorescence imaging using a 3-axis micromanipulator. At least 20 pressure transients for each group were measured leading to a standard deviation of less than 10%.

#### 4.3.5 Statistical analysis

Statistical comparison of metrics is performed with a 2-sided unpaired student's t-test. Error bars reported are standard deviation (SD) between imaging experiments. Statistical significance is denoted graphically with asterisks, where \* represents  $p < 0.05$  and \*\*\* represents  $p < 0.001$ .

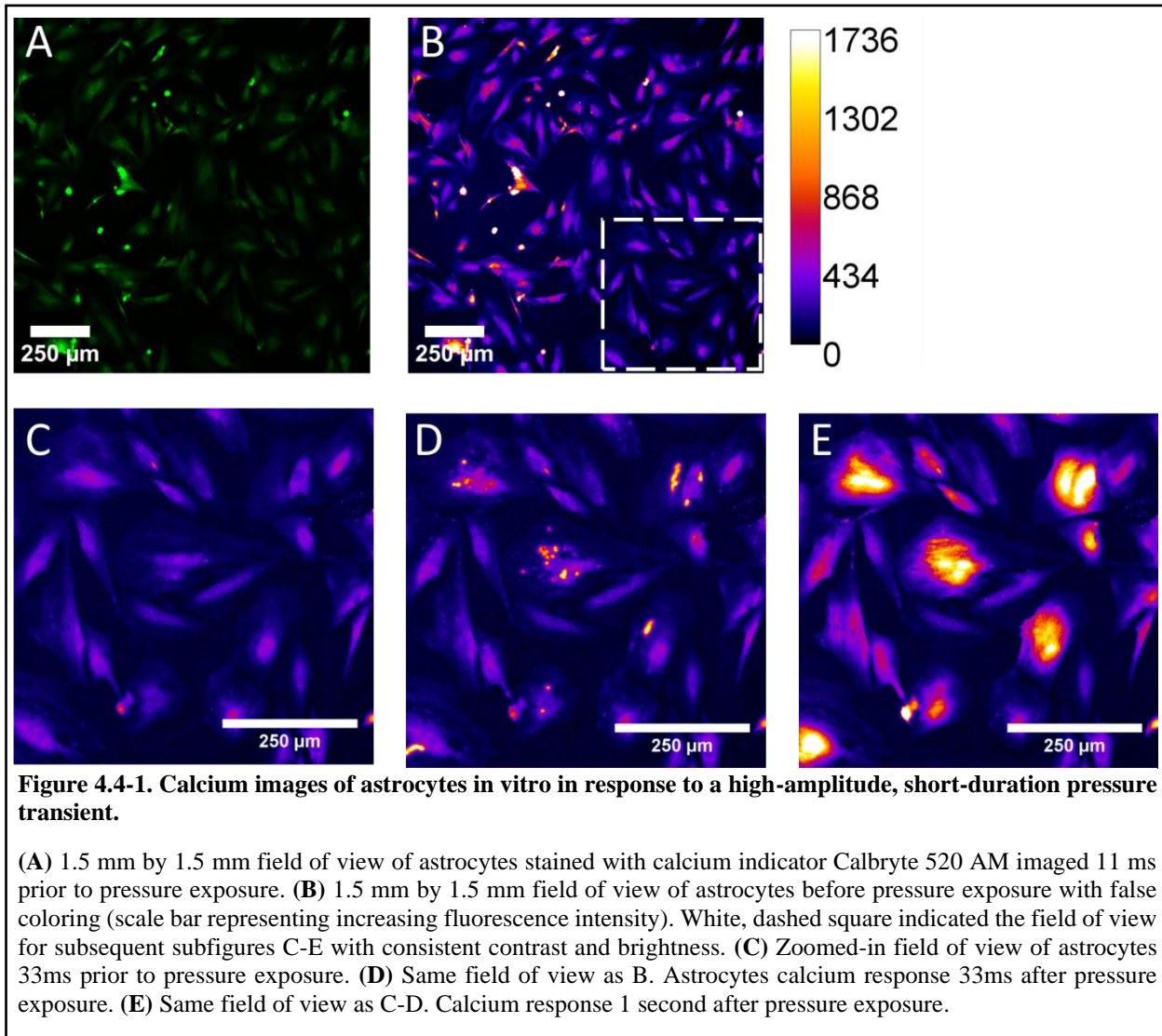
## 4.4 Results

### 4.4.1 High-amplitude, short-duration pressure transients initiate localized spots of intracellular calcium uptake

Figure 4.4-1 illustrates the response of astrocytes to a single pressure transient of 4.65 MPa peak positive pressure. The green emitting calcium indicator shows a basal activity in astrocytes in vitro (Figure 4.4-2A), though it is more easily seen with false coloring representing the fluorescence intensity (Figure 4.4-3B). Using the single fluorescence image taken 33 ms before pressure exposure (Figure 4.4-4C) as a comparison, the pressure transient causes localized spots to appear in the frame (Figure 4.4-5D). The calcium fluorescence dissipates to the rest of the cell from these localized spots as seen in the image 1 second after pressure exposure (Figure 4.4-6E). Astrocytic calcium responses initiated by these localized spots occurred earlier than calcium responses from adjacent astrocytes without obvious localized calcium increase spots.

Figure 4.4-2 depicts the response of astrocyte to high-amplitude, short duration pressure transients. Intracellular calcium transients are evoked directly after exposure to varying peak positive pressures from 0.85-4.65 MPa at  $t=0$  s. The intracellular calcium transients are characterized by a sharp rise in  $\Delta F/F$  followed by a sharp fall in  $\Delta F/F$  to slightly elevated baseline levels of intracellular calcium (Figure 4.4-2A). The percentage of cell that respond over a 0.1 increase in  $\Delta F/F$  varies from 0% to 90% of the cells in the fields of view as shown in figure 4.4-1. Fifteen percent of cells in the field of view responded to 0.85 MPa, which increases to the nearly saturated percentage of cells responding of 89% at 1.83 MPa. At 4.65 MPa, 90% of cells respond to high-amplitude, short-duration pressure transients, well within variance of the 1.83 MPa pressure transient (Figure 4.4-2B). The average maximum  $\Delta F/F$  for activated cells increases from 0.85 MPa to 1.83 MPa but then levels off when further increasing the pressure amplitude exposure

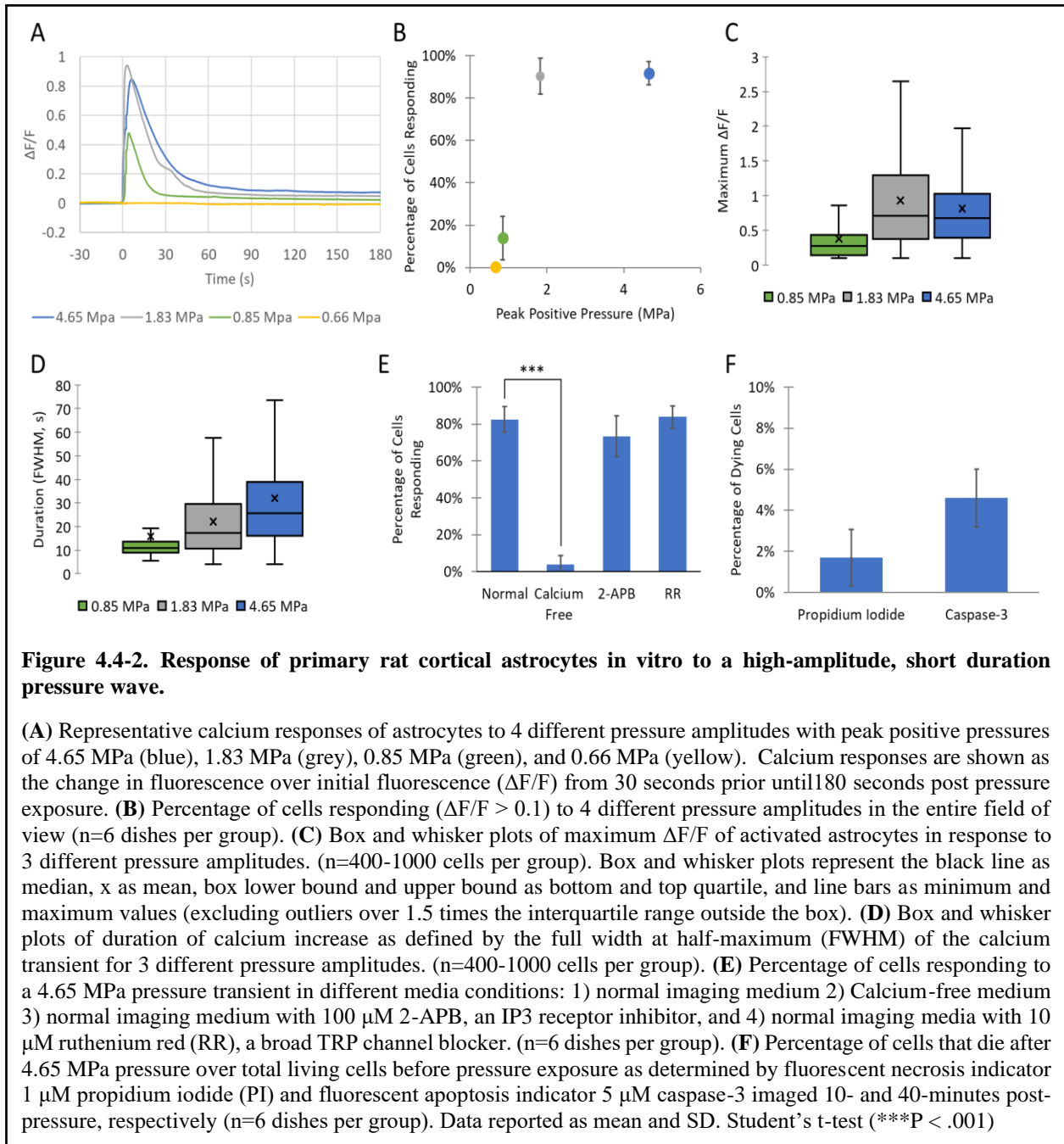
from 1.83 MPa to 4.65 MPa (Figure 4.4-2C). The duration of the calcium response for activated cell is defined as the full-width in seconds of half the maximum  $\Delta F/F$  (FWHM). The average duration increases for each step in peak positive pressure (Figure 4.4-2D). The origination of the calcium response was determined by changing the extracellular environment of the cells. In comparison to standard imaging media, calcium-free media significantly reduces the percentage of cells responding a 4.65 MPa pressure transient, from 83% to 5%, with a p-value well below 0.001. Imaging media with IP<sub>3</sub> receptor blocker 100  $\mu$ M 2-APB did not have a significant effect on the number of cells responding to the highest pressure (4.65 MPa) transient. Imaging media with 10  $\mu$ M RR, a broad TRP channel blocker, also did not significantly change the number of cells responding to 4.65 MPa (Figure 4.4-2E). Peak positive pressure of 4.65 MPa increased the uptake of propidium iodide by only 2% and the uptake of caspase-3 by less than 5% (Figure 4.4-2F).



#### 4.4.2 Microglia respond to high-amplitude, short-duration pressures via intracellular calcium transients without irreversible damage

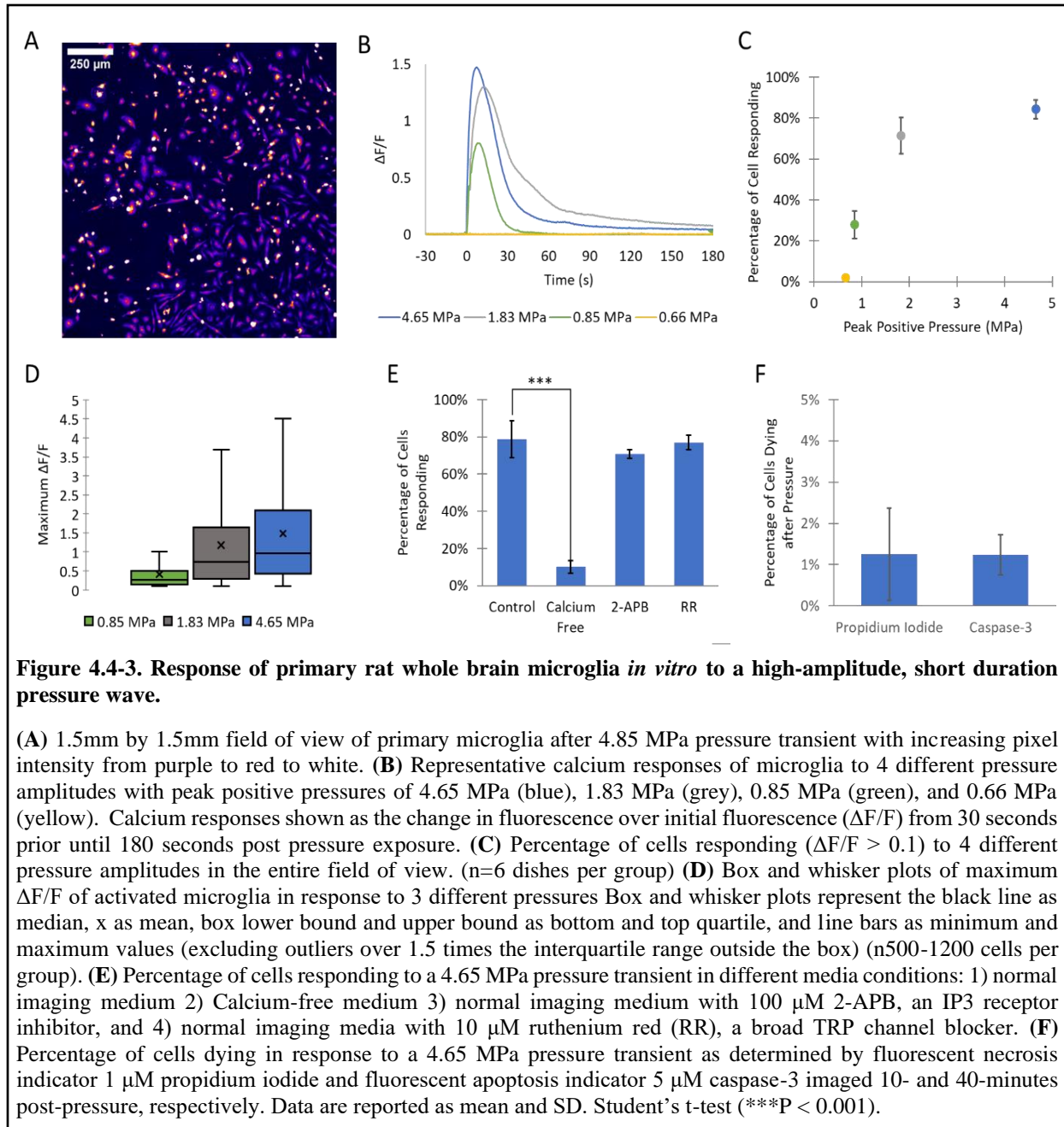
Figure 4.4-3 illustrates the response of primary microglia to high-amplitude, short duration pressure transients. An image of activated microglia with false coloring representing the fluorescence intensity is shown in Figure 4.4-3A. Intracellular calcium transients are evoked immediately after peak positive pressures from 0.85-4.65 MPa at  $t=0$  s. Similar to astrocytes, the calcium response follows a quick rise and fall of  $\Delta F/F$  (Figure 4.4-3B). The percentage of cell that

respond with a greater than 0.1 increase in  $\Delta F/F$  varies from 0% to 84% in the fields of view. Fourteen percent, seventy-one percent, and 85 percent of cells in the fields of view responded to 0.85 MPa, 1.83 MPa, and 4.65 MPa peak positive pressure, respectively (Figure 4.4-3B). The average maximum  $\Delta F/F$  for activated cells increases as the pressure increases (Figure 4.4-3D). The origin of the calcium response was determined by modulating the extracellular environment of the cells. In comparison to standard imaging media, calcium-free media significantly reduces the percentage of cells responding to a 4.65 MPa pressure transient, from 79% to 10%, with a p-value well below 0.001. Imaging media with IP<sub>3</sub> receptor blocker 2-APB did not have a significant effect on the number of cells responding to the highest-pressure amplitude (4.65 MPa). Imaging media with 10  $\mu$ M RR similarly did not significantly change the number of cells responding to the 4.65 MPa amplitude pressure transient (Figure 4.4-3E). Pressure transients with a peak positive pressure of 4.65 MPa increased the uptake of propidium iodide by about 1% and the uptake of caspase-3 by about 1% (Figure 4.4-3F).



#### 4.4.3 Neurons exhibit a two-phenotype response to high-amplitude, short-duration pressures

Figure 4.4-4 characterizes the response of primary neurons to high-amplitude, short duration pressure transients. An image of activated neurons with false coloring representing the fluorescence intensity is shown in Figure 4.4-4A. Intracellular calcium transients are evoked immediately after peak positive pressures from 1.83-4.65 MPa at  $t=0$  s. Unlike the responses from



glia, two phenotypes of response emerged, especially when exposed to 4.65 MPa. One phenotype can be described as a “fast calcium transient” and is characterized by a calcium transient that peaks within 180 seconds and reduced to at least half the maximum  $\Delta F/F$  by 180 seconds. The other phenotype is described as a “slow calcium transient” and is characterized by a calcium transient about 0.1  $\Delta F/F$  and does not reduce to or below half the  $\Delta F/F$  by 180 seconds. Typical “fast calcium transients” and “slow calcium transients” are provided in Figure 4.4-4B. The percentage of cells that respond to high-amplitude, short-duration pressure transients increase from <5% at 0.66 MPa to 80% at 1.83 MPa and is dominated by slow calcium transients. At 4.65 MPa, the overall percentage of cells responding does not change from 1.83 MPa, but the ratio of fast to slow calcium transient phenotypes does. The ratio of fast is nearly 1:1 with the “slow calcium transient” phenotype making up 54% of the cells responding and the “fast calcium transient” consisting of 46% of the cells responding (Figure 4.4-4C). As with the glia cells, an increase in the peak positive pressure causes an increase in the maximum  $\Delta F/F$  (Figure 4.4-4D). The cell viability changes significantly from 1.83 MPa, where nearly no cells experience necrosis due to pressure exposure, to 4.65 MPa where about 27% of cell die within 10 minutes of pressure exposure (Figure 4.4-4E). Due to the use of simultaneous calcium and propidium iodide imaging, an association between calcium transient phenotypes and their subsequent cell viability can be made. A majority of the cell death occurred in cells initiating a “fast calcium transient” in response to the 4.65 MPa pressure pulse. 55% of all cells exhibiting a “fast calcium transient” phenotype died via necrosis 10 minutes post-pressure exposure, while only 4% of cells exhibiting the “slow calcium transient” phenotype up took the propidium iodide dye (Figure 4.4-4F).

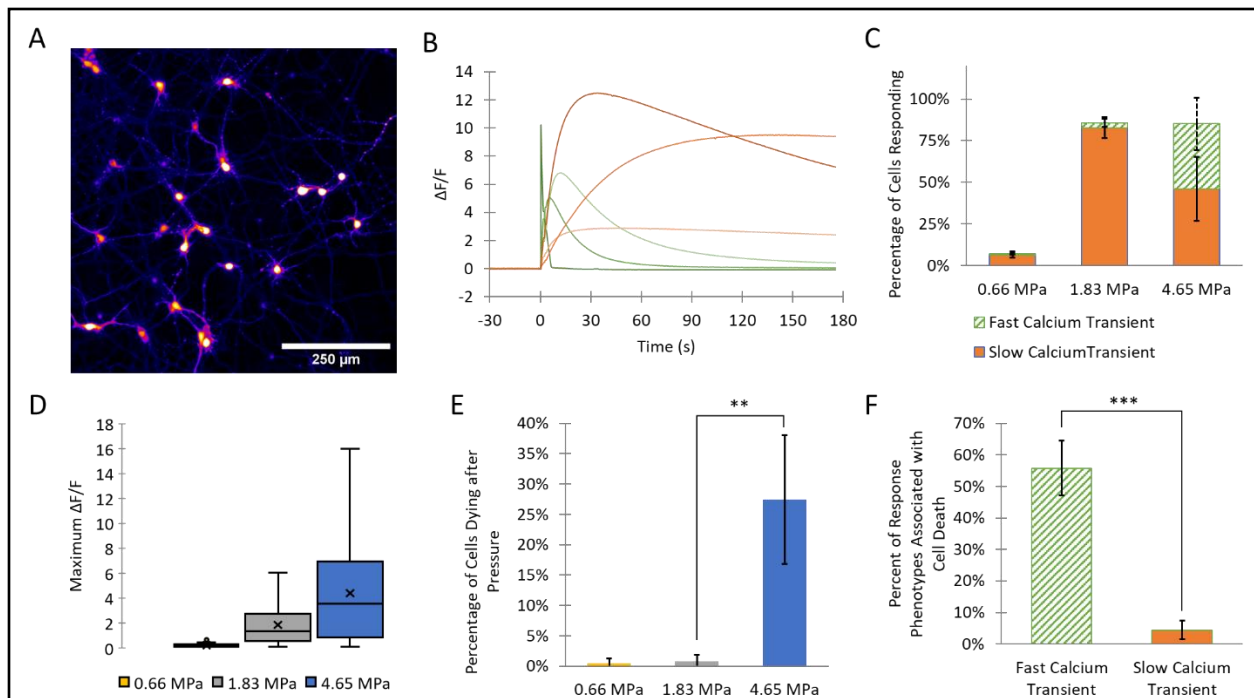


**Figure 4.4-4. Response of primary rat cortical neurons *in vitro* to a high-amplitude, short duration pressure wave.**

(A) 1.5mm by 1.5mm field of view of primary neurons after 4.65 MPa pressure transient with increasing pixel intensity from purple to red to white representing the fluorescence intensity of the calcium indicator dye. (B) Representative calcium responses of neurons to high-amplitude, short duration pressure transients demonstrating two phenotypes of response: 1) calcium responses characterized by a fast calcium transient (green shades) and 2) slow calcium transient (orange shades). Calcium responses shown as the change in fluorescence over initial fluorescence ( $\Delta F/F > 0.1$ ) from 30 seconds prior until 180 seconds post-pressure exposure. (C) Percentage of cells responding ( $\Delta F/F > 0.1$ ) to 3 different pressure amplitudes in the entire field of view and characterized by calcium response phenotype. Durations less than 180 seconds (striped, green) and durations greater than 180 seconds (solid orange). The sum of the two phenotype percentages represents the overall percentage of cells responding. (n=5 dishes per group). (D) Box and whisker plots of maximum  $\Delta F/F$  of activated neurons in response to 3 different pressure amplitudes. (n= <50 cells for 0.66 MPa due to few responders, 500-100 cells for higher pressures) (E) Percentage of cells dying in response to 3 different pressure amplitudes as determined by fluorescent necrosis indicator 1  $\mu$ M propidium iodide. (n=5 dishes per group). (F) The percentage of each calcium response phenotype associated with subsequent cell death after exposure to a 4.65 MPa pressure transient as determined by simultaneous imaging with Calbryte 520 AM and propidium iodide 10 minutes post-pressure on the same cells (n= 5 dishes). Data are reported as mean and SD. Student's t-test (\*\*P <0 .01, \*\*\*P <0 .001).

#### 4.4.4 Comparing the responses of astrocytes, microglia, and neurons to high-amplitude, short-duration blast.

A comparison of the responses of each cell type is provided in Figure 4.4-5. All three cell types increase in percentage of cells responding to pressure as the peak positive pressure is increased (Figure 4.4-5A). A similar percentage of activated cells occurs at the lowest pressure of 0.66 MPa and all cell types are near saturated percent-activated at 1.83 MPa peak positive pressure.

Comparing the percentage of cell that die within 10 minutes of 4.65 MPa pressure exposure using propidium iodide shows a clear difference between neurons and glia (Figure 4.4-5B). Apoptosis stain caspase-3 reveals a small, but significant difference in the percentage of cells that take up the dye 40 minutes after pressure exposure between microglia, 1%, and astrocytes, 5%. The mechanism by which intracellular calcium transient are initiated appears to be largely due to extracellular calcium for both astrocytes and microglia as less than 10% cells activated in the absence of extracellular calcium (Figure 4.4-5C).

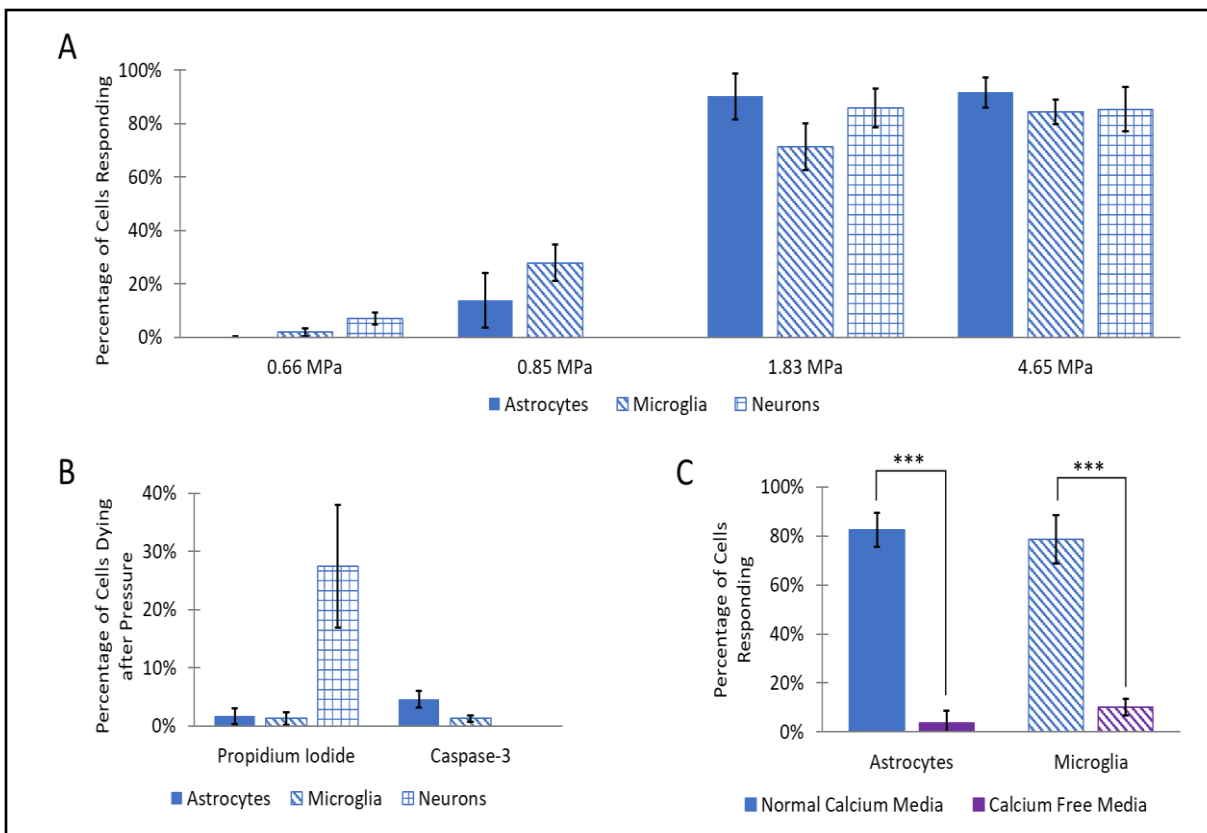
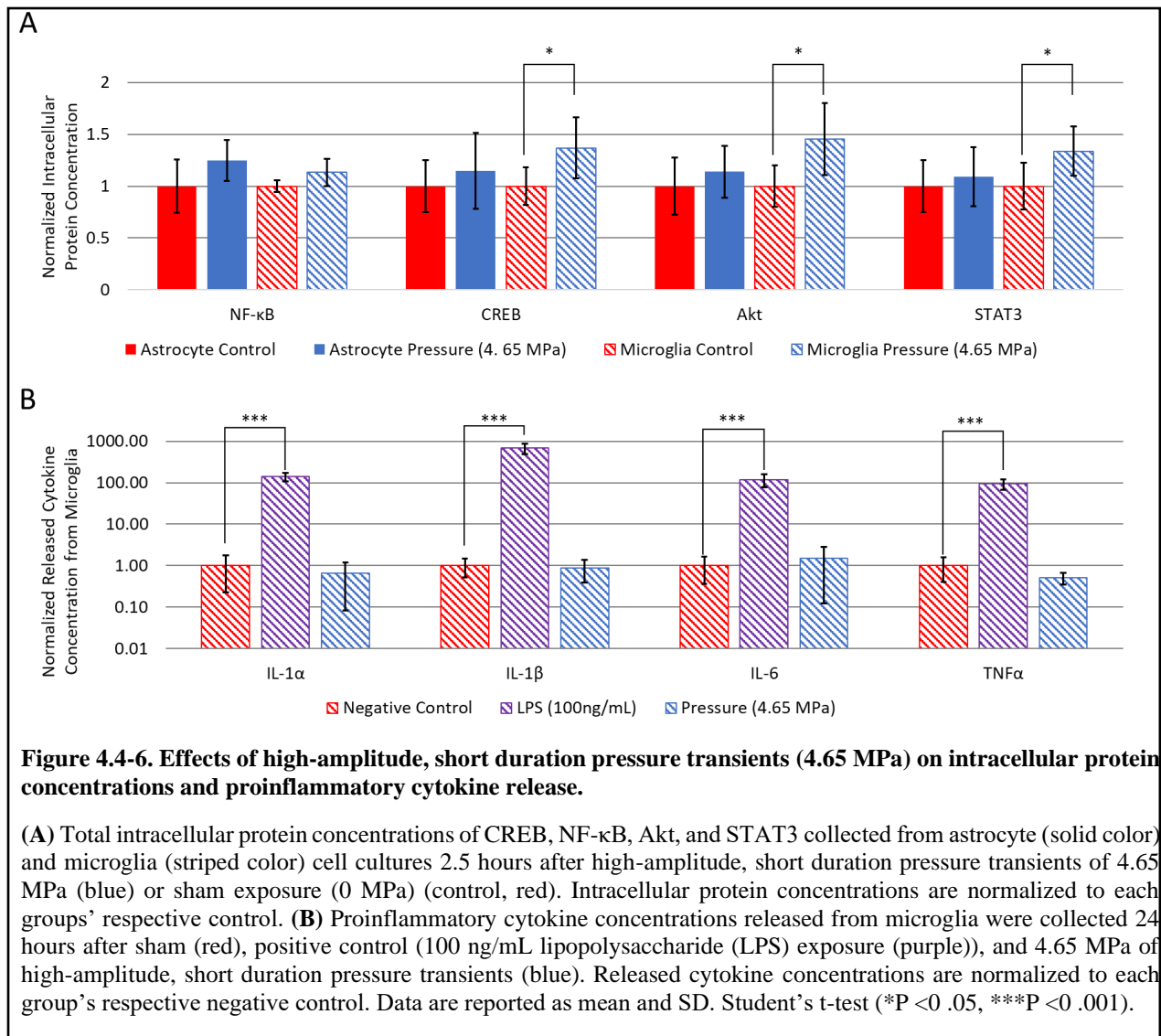


**Figure 4.4-5. Comparison of responses of primary astrocytes, microglia, and neurons to high-amplitude, short duration pressure transients.**

(A) Percentage of astrocytes (solid), microglia (diagonal striped), and neurons (grid) responding ( $\Delta F/F > 0.1$ ) to 4 different pressure amplitudes of 0.66, 0.85, 1.83, and 4.65 MPa peak positive pressures respectively. (B) Percentage of astrocytes, microglia, and neurons taking up necrosis and apoptosis stains in response to 4.65 MPa pressure exposure. (C) Percentage of astrocytes and microglia responding to 4.65 MPa pressure exposure via intracellular calcium transients in normal imaging medium (blue) and in calcium-free imaging medium (purple). Data are reported as mean and SD. Student's t-test (\*\*\*)  $P < 0.001$ .

#### 4.4.5 Immune responses of astrocytes and microglia

Figure 4.4-6 highlights immunological signaling responses of astrocytes and microglia to high-4.65 MPa pressure exposure. Astrocytes produce small but insignificant changes in concentrations of intracellular proteins NF- $\kappa$ B, CREB, Akt, and STAT3 180 minutes after 4.65 MPa pressure exposure. Microglia do not show a significant increase in concentrations of proinflammatory mediator NF- $\kappa$ B due to a 4.65 MPa pressure transient but do have significant ( $p < 0.05$ ) protein concentration increases of 33%, 45%, and 34% in CREB, Akt, and STAT3, respectively, 180 minutes after 4.65 MPa pressure exposure (Figure 4.4-6A). Twenty-four hours after pressure exposure, concentrations of released proinflammatory cytokines IL-1a, IL-1b, IL-6, and TNF $\alpha$  did not significantly change (Figure 4.4-6B) in comparison to a positive control for the pro-inflammatory response of primary microglia (100 ng/mL lipopolysaccharide (LPS) was added to culture media 24 hours prior to collection). The concentrations of the four pro-inflammatory cytokines increased by at least 2 magnitudes in response to 24 hours of LPS exposure.



## 4.5 Discussion

This work aims to better understand the effects of high-amplitude, short-duration pressure transients on different cell types in the brain in the immediate timeframe post exposure through intracellular calcium imaging and short-term immune function assessment.. We have demonstrated 1) a similarity in astrocytes, microglia, and neurons to stimulate intracellular calcium transients to full effect at 1.83 MPa pressure exposure from the described high-amplitude, short duration pressure transients, with nearly no activation at 0.66 MPa pressure exposure, 2) a similarity in astrocytes and microglia calcium transient characteristics in which the increased intracellular calcium quickly rises and falls within ~30 seconds, 3) neuronal calcium transients that are different from the glial calcium transients and in which there are two transient phenotypes of neuronal calcium activation; fast and slow, 4) a similarity in glia cell calcium origination as extracellular calcium is necessary for calcium activation in both microglia and astrocytes, but is not TRP channel dependent in either, 5) a similarity in glia cells in which they are resistant to cell necrosis the first 10 minutes post exposure and apoptosis the first 40 minutes post exposure up to 4.65 MPa high-amplitude, short-duration pressure exposures, 6) a difference between glia and neurons, where pressure transients at 4.65 MPa cause irreversible damage in a significant fraction of neurons but not in glia, 7) a significant increase in microglia intracellular pathway proteins CREB, Akt, and STAT3, but a nonsignificant increase in cytokine precursor NF- $\kappa$ B, and 8) a lack of released proinflammatory cytokine increase of IL-1 $\alpha$ , IL-1 $\beta$ , IL-6, and TNF $\alpha$  24 hours after pressure introduction in primary microglia.

#### 4.5.1 Astrocytes and microglia respond to high-amplitude, short-duration pressure exposures via intracellular calcium transients

Intracellular calcium transients are a ubiquitous second messenger of many physiological responses, it's the spatio-temporal patterning and decoding of the transient that determines downstream implications.<sup>25</sup> The calcium responses of astrocytes and microglia to high-amplitude, short-duration pressure exposures share many similarities, including the percentage of cells responding at varying pressures, time to peak  $\Delta F/F$ , and duration of responses. The trends of increasing maximum  $\Delta F/F$  as pressure increases (until saturation) and increasing duration as pressure increases (until saturation) are present in both glial cells as well. The similarities in spatio-temporal patterning suggest that a common pathway of pressure-induced intracellular calcium transients may exist. As glial cells function to support and maintain the health of the CNS, astrocytes and microglia share many functional pathways. The specific nature of that pathway is not clear, and more work is needed to definitively answer this question.

Current literature on blast-mediated calcium transients suggests purinergic signaling<sup>26</sup> and mechanosensitive channels<sup>27</sup> are the main proponents of calcium activation. Purinergic signaling may not be the target of high-amplitude, short-duration pressure transients due to complimentary observations within this work. The extracellular ATP needed to initiate purinergic signaling is thought to be released from the high concentrations of basal ATP in cells during damage and cell death. In our experiments though our microglial and astrocyte experiments show only limited cell death in monocultures<sup>28</sup>. It is possible that increased extracellular ATP occurs through non-damage mechanisms, but we present no evidence to support this. In general, cell to cell signaling is unlikely to be a cause of the immediate calcium response since the diffusion speed extracellularly<sup>29</sup> is on the order of 10  $\mu\text{m/s}$  and intracellular calcium transients were observed within 11-33 ms post-

pressure. This would result in signaling molecules moving less than 1  $\mu\text{m}$  in that time, which is shorter than cell separations in experiments. A main mechanosensitive family of channels, TRP channels, was determined to have little effect on the ability of astrocytes and microglia to induce intracellular calcium transients after high-amplitude, short-duration pressure transients via broad TRP blocker, ruthenium red; meaning that TRP channels cannot be the sole mechanism of extracellular calcium influx, if they are involved at all. There was a small, but significant decrease in the average maximum  $\Delta F/F$  in the presence of RR for microglia (data not shown) that may suggest a role of TRP channels in maximizing intracellular calcium responses, but the trend of low TRP involvement for initiation purposes remains.

An unexpected result from this work was the observation of localized, subcellular spots of increased intracellular calcium in astrocytes, and to a lesser extent microglia, which manifest themselves as fluorescence ‘hot spots’ within 11-33 milliseconds of pressure exposure (Figure 4.4-1). Given the extracellular origin of this response, one theory for this observation is the induction of micropores or nanopores in the bilipid membrane. As the name implies, nanopores are nanometer sized holes. Qualitatively, the localized spots can appear both near and far from nucleus, and the number of pores can range from one to twenty per cell. A channel-based mechanism would likely occur at many locations throughout the cells. A study<sup>29</sup> on nanoelectroporation-induced calcium transients in mammalian cells demonstrate similar calcium transient characteristics, such as sub-50 second durations and response onset within seconds of stimuli, as this study. Though the sources of calcium were both intracellular and extracellular. Further investigation is needed to better understand the meaning of these localized increases in intracellular calcium to determine calcium origin and functional effects.

#### 4.5.2 Neuronal intracellular calcium responses to high-amplitude, short-duration pressure exposures

Neurons, being the base unit for the entire nervous system, could cause profound, detrimental effects to brain function if affected by high-amplitude, short-duration pressures. Unlike astrocytes and microglia, neurons are non-dividing cells and damage may be permanent due to blast. Unlike the glial intracellular calcium responses at the same pressure exposures, neurons exhibited two phenotypes of calcium transients, especially at 4.65 MPa pressure exposures. The “fast calcium transient” phenotype, while often similar in shape and duration as glial calcium responses, was strongly associated with subsequent cell death via necrosis staining. This is unlike the glial calcium transients as only small changes in cellular viability were observed. The “slow calcium transient” phenotype observed in neurons differs greatly in overall shape and duration from their glial counterparts, suggesting a different physiological pathway may be involved. It is also notable that the two phenotypes may be independent of one another, as the “slow calcium transient” phenotype was observed without large number of cells presenting the “fast calcium transient phenotype”. If true, the dual responses of neurons may be purely a function of the photomechanical insult rather than due to communication between cells. The functions of the neuronal “slow calcium transient” phenotype need further investigation, though known functions of calcium transients in neurons can guide the prediction of potential downstream effects. An obvious role of intracellular calcium transients in neurons is neuroexcitability, but calcium transient with durations over 100 seconds from high-amplitude, short-duration pressure differs greatly from normal neuronal spiking of only a few seconds<sup>11,30</sup>. The origin of high-amplitude, short-duration pressure calcium transients in literature remains unclear, with different studies suggesting extracellular origin<sup>26</sup> and intracellular origin<sup>31</sup>.

#### 4.5.3 High-amplitude, short-duration pressure transients can affect cell viability

Cell death is a major driver of pathology for bTBI. Blast-mediated damage can occur in neurons, astrocytes, and microglia, with a particularly damaging effect on neurons.<sup>32-34</sup> The effects of high-amplitude, short-duration pressure transients on CNS cell health have not been well defined. This work highlights the particular sensitivity of primary neurons to high-amplitude, short-duration pressure exposures as 27% of neurons up took necrosis indicator, propidium iodide, 10 minutes after 4.65 MPa pressure exposure compared to 2% and 1% for astrocytes and microglia, respectively. Only a small percentage of astrocytes, ~5%, and microglia, 1%, showed signs of apoptosis 40 minutes after 4.65 MPa pressure exposure.<sup>35,36</sup> The “fast calcium transient” phenotype of neurons described in this work was highly associated with later necrosis. The short duration of this response may be due to the loss of integrity of the bilipid membrane in which the calcium reporter would no longer be spatially confined. This would result in a decrease in baseline calcium fluorescence after pressure transients, which was observed in a subset of the phenotype responders.

This work suggests death-initiated events, such as astrocyte and microglia reactivity, neuroinflammation, and excitotoxicity<sup>35,36</sup>, may be driven solely by secondary effects from neuronal cell death. This could be further investigated using co-cultures of various CNS cell types to better understand their interconnected responses. A limitation to this work is the cell viability ramifications of high-amplitude, short-duration pressure exposures were investigated for only 40 minutes after pressure exposure. While caspase-3 is a main driver of apoptosis, it is possible that other apoptosis pathways are activated by these pressure characteristics.

#### 4.5.4 Immune signaling responses of microglia and astrocytes to high-amplitude, short-duration pressure transients

Ultimately, the debilitating effects of bTBI are long-term changes in anatomy and physiology, including neuroinflammation and its impact on the brain. The mechanism behind the resultant inflammation has been described as both a direct effect<sup>24</sup> and solely an indirect<sup>37</sup> effect of blast overpressures. Therefore, this work investigated the possible activation of immune response in astrocytes and microglia through the increase of intracellular pathway proteins and release of proinflammatory cytokines. Microglia showed a significant increase in intracellular concentrations of CREB, Akt, and STAT3 when measured 2.5 hours after a 4.65 MPa pressure transient. The significance of these three intracellular proteins is they all can drive microglia into a neuroprotective state: promoting proliferation, suppressing inflammation, clearing dead cells, and aiding neurogenesis and tissue recovery. The impact of STAT3 is more complex as it has pro-inflammatory and anti-inflammatory properties<sup>21</sup>. Other modalities to study TBI converge to a similar finding<sup>8,38,39</sup>, that glial cells initially are neuroprotective after injury, though most findings occurred *in vivo*.<sup>21</sup> In contrast, the proinflammatory precursor NF- $\kappa$ B did not increase significantly in microglia after a high-amplitude, short-duration pressure transient. Further validation of high-amplitude, short duration pressure transients lack of initial proinflammatory response comes as there were no significant changes in released proinflammatory cytokine concentrations, IL-1 $\alpha$ , IL-1 $\beta$ , IL-6, and TNF $\alpha$  24 hours after pressure exposure.

Astrocytes also play an important role in the immune response of the central nervous system. That same immune signaling proteins were quantified for astrocytes and increases in neuroprotective pathway proteins were not observed after pressure exposure. It should be noted that other researchers have found increases in CREB, Akt, and STAT3<sup>40,41</sup> concentrations in

astrocytes after TBI initiation. This discrepancy may be due to the early measurement point of 2.5 hours after pressure exposure and further investigation into the temporal aspect of intracellular pathway protein upregulation would yield similar results.

From this work we propose high-amplitude, short-duration pressure transients stimulate microglial neuroprotective functions within hours after insult. Most TBI literature use an *in vivo* model system to investigate immune and inflammatory responses. The advantage of our experimental design is the isolation of each cells type to determine the direct effects of a pressure transient and eliminates effects of communication between cell types. This work suggests that neuroprotective states may be at least partially activated due to direct overpressure of a blast rather than only responses to neuronal damage or other extracellular signals.

#### 4.5.5 Comparing high-amplitude, short-duration pressure to other blast modalities

The high-amplitude, short-duration pressure transient in this work is used to mimic the initial peak of pressure due to a blast event. The initial peak of explosive blasts in the field has maximum pressures on the order of 10's to 100's of kPa instead of single MPa and durations on the order of single  $\mu$ s rather than sub-100 ns.<sup>42</sup> The need for higher maximum peak pressures is likely due to multiple mechanisms driving the impact of blast on the brain. The multitude of factors that can impact the brain during blast include head acceleration, deacceleration, impulse, and shear strain.<sup>43</sup> The impulse, integral of pressure over time (P•s), is thought to be a main driver of damage.<sup>44</sup> The impulse in this work is 1-2 magnitudes lower than impulses from shock tube needed to induce bTBI.<sup>32</sup> Given this discrepancy, impulse is unlikely to be the sole driver of physiological changes and high-amplitude, short-duration pressure transients likely play a role in determining physiological outcomes. This new-formed knowledge may help to development of new countermeasures of bTBI since either a reduction of the high frequency component of blasts or a

reduction in the high-amplitude, short-duration pressure effects on neurons could potentially lessen severity and frequency of bTBI.

## 4.6 Conclusion

In conclusion, we have demonstrated the impact of high-amplitude, short-duration pressure transients on monocultures of astrocytes, microglia, and neurons and their individual roles in short-term physiological responses. Specifically, we found that 1) a similar percentage of cells from all three types respond to each peak positive pressure tested, 2) astrocytes and microglia respond similarly to high-amplitude, short-duration exposures in calcium transient characteristics, origin of calcium response, and lack of proinflammatory response, 3) microglia drive neuroprotective pathways in response to these pressure transients, 4) neurons initiate two phenotypes of calcium response, one of which is highly associated with cell damage and 5) neurons are most susceptible to immediate cell death following high-amplitude, short-duration pressure transients once the amplitude exceeds a threshold (1.83 MPa). Through this work, we now understand that the initial peak in pressure transients associated with blast may be capable of directly eliciting physiological responses and damage in CNS cells. The negative effects of primary blast may be most driven by damaged neurons and not the neuroinflammatory impact of glial cells. Countermeasures designed to reduce the high frequency component of blast or reduce the neuronal susceptibility to high-amplitude, short-duration component of blast may help reduce the severity and number of bTBIs on the battlefield.

## 4.7 References

1. Frieden, T. R., Houry, D. & Baldwin, G. Traumatic Brain Injury In the United States: Epidemiology and Rehabilitation. *Centers for Disease Control and Prevention* (2015)
2. Ling, G., Bandak, F., Armonda, R., Grant, G. & Ecklund, J. Explosive Blast Neurotrauma. *Journal of Neurotrauma* **26**, 815–825 (2009).
3. Defense and Veterans Brain Injury Center (DVBIC). DoD worldwide numbers for TBI. [https://dvbic.dcoe.mil/system/files/tbi-numbers/worldwide-totals-2000-2018Q1-total\\_jun-21-2018\\_v1.0\\_2018-07-26\\_0.pdf](https://dvbic.dcoe.mil/system/files/tbi-numbers/worldwide-totals-2000-2018Q1-total_jun-21-2018_v1.0_2018-07-26_0.pdf). (2019).
4. NAE Website - TBI Clinical Trials: Past, Present, and Future. <https://www.nae.edu/152165/TBI-Clinical-Trials-Past-Present-and-Future>. (2022).
5. Nakagawa, A. *et al.* Mechanisms of primary blast-induced traumatic brain injury: Insights from shock-wave research. *Journal of Neurotrauma* **28**, 1101–1119 (2011).
6. Vogel, A. & Venugopalan, V. Mechanisms of Pulsed Laser Ablation of Biological Tissues. *Chem. Rev.* (2003)
7. Hicks, R. R., Fertig, S. J., Desrocher, R. E., Koroshetz, W. J. & Pancrazio, J. J. Neurological Effects of Blast Injury. *J Trauma* **68**, 1257 (2010).
8. Bu, W. *et al.* Mild Traumatic Brain Injury Produces Neuron Loss That Can Be Rescued by Modulating Microglial Activation Using a CB2 Receptor Inverse Agonist. *Frontiers in Neuroscience* **10**, 449 (2016).
9. Burda, J. E., Bernstein, A. M. & Sofroniew, M. v. Astrocyte roles in traumatic brain injury. *Exp Neurol* **275**, 305 (2016).

10. Simon, D. W. *et al.* The far-reaching scope of neuroinflammation after traumatic brain injury. *Nature Reviews Neurology* 2017 13:3 **13**, 171–191 (2017).
11. de Melo Reis, R. A., Freitas, H. R. & de Mello, F. G. Cell Calcium Imaging as a Reliable Method to Study Neuron–Glial Circuits. *Frontiers in Neuroscience* **14**, 975 (2020).
12. Brini, M., Calì, T., Ottolini, D. & Carafoli, E. Neuronal calcium signaling: Function and dysfunction. *Cellular and Molecular Life Sciences* **71**, 2787–2814 (2014).
13. Semyanov, A., Henneberger, C. & Agarwal, A. Making sense of astrocytic calcium signals — from acquisition to interpretation. *Nature Reviews Neuroscience* 2020 21:10 **21**, 551–564 (2020).
14. Umpierre, A. D. *et al.* Microglial calcium signaling is attuned to neuronal activity in awake mice. *Elife* **9**, 1–24 (2020).
15. Harteneck, C. & Leuner, K. TRP Channels in Neuronal and Glial Signal Transduction. *Neurochemistry* (2014) doi:10.5772/58232.
16. Kania, E., Roest, G., Vervliet, T., Parys, J. B. & Bultynck, G. IP3 receptor-mediated calcium signaling and its role in autophagy in cancer. *Frontiers in Oncology* **7**, 140 (2017).
17. Lilienbaum, A. & Israël, A. From Calcium to NF- $\kappa$ B Signaling Pathways in Neurons. *Molecular and Cellular Biology* **23**, 2680 (2003).
18. Zhang, J. M. & An, J. Cytokines, Inflammation and Pain. *Int Anesthesiol Clin* **45**, 27 (2007).
19. Wen, A. Y., Sakamoto, K. M. & Miller, L. S. The Role of the Transcription Factor CREB in Immune Function. *J Immunol* **185**, 6413 (2010).

20. Kang, J. Q., Chong, Z. Z. & Maiese, K. Akt1 protects against inflammatory microglial activation through maintenance of membrane asymmetry and modulation of cysteine protease activity. *Journal of Neuroscience Research* **74**, 37–51 (2003).
21. Mao, J. H. *et al.* Microglia polarization in ischemic stroke: Complex mechanisms and therapeutic interventions. *Chinese Medical Journal* **134**, 2415–2417 (2021).
22. Borrachero-Conejo, A. I. *et al.* Stimulation of water and calcium dynamics in astrocytes with pulsed infrared light. *FASEB J* **34**, 6539–6553 (2020).
23. Hernandez, A. *et al.* Exposure to mild blast forces induces neuropathological effects, neurophysiological deficits and biochemical changes. *Molecular Brain* **11**, (2018).
24. Simon, D. W. *et al.* The far-reaching scope of neuroinflammation after traumatic brain injury. *Nature Reviews Neurology* 2017 13:3 **13**, 171–191 (2017).
25. Bagur, R. & Hajnóczky, G. Intracellular Ca<sup>2+</sup> sensing: role in calcium homeostasis and signaling. *Mol Cell* **66**, 780 (2017).
26. Ravin, R. *et al.* Blast shockwaves propagate Ca<sup>2+</sup> activity via purinergic astrocyte networks in human central nervous system cells. *Scientific Reports* 2016 6:1 **6**, 1–14 (2016).
27. Maneshi, M. M., Sachs, F. & Hua, S. Z. A Threshold Shear Force for Calcium Influx in an Astrocyte Model of Traumatic Brain Injury. *Journal of Neurotrauma* **32**, 1020–1029 (2015).

28. Moro, N., Ghavim, S. S. & Sutton, R. L. Massive efflux of adenosine triphosphate into the extracellular space immediately after experimental traumatic brain injury. *Experimental and Therapeutic Medicine* **21**, (2021).
29. Bo, W. *et al.* Probing Nanoelectroporation and Resealing of the Cell Membrane by the Entry of Ca<sup>2+</sup> and Ba<sup>2+</sup> Ions. *International Journal of Molecular Sciences* 2020, Vol. 21, Page 3386 **21**, 3386 (2020).
30. Ali, F. & Kwan, A. C. Interpreting in vivo calcium signals from neuronal cell bodies, axons, and dendrites: a review. *Neurophotonics* **7**, 011402 (2019).
31. Gomez Godinez, V. *et al.* High-amplitude, short-duration Shockwave (LIS) to Study Neuronal Ca<sup>2+</sup> Responses. *Frontiers in Bioengineering and Biotechnology* **9**, 97 (2021).
32. Miller, A. P. *et al.* Effects of Blast Overpressure on Neurons and Glial Cells in Rat Organotypic Hippocampal Slice Cultures. *Frontiers in Neurology* **6**, (2015).
33. Miller, A. P. *et al.* Acute death of astrocytes in blast-exposed rat organotypic hippocampal slice cultures. *PLoS ONE* **12**, (2017).
34. Rama Rao, K. v. *et al.* A single primary blast-induced traumatic brain injury in a rodent model causes cell-type dependent increase in nicotinamide adenine dinucleotide phosphate oxidase isoforms in vulnerable brain regions. *Journal of Neurotrauma* **35**, 2077–2090 (2018).
35. Carson, M. J., Cameron Thrash, J. & Walter, B. The cellular response in neuroinflammation: The role of leukocytes, microglia and astrocytes in neuronal death and survival. *Clinical Neuroscience Research* **6**, 237–245 (2006).

36. Karve, I. P., Taylor, J. M. & Crack, P. J. The contribution of astrocytes and microglia to traumatic brain injury. *British Journal of Pharmacology* **173**, 692–702 (2016).
37. Gama Sosa, M. A. *et al.* Lack of chronic neuroinflammation in the absence of focal hemorrhage in a rat model of low-energy blast-induced TBI. *Acta Neuropathol Commun* **5**, 80 (2017).
38. Bhat, S. A. *et al.* Enhanced Akt/GSK-3 $\beta$ /CREB signaling mediates the anti-inflammatory actions of mGluR5 positive allosteric modulators in microglia and following traumatic brain injury in male mice. *J Neurochem* **156**, 225–248 (2021).
39. Zheng, Z. V. *et al.* Novel role of STAT3 in microglia-dependent neuroinflammation after experimental subarachnoid haemorrhage. *Stroke and Vascular Neurology* **7**, 62–70 (2022).
40. Chiareli, R. A. *et al.* The Role of Astrocytes in the Neurorepair Process. *Frontiers in Cell and Developmental Biology* **9**, 1304 (2021).
41. LeComte, M. D., Shimada, I. S., Sherwin, C. & Spees, J. L. Notch1-STAT3-ETBR signaling axis controls reactive astrocyte proliferation after brain injury. *Proc Natl Acad Sci U S A* **112**, 8726–8731 (2015).
42. Misistia, A. *et al.* Sensor orientation and other factors which increase the blast overpressure reporting errors. *PLOS ONE* **15**, e0240262 (2020).
43. Bryden, D. W., Tilghman, J. I. & Hinds, S. R. Blast-Related Traumatic Brain Injury: Current Concepts and Research Considerations. *Journal of Experimental Neuroscience* **13**, (2019).

44. Blast Injuries and Blast-Induced Neurotrauma. *Brain Neurotrauma: Molecular, Neuropsychological, and Rehabilitation Aspects* **45** (2015).

## **Chapter 5**

### **Summary and Concluding Remarks**

## 5.1 Summary and Major Conclusions

### 5.1.1 Summary

The overall goal of this dissertation was to uncover the impact of directed energies on CNS immune cell function and pro-inflammatory immune signaling. The parameter space of directed energies could be infinite, therefore we focused on parameters relevant to potential modulators for inducing or treating neurological chronic diseases. Specifically, known photothermal parameters were used to block the propagation of pain-carrying neuronal signals, and photomechanical parameters used simulate a component of explosion blast pressure transients experienced by service men and women on the battlefield. Understanding the impact of these photothermal and photomechanical stimuli on immediate physiological change indicators and short-term pro-inflammatory immune signaling could further the development of preventions or treatments of chronic pain and blast-induced traumatic brain injury (bTBI); two neurological chronic disease processes that are in urgent need of improved prophylactics and therapeutics.

Chapter III aimed to characterize the impact of infrared neural inhibition (INI)-specific photothermal effects on microglia *in vitro*. Microglial inflammatory immune signaling plays a critical role in the chronification of pain. Understanding the impact of pulsed IR on microglial physiology will produce insights into the potential long term beneficial or detrimental nature of INI on immune signaling. Widefield calcium imaging uncovered three distinct calcium transient phenotypes, ranging from 20 seconds to 20 minutes in duration, which initiate within one second of full-dose pulsed IR exposure. The three distinct intracellular calcium transient phenotypes (“low energy”, “high energy”, “death”) were associated with statistically significant, distinct temperature rises (16.7 °C, 19.7 °C, and 35 °C, respectively) and radiant exposures (540 J/cm<sup>2</sup>, 714 J/cm<sup>2</sup>, and 1410 J/cm<sup>2</sup>, respectively). Plate-reader calcium imaging measured subsequent ligand-

transmembrane channel activation (capsasin-TRPV1 activation), which showed attenuated intracellular calcium responses by a pre-exposure of pulsed IR from 5 to 15 minutes prior to ligand introduction. This effect was found at temperature rises over  $\sim 18$  °C from room temperature and radiant exposures over  $44 \text{ J/cm}^2$ . Heat sensitive channel TRPV1 was investigated for its role in this phenomena, but was determined to play only a small role in pulsed IR-induced basal calcium increases.

Ultimately, the impact of pulsed IR on pro-inflammatory immune response was the focus of this chapter, since increased pro-inflammatory cytokine release may suggest a detrimental impact of INI on innate immune function. Concentrations of released pro-inflammatory cytokine IL-6 from basal BV2 cells measured at 4 hours post-exposure did not significantly change after pulsed IR exposure; suggesting INI may not induce an inflammatory response. Surprisingly, the short duration pulsed IR train (40-80 seconds) reduced the concentrations of released IL-6 when microglia were given a pre-exposure of pulsed IR prior to innate immune insult; suggesting that pulsed IR may prevent pro-inflammatory immune signaling after insult. While microglial immune activity and inflammatory signaling are important aspects of their function, it was critical to show that pulsed IR did not cause non-reversible damage. Pulsed IR did not induce necrosis or apoptosis at radiant exposures and temperatures needed to induce calcium transients but did reduce cell viability by up to 20% after pulsed IR exposure for cytokine quantification experiments. The reduction in cytokine release ( $\sim 95\%$ ) was much greater than the loss of cell viability.

Chapter IV aimed to identify the impact of blast-like photomechanical effects on neuroimmune function *in vitro*. Explosive blast overpressure consists of a microsecond initial peak in positive pressure followed by a millisecond exponential-like decay. The former component of explosive blast can be simulated by laser-induced pressures. Unlike the previous chapter where

neuronal responses to similar photothermal parameters had been well characterized previously<sup>1-4</sup>, the impact of high-amplitude, short-duration pressure transients on any CNS cell type were unknown. Therefore, this chapter focused on understanding the impact of high-amplitude, short-duration pressure transients on neuronal, astrocytic, and microglial functions and the associated inflammatory immune signaling.

Using fast, widefield calcium imaging, each cell type was found to illicit intracellular calcium transients at similar peak positive pressures; with near full community response (~80%) at 1.83 MPa and low community response (<10%) at 0.6 MPa. The glial cells, astrocytes and microglia, shared similar characteristics in their pressure-induced calcium transient phenotypes, extracellular origin of calcium transients, and levels of induced damage at less than 5%. Neuronal calcium responses exhibit two intracellular calcium transient phenotypes: “fast” and “slow”. The percentage of cells presenting each phenotype varied as the pressure increased. At 1.83 MPa, the dominate calcium response phenotype was “slow”. While at 4.65 MPa, the “fast” and “slow” phenotypes were nearly 1:1 in percentages of cells responding. A fluorescent necrosis stain identified that cells responding with the “fast” phenotype were highly associated with necrosis (55% of cells with this phenotype) within 10 minutes of exposure, but not the “slow” phenotype.

Using multiplex assays for protein quantification, immune signaling response of microglia to 4.65 MPa pressures indicated a lack of pro-inflammatory signaling in four major cytokines 24 hours after pressure exposure. Similarly, concentrations of pro-inflammatory mediator NF- $\kappa$ B were not upregulated at 2.5 hours after 4.65 MPa pressure exposure in neither astrocytes nor microglia. Statistically significant upregulation of CREB, Akt, and STAT3 in microglia occurred 2.5 hours after 4.65 MPa pressure exposure; highlighting the potential neuroprotective role of microglia in response to high-amplitude, short-duration pressure transients.

### 5.1.2 Major Conclusions

In summary, this dissertation set out to uncover the impact of directed energies on CNS immune cell function and pro-inflammatory immune signaling; motivated by the lack of safe, effective prophylactics and treatments for chronic pain and bTBI. Certain persistent symptoms of either can be traced to chronic inflammatory origins. The work contained in this dissertation highlights the impact of treatment-relevant photothermal exposures on the broad modulation of microglial physiology and altering pro-inflammatory signaling in basal and pro-inflammatory phenotypical states. The major conclusions from chapter III are **proposed mechanisms of action in which the temperature rise associated with pulsed IR 1) induces multiple, distinct intracellular calcium transient phenotypes that are associated with varying temperature rises, 2) which reduces the effects of innate immune receptor targeted danger signals, and 3) results in a reduction of pro-inflammatory immune signaling after innate immune insult**. In cell culture, the temperature rise necessary to trigger BV2 physiology changes was 15-25 °C from room temperature (20 °C). To the author's knowledge, this was the first evidence of acute photothermal exposures modulating a source of the chronification of pain; pro-inflammatory cytokine release.

This work also highlights the impact of photomechanical, high-amplitude, short-duration pressure transients on CNS cell intracellular calcium responses and inflammatory immune signaling. The major conclusions from this work are **1) high-amplitude, short-duration pressure transients directly induce physiological responses in neurons, astrocytes, and microglia at comparable peak positive pressures, 2) neurons are more susceptible to high-amplitude, short-duration pressure-induced damage than astrocytes and microglia, and 3) microglia do not initiate pro-inflammatory precursors in response to high-amplitude, short-duration,**

**pressure transients, but rather indicate a potential activation of neuroprotective immune signaling pathways.** A novel mechanism of extracellular calcium entry in CNS cells after high-amplitude, short-duration, photomechanical pressure may have been discovered, but further experimentation would be needed before such a claim could be made. To the author's knowledge, this is the first comprehensive study on the immunological impact of high-amplitude, short-duration, photomechanical pressure transients on neurons, astrocytes, and microglia in isolation.

## 5.2 Implications

### 5.2.1 Directed energies share similarities in microglial response while biophysical mechanisms may vastly differ

Through this work, a trend became evident from microglial physiological responses and pro-inflammatory immune signaling after directed energy exposure. Both photothermal and photomechanical stimuli induced intracellular calcium transients that share spatio-temporal characteristics, revealed a lack of pro-inflammatory immune signaling, responded in a dose-dependent manner, and induced calcium transients below damage thresholds.

Intracellular calcium transients are a highly sensitive indicator of a wide range of physiological changes. The exact pathways that are initiated by pressure-induced intracellular calcium transients can be difficult to determine and usually need substantial pharmacological studies and knock-out models to confirm the mechanisms. The spatio-temporal patterning of intracellular calcium response plays a role in driving the functional outcome. Both photothermal and photomechanical exposures induced a dose-dependent intracellular calcium response in microglia. A subset of calcium responses shared similarities in calcium transient phenotype, which is characterized by a near-immediate increase in intracellular calcium which peaks within 15 seconds of exposure and then falls to near baseline levels of intracellular calcium within 60 seconds of onset. This commonality implies a potentially similar functional outcome of these responses. This argument is strengthened by the observation of similar functional output in terms of pro-inflammatory immune signaling, as described in the next paragraph. It should be noted that calcium alone does not dictate the functional outcome, but also the position, concentration, and modulation of calcium-sensing elements. A difference between these two directed energies is that

photothermal exposure induces two distinct intracellular calcium transient phenotypes, while only one intracellular calcium transient phenotype was observed by the photomechanical parameters used.

Heat and pressure can have detrimental effects on the health of the brain and spinal cord<sup>5-7</sup>. However, both directed energies investigated showed a lack of pro-inflammatory immune signaling at sub-damage activation thresholds. Photothermal effects of BV2 cells indicated a lack of initial pro-inflammatory signaling up to temperature rises able to damage the cells. Photomechanical effects of primary microglia demonstrated a lack of initial pro-inflammatory immune signaling up to pressure amplitudes able to damage neurons. Furthermore, there is evidence that these directed energies trend toward anti-inflammatory immune signaling. Chapter IV found potential evidence of microglia driving toward anti-inflammatory physiology after photomechanical exposure through the upregulation of CREB, Akt, and STAT3. While these three proteins are associated with a number of intracellular pathways, they have been associated with neuroprotective signaling after TBI.<sup>8</sup> After photothermal exposure, the LPS-stimulated BV2 cells showed a reduction in pro-inflammatory cytokine concentrations, which is not necessarily neuroprotective but rather trending away from neurotoxic. Other studies have found the effect of long-term hyperthermia of microglia to similarly reduce IL-6 release after innate immune insult, but also demonstrated an increase in anti-inflammatory cytokine, IL-10.<sup>9</sup> While the heating parameters were much different between these studies, the trend of driving anti-inflammatory immune signaling may remain for pulsed IR.

While the measured responses from each directed energy share similarities in driving the inflammatory response away from pro-inflammatory, the mechanisms of activation may diverge. Firstly, the temporal and spatial extent of each stimuli is much different. In this work, the

photothermal effects were driven using sub-cm spatial resolution and temporal resolution on the order of 10's of seconds. Conversely, the photomechanical stimuli were expanding pressure waves that would impact cells for sub- $\mu$ s. There are channels, such as TRP channels, that can be both temperature and pressure sensitive. Though this family is unlikely to be a major driver of these similarities since both chapters III and IV show the use of TRP blockers to have little effect on calcium transients. There may be other cellular components that are similarly impacted by both directed energies or the mechanisms may converge further downstream.

### 5.2.2 Potential therapeutic target for infrared neural inhibition

Infrared neural inhibition (INI) has been investigated for the past decade as a technique to block neural transmission associated with pain. It differentiates itself from other neuromodulation techniques by its proposed mechanism of modulating voltage-gated potassium channels<sup>4</sup> and small axon diameter fiber selectivity<sup>2</sup>. Yet another differentiating aspect of INI may be through its impact on pro-inflammatory immune signaling. The parameters used for this dissertation slightly differ from the classical INI parameters. This dissertation found that pulsed IR parameters resulting in temperature rises of 15-25 °C from room temperature (20 °C) for 10's of seconds impacted pro-inflammatory signaling, while for INI, temperature increases as low as 3-6 °C from 37 °C for second(s) could impact neural conduction. If the effects of both functional outcomes are due to a temperature threshold, rather than a temperature gradient, there is a striking similarity in temperature thresholds need to impact cellular physiology of 40-45 °C. As mentioned, evidence points toward voltage-dependent potassium channel modulation as a mechanism for neural inhibitory effects of pulsed IR. Interestingly, voltage-dependent potassium channels in macrophages are necessary for LPS-induced cytokine production<sup>10</sup> and may play a role in the inhibition of cytokine release by pulsed IR.

Findings from this chapter are 2-fold: 1) pulsed IR exposure did not increase pro-inflammatory cytokine release in basal microglia and 2) LPS-stimulated microglia showed a reduction in released IL-6 after pulsed IR. The former finding suggests that INI does not induce pro-inflammatory cytokine signaling in microglia, which is essential for the continued development of INI towards clinical relevance. The later finding suggests a new potential target for pain modification by INI. Therefore, pulsed infrared light has the potential to intervene not only in the symptomatic experience of chronic pain but also provide disease modification through targeting pro-inflammatory immune signaling.

### 5.2.3 Acute heating in the brain induced by other directed energies

Parameters of heating are likely import in modulating physiology, as seen by the Arrhenius model, in which thermal damage is a consequence of the temperature and duration of elevated temperatures.<sup>11,12</sup> If the dependance on temperature and time is also driving the temperature-induced sub-damage inflammatory effects, then other heating modalities may also impact inflammatory immune signaling. Certainly, thermal directed energies have had more utility than just blocking pain signals in preclinical models, since there are clinically relevant thermal-mediated therapies and unintended heating from therapies and diagnostics. A thermally mediated therapy that shares similarities in the modality and parameters used in this dissertation is laser interstitial thermal therapy (LITT), a minimally invasive surgical procedure that uses thermal ablation to destroy unhealthy brain tissue, such as cancer or epilepsy centers.

The clinical LITT heating parameters can vary depending on device and context of the surgery. In general, the temperature required for thermal ablation is over 43 °C, but some LITT can generate temperatures up to 90 °C with a duration on the order of minutes<sup>13</sup>. Thermal ablation occurs earlier for high temperatures and later for lower temperatures. This dissertation has

demonstrated a temperature rise of 15 °C to 25 °C in 10's of seconds is needed for reduction of pro-inflammatory immune signaling. There are many tissue and cellular differences between the rodent cell culture-based temperature changes from this work and pathological human brain, so further investigation is needed for fully understand the relevance of this dissertation's findings for LITT clinical use and development.

The zone outside of the non-reversible thermal damage area from LITT experiences temperature increases as well, but the inflammatory ramifications are not well understood. This dissertation suggests that temperature rises below 40-45 °C in the surrounding zones may not induce pro-inflammatory immune responses and may reduce pro-inflammatory immune signaling in ablation of cancer, which itself induces characteristic abnormal inflammation. Results in this dissertation suggest that pro-inflammatory cytokines are not produced up to a temperature increase necessary to impact cell viability, which may suggest the LITT surrounding zone may not have induced pro-inflammatory immune signaling from non-damaging temperature rise. Though, this dissertation did not investigate the later effects of cell-cell communication that may well influence delayed pro-inflammatory cytokine release. A potential application of findings from this dissertation is to pre-dose or prime the pathological area and surrounding areas with heat prior to LITT ablation to induce a potential neuroprotective environment, as will be discussed in Section 5.3.

#### 5.2.4 Mechanism behind pressure-induced calcium transients

In Chapter 4, the findings included the appearance of localized, subcellular spots of increased intracellular calcium that occurred at the earliest measurable time points of imaging (11-33 ms) in the astrocytes and microglia. The intracellular calcium transients were found to be of extracellular origin since calcium transients could not be initiated when calcium was taken out of

the imaging media. A potential theory of the mechanism behind the calcium “hot spots” is inducing poration in the bilipid membrane from the high-amplitude, short-duration pressure transients. Intense intracellular calcium transients would likely occur cause poration due to both chemical and electrical gradients between the extracellular and intracellular spaces. There is a ~7 magnitude difference<sup>14</sup> in concentrations of extracellular calcium as opposed to intracellular calcium in astrocytes, making diffusion a likely contributor to calcium entry through non-selective holes in the membrane. Similarly, astrocytes have a resting membrane potential from -50 to -70 mV, yet then Nernst potential for calcium is +130 to +140 mV. Therefore, there is a large driving force (> 180 mV) for calcium to enter the cell through pores in the membrane.

Other qualitative evidence suggests poration may be a mechanism. The location of the calcium entry spots occurred at the astrocyte end feet, as well as more centrally, suggesting it is not a channel membrane that is location specific. Other researchers have shown that nanoporation can induce calcium transients that share many characteristics as those observed from high-amplitude, short-duration pressure transients, such as durations below 50 seconds and a calcium response initiation within a second of stimulus.<sup>15</sup> Laser-induced pressure has been investigated for its potential to permeabilize bilipid membranes in non-CNS cells with unclear findings. Some studies have found permeabilization<sup>16</sup>, while others have not<sup>17</sup>, suggesting other factors may be important. Further investigation is needed to better understand the meaning of these localized increases in intracellular calcium to determine calcium origin and functional effects.

#### 5.2.5 Isolation of initial peak of explosive blast

A blast overpressure usually consists of an initial peak pressure on the order of 10’s to 100’s of kPa that maximizes within a few microseconds followed by an exponential-like decay to near baseline. The majority of research looking at mechanisms and consequences use pressure

transients that mimic those characteristics of blast<sup>18,19</sup>. An important component of blast that is largely ignored is the initial microseconds of peak pressure at the onset of the pressure transient. Laser-induced pressures allow for an isolation of the initial peak of pressure to better understand its impact on neuronal and glial responses and viability. This dissertation found that higher peak pressures (>1 MPa) are needed for non-damaging intracellular calcium transient initiation than what other modalities need to induce neuronal damage. This may be due to multiple mechanisms of pressure-induced physiological and viability changes that are unrelated to the mechanism behind this work. Other studies suggests that many of the effects from blast are due to the impulse (integral of the pressure-time wave) of the pressure transient, though this dissertation suggests that high-amplitude, short-duration transients can impact physiology at impulses 10-100 times lower. To confirm the relevance of this dissertation's findings from high-amplitude, sort durations pressure transients, investigation is needed from more blast-representative techniques, such as shock tube. Therefore, laser-induced pressures should be used as a complement to other techniques in efforts to determine primary blast effects.

#### 5.2.6 Initial pro-inflammatory immune signaling effects from blast are unlikely to drive bTBI pathology

A major advantage of monoculture-based research is the isolation of cellular effects away from the influence of other cell types. Cell isolation allowed this dissertation to compare and contrast the pressure-induced effects on three main CNS cell types: neurons, astrocytes, and microglia. Given the central role microglia play in the CNS, a focus of this work was the pro-inflammatory immune response of microglia to directed energies. Microglia did not induce pro-inflammatory immune signaling via IL-1 $\alpha$ , IL-1 $\beta$ , IL-6, nor TNF $\alpha$  in response to the largest high-amplitude, short-duration pressure transients tested. Investigation into the intracellular mediators

of the inflammatory immune response found a nonsignificant increase in pro-inflammatory mediator NF- $\kappa$ B after 2.5 hours, which agrees with the lack of pro-inflammatory cytokine response. Rather, significant increase in CREB, Akt, and STAT3 concentrations were measured 2.5 hours after the highest peak pressure exposure. These three intracellular pathway proteins have an association with downstream neuroprotective responses, including morphological state changes and the release of anti-inflammatory cytokines.<sup>8</sup> In contrast, the same peak positive pressures that are non-damaging and potentially neuroprotective for microglia were found to be damaging to neurons through the uptake of a necrosis indicator, propidium iodide.

Other modalities that more accurately demonstrate an explosive-like blast have found a similar finding in initial neuroprotective signaling, though usually *in vivo*. The initial response of glia tends to express neuroprotective qualities rather than neurodegenerative qualities. While microglia are likely neuroprotective initially, they can functionally change to a pro-inflammatory state days after an explosive blast. The results from this dissertation suggest that high-amplitude, short-duration pressure transients are capable of inducing physiological change through induced intracellular calcium transients that are unrelated to pro-inflammatory immune signaling response. Furthermore, evidence suggests that microglia may be initially driven into a neuroprotective state. A potential theory that arises from this work is chronic inflammatory responses associated with bTBI may be driven by immune responses to damaged and unhealthy neurons rather than a direct response of primary blast on microglia. Further investigation into the high-amplitude, short-duration pressure transients on later inflammatory immune signaling and communication between cell types is needed to strengthen this theory.



### 5.3 Future Directions

This dissertation has focused on understanding the impact that directed energies have on the central nervous system in the context of inflammatory immune signaling and broad physiological changes. While this work has provided insights into photothermal and photomechanical effects potentially driving inflammatory immune signaling away from pro-inflammatory phenotypes, there are many questions that remain and many potential paths to continue this research into the future. Potential future projects will be discussed in this section.

#### 5.3.1 Photothermal effects on Spinal Cord *ex vivo*

As discussed at great lengths, this work discovered the potential utility of pulsed infrared light to prevent initiation of pro-inflammatory immune signaling after innate immune insult. This discovery was made in an immortalized cell line at room temperature in the absence of other cell types to form the neuroimmune interface. To better determine the legitimacy, robustness, and impact of pulsed IR in reducing pro-inflammatory signaling, a study should aim to investigate the reduction of pro-inflammatory cytokines in a higher order model with immune and cell environments closer to *in vivo* human. Acute *ex vivo* rodent spinal cord<sup>163</sup> would be an ideal model to use as the next step in development given its reduction in animal suffering (compared to *in vivo*), ease of access to relevant spinal regions of interest, relatively thin<sup>164</sup> for improved light penetration, and less acute damage and subsequent immune response in regions of interest (compared to a slicing protocol, as discussed in Appendix B). The leading research question for this future direction is: **Does pulsed IR light impact inflammatory immune signaling in heated, rodent, *ex vivo* spinal cord before and after innate immune insult?** If the answer is yes, then I would propose further advancement of this research into *in vivo* animal models to confirm previous

results, investigate the time aspect of pro-inflammatory cytokine reduction, and uncover the potential pain relief of this technique.

Firstly, a physiological response, perhaps through intracellular calcium transients, of microglia to the photothermal stimuli would need to be confirmed to verify the correct light and thermal parameters in this unexplored setup. A region of interest for this is the spinal dorsal horn because central sensitization can occur at the synapse between the nociceptive sensory neuron and the second-order nociceptive projection neuron.<sup>2</sup> To determine the prevention of a pro-inflammatory immune signaling response, innate immune insult can be initiated either through an induced chronic injury *in vivo* or with LPS within an *ex vivo* setup<sup>25</sup>. Both approaches should be used as they can help answer different questions. An induced chronic injury would be more representative of an innate insult and could detail the impact of pulsed IR on halting or reversing inflammatory signaling after it had already been induced. This question was not answered through the work in this dissertation but could widen the potential utility of pulsed IR immensely. Tissue can then be excised and processed for protein quantification by either ELISA or multiplex array to determine the consistency of results in this setup. An area that begs for more exploration is the ability of pulsed IR or heat to reverse the pro-inflammatory immune response after chronic inflammation has already occurred, which was not addressed in this dissertation. This is likely a more clinically impactful use of pulsed IR as preventing inflammation means it must be predicted rather than have already occurred.

Another aspect of great interest is the potential synergy in using pulsed IR to both inhibit the propagation of a pain signals and reverse pro-inflammatory responses to eliminate the source of chronic pain. An *ex vivo* spinal cord setup could be used for electrophysiology studies concurrent with inflammatory response studies.<sup>166</sup> Stimulation and recording electrodes upstream

and downstream of the dorsal root ganglia or dorsal root horn could measure the transmission of neural signals, which would imitate nociceptive signals in this context. If prior inflammation was induced in this setup, the tissue could be processed post-experiment to determine pro and anti-inflammatory immune signaling responses in response to pulsed IR parameters used in INI. This could help prove the dual purpose of pulsed IR to impact chronic pain from multiple mechanisms.

Lastly, this may be an ideal setup to test the safety and efficacy of other heating modalities. Of particular interest for nerve inhibition is a heated coil nerve cuff, similar to a prototype designed and built by Junqi Zhuo in the Dr. Michael Jenkins lab at Case Western Reserve University. While pulsed IR light has certain innate advantages, other modalities benefit from great penetration in biological tissue and are more energy efficient. Techniques such as focused ultrasound may allow for heating to originate outside the body, rather than need an implanted device. As this research progresses into larger animal models and human models, I would suggest further analysis into the proper technique to induce heating that are practical, efficacious, and safe.

### 5.3.2 Photothermal effects on inflammatory response during LITT

This dissertation focused on the role of photothermal effects on inflammatory signaling which makes its particularly translatable to other laser-based heating methods with similar time, space, and thermal characteristics used in the brain. One such technique is laser interstitial thermal therapy (LITT) which involves precise thermal ablation of targeted brain structures, such as a brain tumor, basal nuclei for epilepsy, or radiation necrosis<sup>26</sup>. Radiation necrosis is a severe local tissue inflammatory reaction that occurs 3-12 months after the completion of radiation therapy for metastatic brain tumors.<sup>27</sup> It is a common side effect that affects 5-9% of patients undergoing radiation therapy for metastatic brain tumors.<sup>28</sup> LITT is gaining prominence in the treatment of radiation necrosis for the ablation of the necrotic lesions. A temperature threshold must be met for

necrosis to occur and the surgical outcome to be successful. During this process there is a layer outside the coagulated tissue that experiences an acute temperature increase that does not coagulate, yet little is known about the impact of these sub-coagulation temperature rises within neurodegenerative brain environments. To realize a direct clinical impact of this work, a study could be performed with a goal to understand the impact of temperature rises on inflammatory immune signaling and downstream inflammation within the context of LITT.

The impact of LITT on the inflammatory response is not well known, and given this dissertation, there may be unintended benefits of temperature rise in the surrounding layers which may be anti-inflammatory in nature. The guiding question for this future direction is: **Is there an inflammatory response in the non-coagulated layer of brain tissue after LITT?** To best understand the thermal impact on inflammatory immune responses, current large animal models used to investigate radiation necrosis should be explored, with a particular emphasis on the brain region impacted, as well as the time between necrosis initiation and LITT application. Using this model, I propose a study in which LITT is applied to the radiation necrosis zone of each subject in 3 experimental groups: sham, temperature threshold, and sub-temperature threshold. A sub-temperature threshold group may be useful in to demonstrate a potential impact of sub-threshold heating to reduce radiation necrosis-related inflammation, which alone may be used to treat radiation necrosis. There are a few paths that this research could follow to quantify the impact of LITT, but I suggest that tissue in and around the radiation necrosis be excised and protein analysis on cytokines and precursors, as well as inflammation quantification, such as T cell counting, should occur. Special attention should be placed on accurately and repeatedly being able to extra a specific thickness of outer-layer shell. I would suggest creating a Monte Carlo model to feed a heating model to best determine the appropriate tissue thickness within a temperature rise range.

This method would give an objective metric for inflammatory impact of LITT rather than a behavioral marker for improvements in the brain. The timing of tissue extraction will impact the relevance of the results, as longer periods between therapy application and tissue extraction may be most clinically relevant.

The impact of this research would better define the impact of heating, but not coagulating, brain tissue. If the inflammatory status of the region becomes anti-inflammatory, then LITT may play a role in reversing the often-inflammatory states during radiation necrosis and tumors. Similar to the potential for INI to impact chronic pain through two mechanisms, LITT may innately impact multiple mechanisms through tissue heating. Furthermore, demonstrating a positive impact of acute heating in this clinical setting may accelerate the acceptance of INI application in the CNS.

### 5.3.3 Origin and function of calcium transients in neurons, astrocytes, and microglia after photomechanical exposure in a less rigid environment

Cell-culture methods with cells attached to glass introduce a rigid barrier in photomechanical stimuli experiments; potentially inducing larger shear stresses on cells than would not be experienced in an *in vivo* model. The shear stress may impact the origin of calcium entry into the cell as well as the functional meaning behind the calcium transients. A model system with cells in a three-dimensional orientation may better reflect the response of cells in *in vivo* settings, which may require different intensities of pressure to induce physiological changes. To better understand the impact of the initial peak in blast pressure, calcium imaging should be performed on a multi-cell setup with less rigid attachment points. The research presented in this dissertation initially used a Mylar film-based dish for cell plating and imaging to achieve the above goals, but imaging artifacts and cell health concerns thwarted those efforts. There are other options to create a less rigid barrier, such as Matrigel, that may perform better than Mylar film. A

comparison between calcium transients induced between a glass-based system and a non-rigid system may give insights into the “best practices” for *in vitro* bTBI research as well as better connect this photomechanical effects on the brain to battlefield blasts. The guiding question for this future direction is: **Does the cell plating and imaging material impact the origin and function of calcium transients after photomechanical stimuli?**

An ideal model for this work would be organotypic cortical brain slices due to their long-term viability, natural cell type distribution, and more anatomically representative morphologies and rigidities. Ultrafast 2D or volumetric imaging using 2 photon fluorescence, such as the MP-SOPi<sup>29</sup> microscope at the Vanderbilt Biophotonics Center, would give insights into the cell type-specific calcium responses after the same pressure exposure. Given the work in this dissertation, the pressure threshold for calcium activation by each cell type would likely be relatively similar, even if all cell types’ activation thresholds are higher than reported in chapter IV. After activation thresholds for each cell type are found, a broader use of pharmacological agents for calcium origin determination would give insights into functional pathways being activated. Pharmacological blockers presented in Chapter IV would be an ideal starting point for this study. This may lead to characterizing the mechanisms by which the central nervous system induces changes after blast and identifying therapeutic targets. It was also shown that calcium transients in glia originated from the extracellular space without an influence of pressure sensitive TRP transmembrane channels. Some evidence from this work postulates that poration may be occurring in the bilipid membrane. This theory should be tested using a non-permeable fluorescent chemical of large size, such as FITC-dextran at 5 kDa or higher.<sup>16,17</sup> Other potential mechanisms that could influence calcium entry are calcium initiation via aquaporin channels, potassium channels, purine channels, and voltage-gated calcium channels. If a probable mechanism is determined with a suitable

antagonist or countermeasure, calcium imaging could be performed on a knock-out mouse model to confirm the dependence on that mechanism.

The impact from this future direction may influence the use of cellular model systems for bTBI research purposes. If activation thresholds and calcium origination do not significantly change when switching to a less rigid plating material, then plating on prototypical glass may be best practice for ease of cell health and imaging considerations. Conversely, a vastly different result would suggest that further improvements are needed for *in vitro* experimentation and more meaningful insight may need to be uncovered in higher animal models.

#### 5.3.4 Inflammatory immune signaling from multi-cell model

This dissertation focused on the response of cells in isolation, without physiologically relevant communication between cell types. Constantly sampling the environment is a key function of microglia, which is certainly impacted by isolating them from neurons and astrocytes. As mentioned prior, the initial impact of the peak during blast pressure on microglia is potentially neuroprotective rather than neurodegenerative within the first 24 hours. *In vivo* studies using more explosive blast-like techniques have found a lagging inflammatory component to bTBI which may result from communication between cells.<sup>30</sup> **Do cellular responses change in the presence of multiple cell types?**

An organotypic brain slice model would be ideal for the same reasons as described in 5.3.3. Similar to Chapter IV, both real-time indicators, calcium, and subsequent indicators, cytokines, can be measured to determine difference between isolated and non-isolated cells. Fluorescence imaging could be used to determine calcium transients induce by photomechanical stimuli with multiple cell types present. Ultrafast imaging would be especially useful to determine true first responders to a blast wave and how communication between cell types is temporally patterned.

Either more robust image segmentation technique will be needed to differentiate the cell types from one another or transgenic animal models with stains may need to be deployed to categorize calcium signals to the proper cell type. To understand inflammatory responses induced communication between cell types, pro- and anti-inflammatory proteins should be quantified at multiple time points (i.e., 24, 48, 96, 168 hours) post high-amplitude, short-duration pressure exposure in a multi-cell model. If pro- or anti-inflammatory cytokine concentrations change over time, it may be due to cell-cell communication rather than direct pressure effects from a single photomechanical blast wave on an immune cell. Assuming that inflammatory responses are altered when in the presence of multiple cell types, cellular communication can be probed using antagonists or chelators for known extracellular communication pathways, such as neurotransmitters, ATP, heat shock proteins, chemokines, etc..

This work may result in a better understanding of the pathways inducing bTBI-related inflammatory signaling as well as the timeframe in which inflammatory immune signaling occurs. Calcium imaging could uncover dynamics at play between different cell types, while inflammatory cytokine quantification may determine how inflammation is impacted by cell communication. There may exist a window in which downstream effects from blast could be blocked with a targeted countermeasure to prevent the chronic implication of bTBI.

#### 5.3.5 Directed energy priming may reduce impact of subsequent insult

A commonality between the photomechanical and photothermal effects was potentially driving inflammatory responses away from pro-inflammatory immune signaling, at least in short-term experiments. As previously discussed, this result was surprising given the known negative impacts of specific direct energies. If the responses are truly anti-inflammatory, then they may be used to benefit overall brain health in specific circumstances. This led to the question: **Could**

**priming the brain with directed energy be a safe and effective prophylactic?** By driving immune cells into anti-inflammatory state, the brain may protect itself or lessen the impact of a potential insult, like blast. Assuming the prophylactic effect, if any, would only induce neuroprotective features on the order of days, it could only be effective if one could accurately predict when an immune insult could occur, such as sending personnel to a battlefield.

A study to determine the potential of directed energies to prime the brain for later insult could take a number of paths given the many types of directed energies. One path with a more impactful clinical relevance would be for TBI-inducing injuries from blast, in which the protectiveness of a prior, lesser blast could be investigated. A rodent model could be a good starting point given the large numbers of animals that may be needed to adequately probe the parameter space. Experimental groups of sham, bTBI, priming blast, and priming blast before bTBI would likely need to be used to best determine the effects of priming in isolation and prior to bTBI insult. The technique for blast creation and priming would need to be experiment-friendly, intensity modifying, and well-characterized. For these reasons, an air gun may be an ideal candidate for both applications. A parametric sweep in priming intensities and timing along with bTBI insult intensities would be needed to determine if a priming-induced neuroprotective window exists. As with previous sections, quantifying the inflammatory response would likely take the form of protein quantification of the affected brain areas. Though, behavioral, but other metrics including edema may be insightful. Behavioral methods may be useful to determine how cognitive injuries are modified from the experimental groups. Further consequences of priming may occur, such as structural reorganization, may occur and would need to be investigated fully prior to moving to human trials. As always with directed energy therapies, the difference in parameters to create therapy and damage need to be well understood.

The impact of this research could be far reaching given the large number of service members often impacted by bTBI in the U.S. alone. One could envision a service member given a priming dose of mechanical energy prior to deployment with follow-up treatments.

## 5.4 Contributions and Societal Impact

### 5.4.1 Scientific Contributions

In the fields of biophotonics, neuromodulation, neuroinflammation, and glial biology, this dissertation demonstrated the sensitivity of microglia to pulsed infrared light directly for the first time. Pulsed infrared light uncovered a dose-dependent nature to modulate distinct physiological signaling responses associated with temperature rise; highlighting the impact of acute temperature rises initiated by research or clinical perturbations. Heating is often assumed to have negative impacts on biology, but this work shows the potential benefit of heating under certain conditions. The ability to modulate pro-inflammatory cytokine signaling with acute photothermal exposures had not been observed prior to this work.

This dissertation demonstrated a novel approach to laser-induced pressure research on neurobiology, where photomechanical exposures impacted a large field of view ( $> 1 \text{ mm}^2$ ) during real-time fluorescence imaging. This work discovered neurons are more susceptible to damage after high-amplitude, short-duration pressures than astrocytes and microglia; suggesting prophylactics should target neurons to lessen the effects of blast on the brain. This work also suggests that microglia and astrocytes are not the initial drivers of a pro-inflammatory response, but rather may be driving anti-inflammatory response immediately after blast. While the theory of neuronal susceptibility to blast has been suggested, this work is another piece of evident to further the scientific communities' acceptance of this proposition. Lastly, further research is needed to compare these photomechanical-based cellular responses to blast-related cellular responses, but this work grows the confidence of laser-based pressure generation for the study of bTBI.

#### 5.4.2 Community and Societal Impact

The work from Chapter III demonstrated the impact of acute photothermal exposure on reducing subsequent pro-inflammatory signaling. This finding is limited in scope for a few reasons, including observed in an in vitro model, only one pro-inflammatory cytokine measures, and temperature rises were from room temperature. A few, if not more, Ph.D. project's worth of work would be required to verify, expand, and develop the potential application of pulsed IR heating to prevent or reverse immune maladaptations of chronic pain. Regardless, the potential societal impact of reducing downstream inflammation in chronic pain conditions with an acute heating event is meaningful. Pairing this potential impact of pulsed IR in reducing pro-inflammatory immune response with the further developed application of pulsed IR to block nociceptive signal transmission could have profound impacts to society. Current device-based neuromodulation techniques target solely the symptomatic nature of pain and require long-term use or implantation, which may not be the case for a dual-target neuromodulation technique that targets both the symptoms and root causes of chronic pain.

The research in Chapter IV initiated in response to the Defense Advanced Research Projects Agency (DARPA) cornerstone program which “aims to protect against blast or impact-induced behavioral and cognitive injury by preventing the initiation of harmful cell signaling cascades”. The identification of a target for prophylactic countermeasures is the long-term goal. Several scientists and engineers that encompass neuroscience, optics, biophotonics, ultrasound, and air blast have been working tirelessly towards identifying the earliest effects of pressure on neurobiology that drives bTBI, in which this work is a small part of. The community impact of this work, in addition to similar, concurrent aspects of the DARPA cornerstone project, is through the continuation of our collective research. What started off as more than one million dollars of

funding for a highly intense year of bTBI research may transition to a multimillion dollar, 5-year project, in part, due to this work. A long-term impact of such a grant would be the support of multiple projects and personnel, as well as strengthening ties between Vanderbilt researchers. The societal impact from the continuation of this work would be protecting those who protect us and our allies from long and short-term deficits of bTBI.

## 5.5 References

1. Duke, A. R. *et al.* Transient and selective suppression of neural activity with infrared light. *Scientific Reports* 2013 3:1 **3**, 1–8 (2013).
2. Lothet, E. H. *et al.* Selective inhibition of small-diameter axons using infrared light. *Scientific Reports* 2017 7:1 **7**, 1–8 (2017).
3. Ford, J. B. *et al.* Optimizing thermal block length during infrared neural inhibition to minimize temperature thresholds. *Journal of Neural Engineering* **18**, 056016 (2021).
4. Ganguly, M., Jenkins, M. W., Jansen, E. D. & Chiel, H. J. Thermal block of action potentials is primarily due to voltage-dependent potassium currents: a modeling study. *Journal of Neural Engineering* **16**, 036020 (2019).
5. Walter, E. J. & Carraretto, M. The neurological and cognitive consequences of hyperthermia. *Critical Care* **20**, (2016).
6. Bryden, D. W., Tilghman, J. I. & Hinds, S. R. Blast-Related Traumatic Brain Injury: Current Concepts and Research Considerations. *Journal of Experimental Neuroscience* **13**, (2019).
7. Miller, A. P. *et al.* Acute death of astrocytes in blast-exposed rat organotypic hippocampal slice cultures. *PLoS ONE* **12**, (2017).
8. Bhat, S. A. *et al.* Enhanced Akt/GSK-3 $\beta$ /CREB signaling mediates the anti-inflammatory actions of mGluR5 positive allosteric modulators in microglia and following traumatic brain injury in male mice. *Journal of Neurochemistry* **156**, 225–248 (2021).

9. Chatzipanteli, K., Alonso, O. F., Kraydieh, S. & Dietrich, W. D. Importance of posttraumatic hypothermia and hyperthermia on the inflammatory response after fluid percussion brain injury: biochemical and immunocytochemical studies. *J Cereb Blood Flow Metab* **20**, 531–542 (2000).
10. Blunck, R. *et al.* New Insights Into Endotoxin-Induced Activation of Macrophages: Involvement of a K<sup>+</sup> Channel in Transmembrane Signaling. *The Journal of Immunology* **166**, 1009–1015 (2001).
11. Welch, A. J. & van Gemert, M. J. C. Optical-thermal response of laser-irradiated tissue. *Optical-Thermal Response of Laser-Irradiated Tissue* 1–958 (2011)
12. Dewhirst, M. W. *et al.* Basic principles of thermal dosimetry and thermal thresholds for tissue damage from hyperthermia. *International Journal of Hyperthermia* **19**, 267–294 (2009).
13. Rahmathulla, G. *et al.* MRI-guided laser interstitial thermal therapy in neuro-oncology: A review of its current clinical applications. *Oncology (Switzerland)* **87**, 67–82 (2014).
14. Parpura, V. & Haydon, P. G. Physiological astrocytic calcium levels stimulate glutamate release to modulate adjacent neurons. *Proc Natl Acad Sci U S A* **97**, 8629–8634 (2000).
15. Roth, C. C. *et al.* Nanosecond pulsed electric field thresholds for nanopore formation in neural cells. *J Biomed Opt* **18**, 35005 (2013).
16. Mulholland, S. E., Lee, S., McAuliffe, D. J. & Doukas, A. G. Cell Loading with Laser-Generated Stress Waves: The Role of the Stress Gradient. *Pharmaceutical Research* 1999 16:4 **16**, 514–518 (1999).
17. Kodama, T., Hamblin, M. R. & Doukas, A. G. Cytoplasmic Molecular Delivery with Shock Waves: Importance of Impulse. *Journal of Biophysics* (2000).

18. Nakagawa, A. *et al.* Mechanisms of primary blast-induced traumatic brain injury: Insights from shock-wave research. *Journal of Neurotrauma* **28**, 1101–1119 (2011).
19. Ravin, R. *et al.* Blast shockwaves propagate Ca<sup>2+</sup> activity via purinergic astrocyte networks in human central nervous system cells. *Scientific Reports* **6**:1 **6**, 1–14 (2016).
20. Biomarkers of Neuroinflammation: Proceedings of a Workshop. *Biomarkers of Neuroinflammation* (2017)
21. Hachisuka, J. *et al.* Semi-intact ex vivo approach to investigate spinal somatosensory circuits. *Elife* **5**, (2016).
22. Ong, H. H. & Wehrli, F. W. Quantifying axon diameter and intra-cellular volume fraction in excised mouse spinal cord with q-space imaging. *Neuroimage* **51**, 1360 (2010).
23. Grace, P. M., Hutchinson, M. R., Maier, S. F. & Watkins, L. R. Pathological pain and the neuroimmune interface. *Nat Rev Immunol* **14**, 217–231 (2014).
24. Ramos, J. M. P. *et al.* Type I IFNs are required to promote central nervous system immune surveillance through the recruitment of inflammatory monocytes upon systemic inflammation. *Frontiers in Immunology* **8**, 1666 (2017).
25. Hachisuka, J. *et al.* Semi-intact ex vivo approach to investigate spinal somatosensory circuits. *Elife* **5**, (2016).
26. Chen, C., Lee, I., Tatsui, C., Elder, T. & Sloan, A. E. Laser interstitial thermotherapy (LITT) for the treatment of tumors of the brain and spine: a brief review. *Journal of Neuro-Oncology* **151**, 429 (2021).

27. Wang, X. S. *et al.* Treatment of cerebral radiation necrosis with nerve growth factor: A prospective, randomized, controlled phase II study. *Radiotherapy and Oncology* **120**, 69–75 (2016).
28. Vellayappan, B. *et al.* Diagnosis and Management of Radiation Necrosis in Patients With Brain Metastases. *Frontiers in Oncology* **8**, 395 (2018).
29. biomiid | Vanderbilt Biophotonics Center | Vanderbilt University.  
<https://www.vanderbilt.edu/vbc/biomiid/index.php>. (2022)
30. Gama Sosa, M. A. *et al.* Lack of chronic neuroinflammation in the absence of focal hemorrhage in a rat model of low-energy blast-induced TBI. *Acta Neuropathol Commun* **5**, 80 (2017).

## **Appendix A**

### **Intraoperative Neuromonitor using Infrared Neural Stimulation Business Plan**

## **A.1 Foreword**

Appendix A is a portion of a Small Business Innovation Research (SBIR) Phase II application that originated from Innovation Realization, an interdisciplinary class, run by Dr. Robert Webster of Vanderbilt University's School of Engineering.

Our team consisted of one PhD candidate, two JD candidates and three MBA candidates, respectively. Logan Jenkins has a strong background in the necessary fields supporting the underlying technology. Anna Choi has experience working in the legal department of a well-known medical device company. Yulin Wu is a licensed Chinese attorney with experience in business formation and merger and acquisitions. Brian Martin has experience developing, patenting, and commercializing new products in his position at Electrolux as a team leader of a product development team. Scott McMann is an experienced sales representative that handles multi-million-dollar market opportunities for Medtronic. Matthew Bowden is a California licensed attorney with a background in healthcare related law and business management.

## A.2 Vanderbeam Technologies Commercialization Plan

### A.2.1 Executive Summary

Surgery will always pose a certain risk of morbidity, but this is especially true of spinal surgeries in which drills, hammers, and knives come within millimeters of the spinal cord in a successful case. The gold standard in assessing and preventing neurological damage during surgery is intraoperative neuromonitoring (IONM), in which the nervous system is constantly stimulated and recorded to guide surgical decision-making. Over 80% of surgeries do not utilize IONM, leading to thousands of patients having worse pain postoperatively than preoperatively. Most surgeons do not use IONM because it suffers with issues in reliability, subjectivity, and usefulness as highlighted by first-hand neurological surgeons' interviews and various studies. Our mission is to improve the safety and efficacy of spinal surgeries by addressing these issues with novel technologies, leading to healthier patients and more effective surgeons.

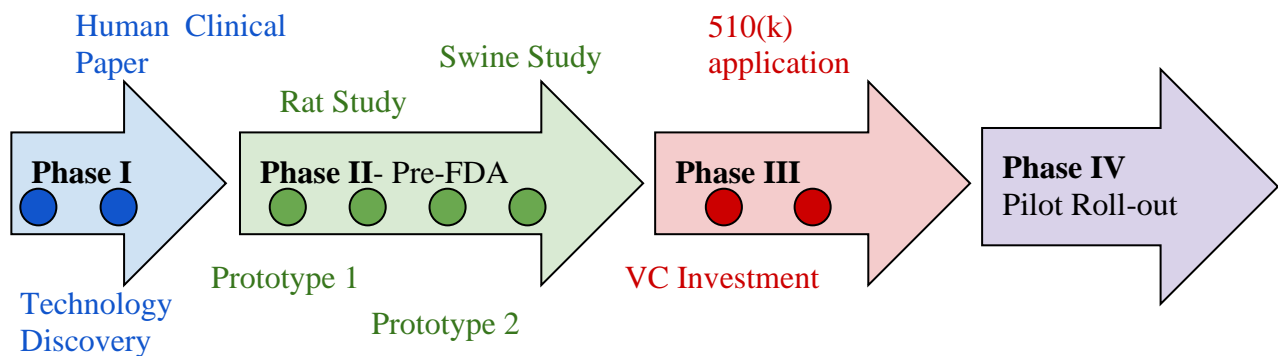
We accomplish this mission by directly monitoring the spinal cord function instead of secondary neural structures, as is the case for current technologies. Directly monitoring the spinal cord becomes more difficult due to the level of specificity needed to adequately discern fine neural tracts from each other. Thanks to pivotal advancements in stimulation techniques, we use a proprietary optical stimulation technique that improves spatial specificity by an order of magnitude over electrical stimulation, called infrared neural stimulation (INS). We are uniquely positioned to revolutionize the spinal IONM market with these two advancements.

The spinal surgery market is a significant segment of medical procedures in the United States, with 1.6 million instrumented procedures annually. Our company will initially develop our device within the cervical region where the technological advantages may present the greatest

differentiator vs. current methods. 80% of the 165 thousand procedures per annum in the cervical spine are Anterior Cervical Discectomy & Fusion (ACDF). 17% of these surgeries use current IONM devices, a result of surgeon's disinterest in the current state of IONM. Total annual hospital reimbursements for IONM during ACDF average over \$12.5million.

We have formed a superb team of experienced business professionals, accomplished lawyers, and innovative engineers. The SBIR funding will play a vital role in developing the minimally invasive stimulation and recording components as well as the software needed to make the best use of our technological advantages. The other required technologies currently exist, easing the integration of our products into operating rooms.

We are perfectly situated to revolutionize the spinal IONM market as we have the right team, the right technology, and the right amount of customer dissatisfaction with current devices. Not only will we make patients healthier, surgeons happier, and hospitals less liable, but we will improve the adoption of future neuromodulation technologies, stemming from the NIH's HEAL and BRAIN initiatives, to the operating room.



### A.3 Value, Outcomes, Impact

**PROBLEM** Anterior cervical discectomy and fusion (ACDF) is a spinal surgery performed 165 thousand times a year in the US to improve the quality of life for those suffering from neck pain and other ailments. Unfortunately, up to three percent of these surgeries result in an exacerbation of myopathy, and another 3 percent suffer from nerve palsy as a direct consequence of the surgery itself (Epstein 2019). Even with these relatively large chances of induced neurological deficits, surgeons have reduced their use of IONM, due to their lack of effectiveness in assessing neurological damage reliably using the current technology. This lack of effectiveness stems from the global, unspecific monitoring of neurological signals, and the inherent nonspecific nature of electrical nerve stimulation generating neurological signals that can be unrelated to a potential injury or defect in nerve tissue. Being unspecific in both stimulation and recording aspects of nerve monitoring recordings can result in a subjective definition of the threshold for neurological damage, as well as potentially higher false positive rate. These can reduce the effectiveness of diagnosis and treatment of postoperative pain.

**SOLUTION** Our device addresses these issues by specifically targeting the damage-prone tracts of the spinal cord in both the stimulation and recording fields. Instead of stimulating and recording the spinal cord by proxy, via brain and muscle signals, our technology directly stimulates and records the spinal cord in the epidural space. Our proposed device is designed to stimulate the fine tracts of the spinal cord in a way that current solutions cannot, by using the optical stimulation technique, INS, instead of electrical stimulation (Cayce 2014).

INS has advantages over electrical stimulation in spatial specificity (sub-millimeter vs. millimeter) and orientation (directed vs. spherical). These advantages create a better solution for

the identification of nerve tracts as well as earlier detection of any damage. Electrical stimulation sites at the brain or periphery often result in unnecessary nerves being stimulated that are unlikely to become damaged. This lack of specificity increases the chances of unintended consequences and suppresses real nerve damage-induced signal loss. Directly stimulating and recording the spinal cord is easily performed through minimally invasive epidural insertion of the device with intraoperative X-ray assistance.

**VALUE** Patients will benefit from this technology through lowered incidences of iatrogenic damage during spinal surgeries. Lowering these incidences will make a patient's decision to have spinal surgery easier, by providing a reliable and safe alternative to simply taking addictive opioids for their pain management.

From the hospital and surgeon's perspective, IONM has a major risk mitigation benefit, reducing the exposure of surgeons to malpractice litigation. Nearly 50% of malpractice spinal surgery cases result in a ruling for the patient, or a settlement, with an average award of \$4 ± 6 million and \$2 ± 2 million, respectively (Daniels 2019). Hospitals reducing their liability through improvements we can offer in IONM technology can result in lowered healthcare cost alongside a reduction in unintended damage to the patients.

This device aligns with many of the NIH's current agendas, including the "BRAIN" and "HEAL" initiatives. More specific stimulation and recording of the spinal cord can work hand-in-hand with future technologies supported by the "BRAIN" initiative. As we begin to better understand the structures, circuitry, and function of the central nervous, higher spatial specificity will be needed to modulate these areas. This device also presents synergistic opportunities to work

with the NIH “HEAL” initiative in developing non-opioid pain management techniques, by making spinal surgery safe and highly effective for patients.

**OUTCOMES** The direct outcome of this program is a highly specific and sensitive stimulation & monitoring of damage-prone neural tracts in the spinal cord during neurosurgery. In turn, this gives neurosurgeons an in-depth analysis tool of the spinal cord health, driving surgical decision-making. To get to this level of impact, our device needs to be developed for animal studies and then clinical human studies. Reaching FDA class II clearance is vital for the success of this device.

While ACDF surgeries are initially targeted as the main application, the other 1.4 million spinal surgeries will very likely benefit from this type of intraoperative neuromonitoring technique. Gaining physician confidence in optical stimulation will lead to further development of the technology, for example hastening adoption of implantable infrared neurostimulators to fight chronic pain or neurological deficits, such as those common in Parkinson’s disease. The investment of the American government into a better understanding of the brain will benefit from a spatially specific stimulation tool to modulate neurological functions.

**IMPACT** Pain has become a national, if not global problem in today’s society. It has driven an opioid epidemic that reduces quality of life and kills an average of 130 Americans every day. Non-opioid treatment options, such as the one our technology offers, are invaluable in fighting both pain and the opioid epidemic. Many sources of chronic pain originate in the spinal cord. Surgical interventions are needed to treat the cause of this kind of pain. Making surgeries safer and more effective can give both patients and surgeons the trust in their technology and techniques needed for more successful outcomes, leading to a healthier society.

### A.3.1 Company Overview

**HISTORY** Vanderbeam was created in 2019 by a dedicated group of six Vanderbilt students during an interdisciplinary collaboration amongst the university's engineering, business and law schools. Our core objective is to revolutionize the intraoperative nerve monitoring space by implementing cutting edge optical technology. Our core competencies include unfettered access to the pre-eminent authorities in the optical intraoperative nerve monitoring space as well as licensed patents for the underlying technology.

Currently, Vanderbeam does not have a history of Federal and non-Federal funding because it does not yet have a commercialized product on the market. Once we receive funding we will complete the remaining research and regulatory steps necessary to bring our product to market.

**PERSONNEL** The company originated from Innovation Realization, an interdisciplinary class, run by Dr. Robert Webster of Vanderbilt University's School of Engineering. Our team consists of one PhD candidate, two JD candidates and three MBA candidates, respectively. Logan Jenkins has a strong background in the necessary fields supporting the underlying technology. His thesis “Infrared Neural Modulation of Neurons and Glia” speaks directly to the concept of nerve monitoring. Anna Choi has experience working in the legal department of a well-known medical device company. In this role she has hands- on experience with the regulatory hurdles to overcome in bringing a device to market. Yulin Wu is a licensed Chinese attorney with experience in business formation and merger and acquisitions. Her experience will help in the formation stages as well as positioning the company for acquisition. Brian Martin has experience developing, patenting and commercializing new products in his position at Electrolux as a team leader of a product

development team. Scott McMann is an experienced sales representative that handles multi-million-dollar market opportunities for Medtronic. His career has been built on building customer relationships in order to bring medical devices to market. Matthew Bowden is a California licensed attorney with a background in healthcare related law and business management.

We will meet critical management functions as our company evolves by leveraging our in-house assets first. Our founding team incorporates a vast pool of skills and knowledge that will assist in the day-to-day management of the firm.

**VISION** Our vision for the short term is to finish the development of our product within five years and consecutively move the product through the FDA Class II process. Once these hurdles have been overcome we expect a market penetration of 15% within 7.5 years. Our long-term vision is to sufficiently de-risk the product and be acquired by one of our competitors.

#### A.3.2 Market, Customer, Competition

**MARKET** Our total addressable market is the 1.6 million instrumented spinal procedures performed annually in the United States, encompassing cervical, thoracic and lumbar. The first marketable product will focus on the cervical spine. There are 165,000 cervical procedures per year. From this amount, 80% of these procedures are ACDF procedures. ACDF is growing 5-6% annually, however, only about 17% (22,000) of ACDF procedures currently use Intraoperative Nerve Monitoring. This will be our initial target market. We are targeting this market first for three reasons: Firstly, there is a higher prevalence of nerve damage and complications in cervical procedures than in the other spinal areas. Secondly, these doctors are already familiar with using Intraoperative Nerve Monitoring. And thirdly, this procedure has a large potential for malpractice claims if the surgeon injures a nerve.

The IONM industry is experiencing healthy growth, both in the U.S. and worldwide (9-10% CAGR US, 4.7% CAGR worldwide). Increasing prevalence of neurological disorder, rising awareness of patient safety, growing neurological centers and favorable reimbursement are the major drivers of the intraoperative neuromonitoring market. Adjacent variables, such as a supply of trained personnel, are the predominant limitations.

**FINANCIAL PROJECTIONS** Our business model will include revenue streams from both disposable and capital equipment. This would allow us to build a recurring revenue model and keep the overall cost of the initial investment low enough to be attractive to the customers. Based on the CPT codes the Average Hospital Reimbursement per case is \$557. Hospitals expect a margin of 30-45% on medical devices. Therefore, we could expect to receive \$390 per procedure. Given this per procedure revenue we could expect the disposable component to provide the following revenue based on market penetration.

This sensitivity analysis provides estimates of market penetration both in the 17% of ACDF procedures currently using IONM and in the 83% of procedures that don't. We anticipate about 10-20% market share in the former. And because of the ease of use of our solution, we expect to convert 1-5% of the remaining non-IONM using market.

Share of New ACDF Market	Share of Existing ACDF Market					
	5%	10%	20%	30%	40%	50%
1%	\$ 864,046	\$ 1,300,827	\$ 2,174,388	\$ 3,047,950	\$ 3,921,511	\$ 4,795,072
2%	\$ 1,291,311	\$ 1,728,092	\$ 2,601,653	\$ 3,475,215	\$ 4,348,776	\$ 5,222,338
5%	\$ 2,573,106	\$ 3,009,887	\$ 3,883,449	\$ 4,757,010	\$ 5,630,572	\$ 6,504,133
10%	\$ 4,709,432	\$ 5,146,213	\$ 6,019,774	\$ 6,893,336	\$ 7,766,897	\$ 8,640,459
20%	\$ 8,982,084	\$ 9,418,864	\$ 10,292,426	\$ 11,165,987	\$ 12,039,549	\$ 12,913,110
30%	\$ 13,254,735	\$ 13,691,516	\$ 14,565,077	\$ 15,438,639	\$ 16,312,200	\$ 17,185,762
40%	\$ 17,527,387	\$ 17,964,167	\$ 18,837,729	\$ 19,711,290	\$ 20,584,852	\$ 21,458,413
50%	\$ 21,800,038	\$ 22,236,819	\$ 23,110,380	\$ 23,983,942	\$ 24,857,503	\$ 25,731,065

Most intraoperative nerve monitoring machines are around \$80,000 when newly purchased. Our expectation is to undercut this amount to build market share. The below chart shows revenue for the capital component given a per device cost of \$50,000. Additionally, we will offer a leasing agreement for our capital equipment in an effort to limit financial barriers to acceptance and drive usage of the higher-margin disposable equipment.

Average Number of Consoles per Center	Number of New Spine Centers per Year (Hospital and ASC)				
	2	5	10	20	40
1	\$ 100,000	\$ 250,000	\$ 500,000	\$ 1,000,000	\$ 2,000,000
2	\$ 200,000	\$ 500,000	\$ 1,000,000	\$ 2,000,000	\$ 4,000,000
3	\$ 300,000	\$ 750,000	\$ 1,500,000	\$ 3,000,000	\$ 6,000,000
4	\$ 400,000	\$ 1,000,000	\$ 2,000,000	\$ 4,000,000	\$ 8,000,000
5	\$ 500,000	\$ 1,250,000	\$ 2,500,000	\$ 5,000,000	\$ 10,000,000

This sensitivity analysis estimates revenue for varying combinations of new spine center implementations per year and the average number of consoles procured by each center. We forecast 5-10 new centers a year with each purchasing 2-3 consoles. With both revenue streams combined, we would expect to have a top line revenue of approximately \$4.5 million dollars by the fifth year.

**CUSTOMER** Our customers are hospitals and ASCs Management including C-Suite Executives, Service Line Directors, Procurement and Vendor Management. In order to get our product in front of these customers we will look for champions among the users of this technology. These users include neuro and spine surgeons, anesthesiologists, IONM technicians and nurses/scrub techs.

We will have three options for a distribution model. The first is direct sales to hospitals. However, this poses access challenges considering the early-stage state of our company. The second option is to work through a distributor with established channels and relationships. Finally,

we could evaluate a distribution partnership with a medical device manufacturer who is already providing ACDF procedure hardware to hospitals. Our offerings would be complementary.

**COMPETITION** The intraoperative neuromonitoring market in the US is highly fragmented with the presence of many manufacturers, local service providers, and implant companies. There are 8 major firms and a number of smaller firms competing in the U.S., driving rivalry up significantly. The firms in the IONM industry are of different sizes, ranging from large manufacturers such as Medtronic and Biotronik to more niche firms such as NuVasive. While these firms still compete for similar procedure and specialty share, the diversity of size has allowed firms to find a niche in the industry, reducing rivalry. many offering IONM in conjunction with other product offerings.

Products in this industry are not highly differentiated. The core technology being utilized has not changed or been significantly improved in the last 2 decades. Switching costs are low considering the same basic functionality of all offerings. This drives rivalry up. As a result, rivals have been driven to differentiate their offering through services provided (i.e., remote IONM), breadth of their portfolio of IONM modalities (SEPs, MEPs, EEG), bundling with additional offerings (robotics and surgical tooling/devices) and software packages.

The production capacity for IONM manufacturers is not limited and can be added in large increments if necessary. These systems have a capital and a disposable component (and very often a software analytics component). Capital equipment is the most limited scalability, though demand is unlikely to be higher than production capacity. As a result, rivalry is driven up.

Exit barriers to the IONM industry are low. Assets used to produce IONM products can likely be leveraged to produce other offerings in a firm's portfolio. Additionally, many companies in the

IONM industry follow acquisition strategy, so the salvage value of assets (overhead and IP) is healthy. This will bring rivalry down. However, in firms that offer multimodal IONM, divesting and exiting specific divisions may be made more difficult due to shared assets and synergies.

There is high excess capacity in the IONM industry. The high number of competing firms combined with under-penetration of use in certain specialties and procedure leads to this excess capacity. This drives rivalry up. Hospitals are already very cost-conscious (and becoming more so). This combined with undifferentiated product offerings from IONM firms leads to low pricing strategies. This makes cost cutting or redistribution imperative for IONM manufacturers, and one tool at their disposal (particularly for the larger firms) is economies of scale. This is harder for smaller, niche manufacturers to leverage. All things considered, this drives rivalry up.

The capital component of IONM can be leveraged by a customer for years. The disposable component (i.e., probes, electrodes) have a finite shelf life of typically 2 years, hence should be considered “perishable”. There is not a significant pressure to sell/use these components. This will bring rivalry down.

All things considered, rivalry in this industry is high. Factors such as a large number of competing firms, relatively undifferentiated product offerings, low customer switching costs, significant excess capacity and a motivation to cut costs (and hence prices) through economies of scale all drive rivalry up. These variables are someone counteracted by the fact that the competing firms are of different sizes and can find a specific niche, the overall IONM industry is growing, low exit barriers and the absence of perishable products.

Overall, our product can reach an attractive market in the cervical spine surgery space and differentiate itself from the competition.

### A.3.3 Intellectual Property

Currently we hold two utility patents:

- Mahadevan-Jansen, A., Cayce, J., Friedman, R., Roe, A., Jansen, E.D., Chernov, M., Konrad, P.E. (2009). *U.S. Patent Application No. 20090069871(A1)*. Nashville, TN. U.S. Patent and Trademark Office.
- Mahadevan-Jansen, A., Cayce, J., Friedman, R., Roe, A., Jansen, E.D., Chernov, M., Konrad, P.E. (2015). *U.S. Patent No. 9,044,596(B2)*. Nashville, TN. U.S. Patent and Trademark Office.

The first protects the method of stimulating neural tissue with infrared light, while the second covers an INS apparatus comprising three components: (1) a capital control console, (2) disposable probes, and (3) recording software. These patents are valid for an additional twelve and seven years, respectively. We anticipate filing for additional utility patents assigned to Vanderbilt University. These patents would protect the delivery method of attaching the disposable probes directly to the respective surgical site, and the source code of the recording software. Since we are outsourcing the development of the recording software, we expect to protect the intellectual property rights to the source code through work-for-hire agreements that contain nondisclosure provisions.

### A.3.4 Financial Plan

**PHASE 1** Our first phase will involve a \$2 million-dollar, 9-month small animal study. We will reach this amount through a Phase 2 SBIR grant at \$1.75 million and Launch TN SBIR match at \$400,000. For personnel outside of our leadership team, we will need one full time graduate student or research technician who will cost approximately \$100,000 with overhead. Vanderbilt facilities and lab space will be utilized to manage and test the animals. We estimate that each rat will cost \$500 when overhead is factored in, and we will need 100 rats. Our company will be developing 100 prototypes iteratively; they will need the required hardware components

on hand. Overall, we expect that our prototypes will cost \$200,000 for parts and labor for all phases.

**PHASE 2** Our second phase will require \$3 million dollars, and a 12-month large animal study. Our personnel requirement will remain static. We will need to collaborate with a private entity to source pigs for this step. We expect that we will need 10-20 pigs and each pig costs \$20,000. We will continue to use Vanderbilt lab space to run the actual testing and to iterate the prototypes. We expect that we will need hardware components for 50 prototypes.

**PHASE 3** Our third phase will require \$10 million dollars and will attend to any FDA mandated studies with our final design. We will need to work with the Vanderbilt University Medical School and source approximately 5 cadavers at an estimated cost of \$500 each. For our FDA submission we will try for the 510(k)-route given the high number of predicate IONM devices, but we may need to submit a De Novo Class II application because of the novelty of our approach. We will meet with the FDA this calendar year to discuss our regulatory pathway and expect to complete our regulatory studies by 18 months, this is even if we use the De Novo Pathway. After FDA approval we expect to launch in 2025.

#### A.3.5 Production and Marketing Plan

**PRODUCT** Although doctors who actually use IONM are the ones that will use the product, they are not the real ‘customer.’ Neurosurgeons and orthopedic surgeons specializing in spinal procedures are, however, important influencers. Our real customers are hospital supply chain and purchasing departments. These organizations will actually make the decision to buy our device. These customer’s needs must be considered along with those of the influencers by our product development process, distribution model, and marketing plan.

Our product is focused on one procedure and in one local area of the spine. This helps to avoid needless complexity or costly variation in the types of devices offered. The only customization we foresee is to offer 3 sizes: small, medium and large, for the varying sizes of cervical spines. This variation affects the disposable component of the IONM system only. There will be no need for, or benefit from, making multiple variations of the same size. In the same way, the capital component of the system will be made in one variant only.

**DISTRIBUTION CHANNEL DESIGN & MANAGEMENT** The distribution model that best fits our product is an indirect one. Vanderbeam will focus on managing the production of devices that will then be sold by an existing medical device sales partner.

The relationship of Vanderbeam to this distributor will be an important one, and our plan is to build into our contract with them provisions and contingencies that encourage the flow of information both up and down the supply chain. From our end users, the doctors, to the purchasing departments, and even from our distributors themselves, we anticipate this communication will help to drive improvements to marketing methods and development of product updates. The key will be to implement processes and contractual contingencies that incentivize the sharing of this information.

One key metric of success is to track customer ‘point of contact’ vs. device sales for both the capital and disposable components of the IONM system. Care must be taken here to ensure that any contractual contingencies put in place will encourage honest reporting of the conversation rate, so that any actions taken can be appropriate, timely and based on good data.

**PROMOTION** In order to drive adoption of our device, we plan to promote to our influencers, the orthopedic or neurosurgeons performing spinal surgeries including ACDF. These

influencers will help to drive purchasing decisions by the appropriate department within the hospital supply chain. The objective of this communication is to emphasize our competitive advantages that improve the surgeon's confidence in patient outcomes.

This is a key pain point identified by our team's interviews with potential end users. By providing a tool that requires less interpretation by a dedicated technician, we put the surgeon that much closer to the data he or she needs by removing a layer of human analysis from the process.

Vanderbeam must also actively coordinate actions and strategy with our distribution partner in a way that leverages their core competencies and previous experience in the medical device sales field. Developing champions for use within the clinical space as well as fostering acceptance and understanding by partnering with professional associations are just two of the tools we foresee using. The groundwork for success in these areas can be laid long before the start of production or product launch.

We anticipate up to 30% of our yearly SG&A allocation to be dedicated to marketing expense. The importance of placing dedicated resources over time cannot be overstated. Relationships and trust are built over time, and we believe that consistent year over year spending will create more value than flooding any ad spaces at launch alone.

**PRICING** Preliminary pricing of the final system has been determined using market research and data. Our prices for each component are calculated using reimbursement-based compensation on the provider side as well as competitor pricing information for similar use-case IONM systems already in the market today. These numbers are explored further in the following section.

### A.3.6 Revenue Stream

The Vanderbeam product portfolio will create two distinct, but correlated, revenue streams. The first will be through the one-time sale of capital control consoles and related, reusable accessories. These sales will carry a price of \$50,000-\$80,000 per console, which is in line or slightly lower than competitive console pricing. While this will drive significant revenue to Vanderbeam, it will drive relatively low profits due to the high cost of goods sold (~25%) and low profit margins. The strategy is to price as low as is sustainable in order to gain early access to hospitals and physicians to begin trialing our systems.

The second revenue stream comes from the recurring sale of disposable accessories used during the procedure, including all non-reusable in-body components. It is through these low-cost sales (<5% COGS) that we will attain higher profit margins. This will support our “depth, not breadth” penetration strategy: instead of targeting a high number of spinal surgeons with our offering, we engage only existing high-volume proceduralists to use the Vanderbeam system for all of their ACDF procedures.

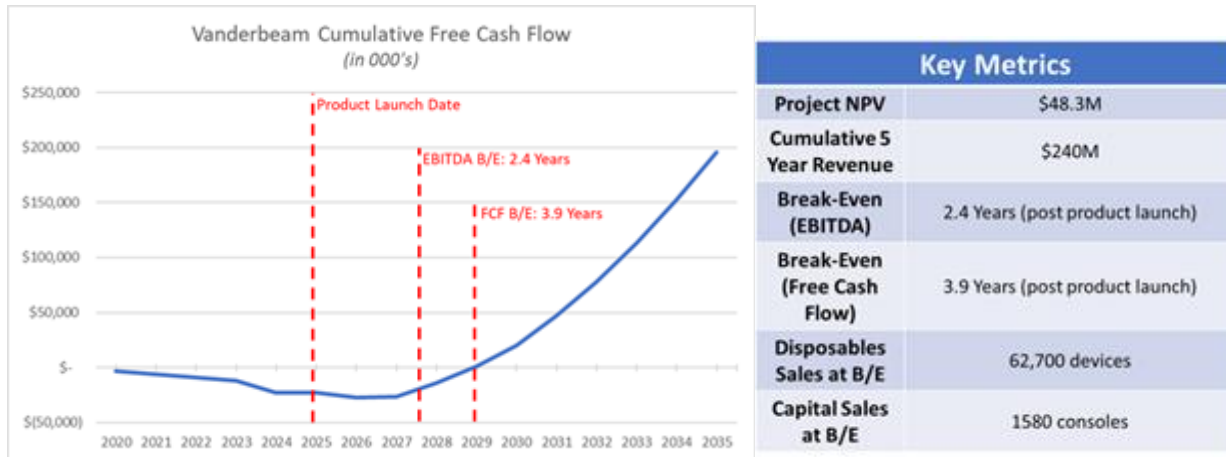
Total revenue and cost are outlined in the financial projections provided below:

	Pre Revenue	Year 1	Year 2	Year 3	Year 4	Year 5	Year 6
Disposables Revenue		\$ 396	\$ 11,070	\$ 11,899	\$ 12,570	\$ 13,138	\$ 13,639
Capital Revenue		\$ 4,700	\$ 22,066	\$ 38,808	\$ 54,916	\$ 70,379	\$ 85,187
<b>Gross Revenue (000s)</b>	<b>\$ -</b>	<b>\$ 5,096</b>	<b>\$ 33,136</b>	<b>\$ 50,707</b>	<b>\$ 67,486</b>	<b>\$ 83,517</b>	<b>\$ 98,825</b>
Disposables COGS	\$ -	\$ (19.80)	\$ (553.51)	\$ (594.94)	\$ (628.52)	\$ (656.88)	\$ (681.94)
Capital COGS	\$ -	(1,175)	(5,516)	(9,702)	(13,729)	(17,595)	(21,297)
<b>Total COGS</b>	<b>\$ -</b>	<b>\$ (1,195)</b>	<b>\$ (6,070)</b>	<b>\$ (10,297)</b>	<b>\$ (14,358)</b>	<b>\$ (18,252)</b>	<b>\$ (21,979)</b>
<b>Gross Profit (000s)</b>	<b>\$ -</b>	<b>\$ 3,901</b>	<b>\$ 16,607</b>	<b>\$ 26,420</b>	<b>\$ 35,781</b>	<b>\$ 44,718</b>	<b>\$ 53,250</b>
R&D	\$ (15,000)	(459)	(2,982)	(4,564)	(6,074)	(7,517)	(8,894)
SG&A		(9,529)	(9,941)	(15,212)	(20,246)	(25,055)	(24,706)
Fixed Cost		(5,000)	(5,000)	(5,000)	(5,000)	(5,000)	(5,000)
<b>EBITDA</b>	<b>\$ (15,000)</b>	<b>\$ (11,086)</b>	<b>\$ (1,316)</b>	<b>\$ 1,644</b>	<b>\$ 4,461</b>	<b>\$ 7,146</b>	<b>\$ 14,650</b>
<b>EBITDA Margin</b>	<b>N/A</b>	<b>-218%</b>	<b>-4%</b>	<b>3%</b>	<b>7%</b>	<b>9%</b>	<b>15%</b>

To drive this revenue growth, we will optimize our targeting by focusing on academic institutions that have a reputation for implementing cutting-edge technology and that currently perform high-volumes of ACDF and other spinal procedures. In addition, we will focus a more granular targeting approach on specific physicians who currently use IONM for their spinal procedures. Our goal with initial targets is not to reinvent their practice and methods by teaching them the value of IONM, but rather to improve their current practice by highlighting the advantages of our novel technology.

However, as a start-up organization, Vanderbeam lacks the infrastructure, reputation and network required to gain quick access to these targets. Speed to market is particularly important considering the timeline on a few of our pivotal patents. For this reason, we will leverage a distributor to sell our system. Numerous nationwide medical device distributors, including AlphaTec Spine, Wenzel Spine, Inc. and Spinal Elements, have well established channels and access to our end users. The selection of the appropriate distributor with whom to partner will be driven by which has optimized access to the highest volume of our predetermined target accounts and physicians as well as which currently carries the most complimentary portfolio of spinal offerings.

Factoring all our revenue streams and costs, we anticipate an EBITDA break-even point approximately 2.4 years after product launch (7.4 years after initiation of product development). At this point, we will have sold 1580 capital consoles and over 62,000 disposable components. This will equate to 5-year cumulative revenue of \$240million and a current valuation of Vanderbeam of approximately \$48million. Refer to graphic below for the projected cumulative free cash flow projections, incorporating a 5-year, \$15million product development runway prior to a product launch in January of 2025.



### A.3.7 Conclusion

Spinal surgeries are life-altering experiences, either positively or negatively. There remains an unmet clinical need of reliable and objective neuromonitors to guide surgical decision making to preserve or improve the health of the spine. Our proposed device harnesses novel technologies to create a never-before-used approach through the epidural space of the spine. Our target market of 22K surgeries a year and reimbursable revenue stream are large enough to sustain a successful business plan and future iterations of this device. We retain the needed intellectual property to protect ourselves from outside competitors and potential litigation. To meet our vision of protecting future patients and surgeons, we first need the support of the NIH SBIR program to jumpstart our 5-year development plan.

#### **A.4 Vanderbeam Technologies Specific Aims**

We propose to design, build, and validate a novel intraoperative neuromonitor (IONM) for spinal discectomies. This purpose of this system is to alert surgeons when life-altering damage is imminent by giving real-time, specific, and digestible information on the health of the spinal cord. This will be achieved by using a novel, spatially specific stimulation technique directly on the spinal cord via an epidural probe.

Only 17% of anterior cervical discectomy and fusion surgeries used IONM in 2014, a figure that dropped from 30% in 2011. All the while, the number of adverse consequences remains in the many thousands per year, with 3% of cases worsening pre-operative pain and 3% of cases creating new pain<sup>2</sup>. Surgeons are rejecting current IONM devices because the devices are frustrating to use. Most of the tens of surgeons interviewed complained about the unreliability and subjectivity of current technology.

Our proposed IONM device uses infrared neural stimulation<sup>3</sup>, a technique developed for over 15 years and proven in a clinical study<sup>4</sup>, to stimulate areas smaller than a square millimeter. This specificity allows for the targeting of specific neural tracts that are most likely to be damaged during surgeries and gather data much more frequently than current technology. We bring this technique right to the spinal cord through an epidural probe; meaning we get the most important data at the right time to prevent long-term neurological damage.

Our developmental approach will be to first test the safety and feasibility of optical stimulation in spinal tissue to prove its value over current technology. Once completed, we will begin to prototype the entire system. Initial testing will be on swine due to their similar nervous system and spinal size. The last steps will be to compare our system to current IONM systems in large animal studies and improve probe placement in cadavers.

### Specific Aim 1: Determine Safety and Feasibility of Underlying Technology

Task 1.1: Quantify Safety of Optical Stimulation in Spinal Tissue. Using histology, damage induced by our light-based stimulation will be evaluated on in vivo rat, ex vivo swine, and cadaver spinal tissue.

Task 1.2: Compare Technology to Current IONM. Determine the sensitivity and specificity of optical and electrical stimulation in detecting crush, stretch, and slice injuries in in vivo rat spinal cord.

### Specific Aim 2: Create Functional Prototypes

Task 2.1: Design Epidural Probe, Console, and Software Package. Model and manufacture initial system prototypes for future swine studies. Design training protocol for 3rd party clinical testing.

Task 2.2: Evaluate Placement Accuracy in ex vivo Swine. Quantify accuracy of X-ray guided probe placement and electrode/optrode placement to surgical sites by newly trained personnel.

### Specific Aim 3: Experimentally Validate System

Task 3.2: Compare Neuromonitors in in vivo Swine. Compare our system to current IONM devices and quantify neural signal delays and amplitude changes during crush, stretch and slice protocols.

Task 3.3: Evaluate placement safety and accuracy in cadavers. Before starting clinical trials, measure safety metrics (pressures, abrasions) on human spinal cord and accuracy of probe placement.

The proposed intraoperative neuromonitor will result in a lower number of adverse consequences in spinal procedures by giving the surgeons more reliable and actionable information. Our technology will be the first IONM device to directly monitor the health of the spinal cord from within the spine. Spatially specific neurostimulation is the next frontier of nervous system therapeutics, as highlighted by the BRAIN and HEAL initiatives. Our proposed device will accelerate the transition of these new technologies from bench to bedside.

## Appendix B

### **Neural responses of rat cortical layers due to infrared neural modulation and photoablation of thalamocortical brain slices**

Text Adapted from:

J. Logan Jenkins<sup>1</sup>, Chris C. Kao<sup>2</sup>, Jonathan M. Cayce<sup>1</sup>, Anita Mahadevan-Jansen<sup>1,2</sup>, E. Duco Jansen<sup>1,2</sup>

1 Department of Biomedical Engineering, Vanderbilt University, Nashville, TN

2 Department of Neurological Surgery, Vanderbilt University Medical Center, Nashville, TN

Proceedings Volume 10052, Optogenetics and Optical Manipulation; 100520L (2017)

<https://doi.org/10.1117/12.2256302>

## B.1 Abstract

Infrared neural modulation (INM) is a label-free method for eliciting neural activity with high spatial selectivity in mammalian models. While there has been an emphasis on INM research towards applications in the peripheral nervous system and the central nervous system (CNS), the biophysical mechanisms by which INM occurs remains largely unresolved. In the rat CNS, INM has been shown to elicit and inhibit neural activity, evoke calcium signals that are dependent on glutamate transients and astrocytes, and modulate inhibitory GABA currents. So far, *in vivo* experiments have been restricted to layers I and II of the rat cortex which consists mainly of astrocytes, inhibitory neurons, and dendrites from deeper excitatory neurons owing to strong absorption of light in these layers. Deeper cortical layers (III-VI) have vastly different cell type composition, consisting predominantly of excitatory neurons which can be targeted for therapies such as deep brain stimulation. The neural responses to infrared light of deeper cortical cells have not been well defined. Acute thalamocortical brain slices will allow us to analyze the effects of INS on various components of the cortex, including different cortical layers and cell populations. In this study, we present the use of photoablation with an erbium:YAG laser to reduce the thickness of the dead cell zone near the cutting surface of brain slices. This technique will allow for more optical energy to reach living cells, which should contribute the successful transduction of pulsed infrared light to neural activity. In the future, INM-induced neural responses will lead to a finer characterization of the parameter space for the neuromodulation of different cortical cell types and may contribute to understanding the cell populations that are important for allowing optical stimulation of neurons in the CNS.

## B.2 Introduction

Neural modulation in brain allows for important applications that could improve modern medicine and neuroscience research. In medicine, there are both clinical therapeutic and diagnostic applications for neuromodulation. Clinical therapeutic uses include cortical implants and deep brain stimulation. Cortical implants have the ability to modulate normal or diseased functional modules in the motor or somatosensory cortex. Deep brain stimulation is a method to suppress symptoms of certain neurological diseases, such as epilepsy and Parkinson's disease.<sup>1</sup> Neuromodulation in the brain can be used for diagnostic tests as well. Example of this are spatial cortical mapping during tumor resections, awake craniotomies, and deep brain stimulator placement. In terms of neuroscience research, tools are needed to specifically stimulate small populations of neurons to better understand their function and how they contribute to macroscopic brain function. The goal to do this has been amplified over the last few years, especially with the creation of the Brain Research through Advancing Innovative Neurotechnologies (BRAIN) Initiative by NIH and similar initiatives elsewhere in the world.

Luigi Galvani paved the path towards our current neuromodulation techniques when he electrically stimulated dead frog leg muscles in the 1700's. Since then, many techniques have been used to modulation nervous systems, such as electrical stimulation, ultrasonic stimulation, magnetic, stimulation, optogenetic stimulation, and infrared neural modulation (INM). INM is a contact-free, artifact-free neural stimulation and inhibition technique with high spatial specificity due to intrinsic properties of tissue. INM entails both infrared neural stimulation (INS) and infrared neural inhibition (INI) which have been shown to be two distinct results with distinct mechanisms. A few mechanisms that appear to play a role in INS have been uncovered, though a full

understanding of how infrared light is transduced into neural activity is still lacking. Wells et. al. demonstrated that INS occurs due to a fast-thermal gradient and ruled out the possible mechanisms of an induced electrical field, photochemical effects, and photomechanical effects.<sup>2</sup> Shapiro et. al. presented that there is a local membrane capacitance change during INS on all bilipid membranes, regardless of neurological origin.<sup>3</sup> This theory is being expanded upon, as presented by Plaskin et. al.<sup>13</sup> Lastly, Albert et. al. demonstrated that heat-sensitive transient receptor potential vanilloid channels (TRPV) are activated by pulsed infrared light.<sup>4</sup>

Our group has used INM in the brain, as demonstrated in previous work. We have used rat thalamocortical brain slices to demonstrate feasibility and to characterize the parameter space.<sup>5</sup> In rat in vivo models, we presented the suppression of spontaneous activity during INM of the somatosensory cortex.<sup>6</sup> We have also shown that INS induced calcium signals are dependent on glutamatergic transients and astrocytes.<sup>7</sup> Lastly, we have shown in in vivo non-human primate experiments activation of single units of the primary visual cortex by INM, as well as the ability to control saccadic eye movements by manipulating the cortex with infrared laser pulses.<sup>8</sup> There are some limitations to these findings. In particular, the in vivo experiments were delivered to cortical surface, meaning that the light is being mostly absorbed by layers I and II of the cortex. These layers are generally composed of astrocytes, inhibitory neurons, and dendrites of lower excitatory neurons. The lower cortical layers (III-VI) are composed of different populations of cells, different densities of cells, and different components of cells. The lower cortical layer responses to INM have not been well defined.

Our method to reach these lower cortical layers is to use thalamocortical brain slices to target the individual layers transversely. Brain slices allow for intact neural connections in one plane and visualization of the cortex and thalamus for electrode and fiber placement. The thalamocortical

brain slice keeps intact a connection from the thalamus to layer IV of the cortex to allow for propagation of neural activity without the thermal artifact that occurs when irradiating the recording electrode.<sup>9</sup> Complications in modulating neural activity with INM directed us towards reducing the dead zone thickness. Dead cell zones on each side of the slice surface are known to be between 50-200  $\mu\text{m}$  thick due to the cutting process, as shown in Figure B.2-1.<sup>10,11</sup> The dead cell zones are responsible for the absorption of optical energy before lower, healthy zones are able to be stimulated. We tested an erbium:YAG laser for precise photoablation of this dead zone due to their low penetration depths in tissue of 1 $\mu\text{m}$ . Photoablation is the use of highly absorbed light to create fast thermal explosions which removes tissue off the surface of some material.<sup>14</sup> There is laser-induced damage due to the transfer of heat during the photoablation process, which means we must be careful to not damage a larger area than we remove.

In this study, we demonstrate the use of erbium:YAG photoablation to reduce the dead zone thickness that is inherent to cutting brain slices for these experiments. We hypothesize that the use of this technique will allow removal of the layer of dead tissue of the cut surface of the brain slice. In turn, this will facilitate INM in the slice model by allowing more optical energy to reach the living zones where a neural signal can be stimulated.

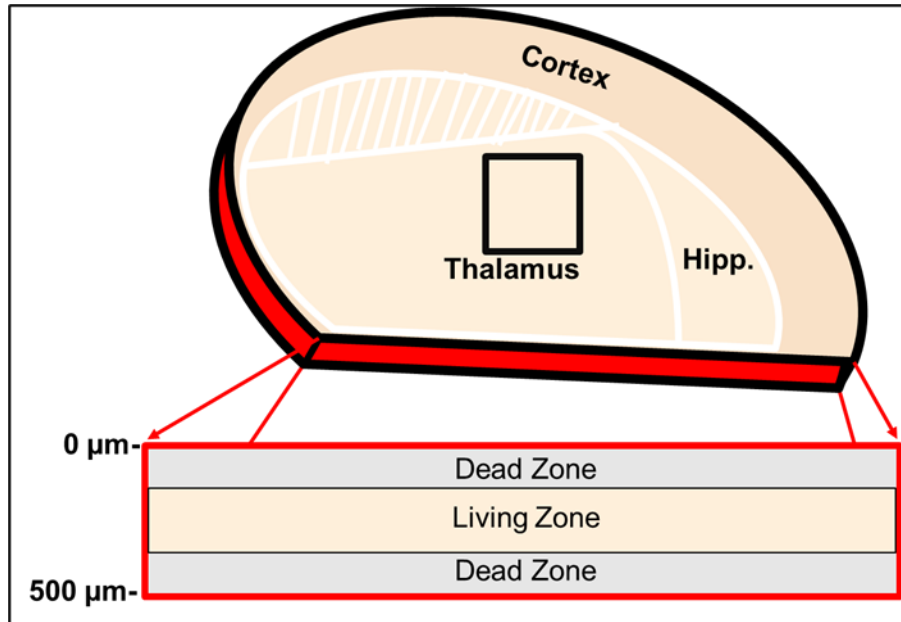


**Figure B.2-1 Representation of the dead zone associated with brain slicing.**

Above: Representation of a brain slice with labeled cortex, thalamus, and hippocampus. Black box represents the approximate imaging area used for Figures B.4-1 and B.4-2. Below: Depiction of the thickness of the brain slice as shown in red above. The top and bottom surfaces of the brain slice have dead zones due to the trauma of the cutting procedure. There is a living zone between the two dead zones of healthy cells that retain neurophysiological function.

## B.3 Methods

### B.3.1 Brain Slice

Sprague-Dawley rats (21 to 35 days old) are anesthetized with inhalation of 4% isoflurane for 1-1.5 minutes and immediately decapitated. The brain is then rapidly dissected from the cranial cavity, and cerebellum will be removed. A parasagittal cut is made at a 55-degree angle from the midline of the brain at 10-degree elevation to allow for the correct orientation during slice preparation.<sup>9</sup> Thalamocortical slices are cut between 450-550  $\mu\text{m}$  thick using a Vibratome 1000 Plus (Vibratome, St. Louis, MO). During slice preparation, the brain tissue is bathed in an artificial cerebral spinal fluid deficient in sodium chloride which is oxygenated throughout slice preparation and experimentation. Once cut, the thalamocortical slices are placed in a similarly oxygenated artificial cerebrospinal fluid (aCSF) solution which is magnesium deficient to induce hyperactivity and the slices are allowed to incubate for 1 hour. The aCSF solution contains the following concentrations (in mM): 124 NaCl, 5 KCl, 1.25  $\text{NaH}_2\text{PO}_4$ , 2  $\text{CaCl}_2$ , 2  $\text{MgCl}_2$ , 26  $\text{NaHCO}_3$ , and 10 glucose. The aCSF was oxygenated using 95%  $\text{O}_2$  / 5%  $\text{CO}_2$  gas concentrations. After incubation, the slices are placed in an interfaced perfusion chamber at room temperature for experiments. Protocols have been approved by Vanderbilt IACUC.

### B.3.2 Electrical Recordings and Stimulation

Electrical recordings were made with glass patch electrodes pulled from borosilicate glass capillaries (World Precision Instrument, Sarasota, FL) using a vertical Narishige PP-83, (Scientific Instrument Lab., Tokyo, Japan). The glass electrodes were filled with aCSF solution to record local action potentials of nearby neurons. Recordings of all electrical signals were made with an Axopatch-200B amplifier (Axon Instruments Inc., Foster City, CA). Electrical recordings were

performed using a silver bipolar electrode. Electrical pulses were generated using an IsoSTIM A365 (World Precision Instruments, Sarasota, FL) at 2-40 Hz and a pulse length of 5  $\mu$ s with an amplitude between 1-10 mA. Electrical recordings of the thalamocortical brain slices demonstrated spontaneous activity and electrical stimulation of the thalamocortical tract between the thalamus and the cortex. The thalamocortical brain slices are 500  $\mu$ m thick and have reproducible results from 8-12 hours after the slicing procedure.

### B.3.3 Photoablation

Photoablation was used to reduce the inherent dead zone thickness as described in the next subsections. A Schwartz Electro-Optics Laser is used with an erbium:YAG cavity. The erbium:YAG has a wavelength of 2.94  $\mu$ m. The pulse width held constant at about 250  $\mu$ s (FWHM). The number of pulses range from 1-50 pulses with each pulse having a radiant exposure of 0.2-0.8 J/cm<sup>2</sup>. The experimental procedure was to place the brain slice on a polydimethylsiloxane (PDMS) block in sodium chloride deficient aCSF. The aCSF was removed using a pipette to keep the surface of the brain slice dry in efforts to avoid ablating the medium rather than the tissue. After ablation, the brain slice was placed back into cold, sodium chloride deficient aCSF for five minutes to recover before being moved to the magnesium deficient aCSF. The beam profile of the erbium:YAG laser is not completely uniform and results in a rough ablation of surface of varying ablation depths. A smoothing technique was used to evenly distribute the energy to better flatten the ablation surface. The smoothing technique entailed translating the brain slice on an X-Y translation stage in by 100  $\mu$ m in one direction between each pulse. The pattern was transverse the brain slice 100  $\mu$ m left, then 100  $\mu$ m up, then 100  $\mu$ m right, and 100  $\mu$ m down to repeat from the starting position.

#### B.3.4 Dead Cell Staining

To quantify the thickness of the dead zones, freshly cut brain slices were incubated in an oxygenated, 0.1 mM concentration of propidium iodide (PI) in aCSF for three hours. The brain slices were then rinsed completely for at least 5 rinses. PI stains the nucleus of broken membranes that we contribute to cell death. PI will not stain healthy cells because it is unable to permeate the bilipid membrane. Two-photon microscopy was used to image the brain slice. The intensity of the fluorescence decreases as the microscope sections deeper into the tissue with a 5 $\mu$ m step size. Dead zone depths were quantified by plotting the normalized fluorescence over depth as shown directly to the right of A.4-1A, A.4-1B, A.4-1A, and A.4-1B. Dead zone thickness was determined when the normalized fluorescence was above  $1/e$  of the maximum fluorescence.

## B.4 Results

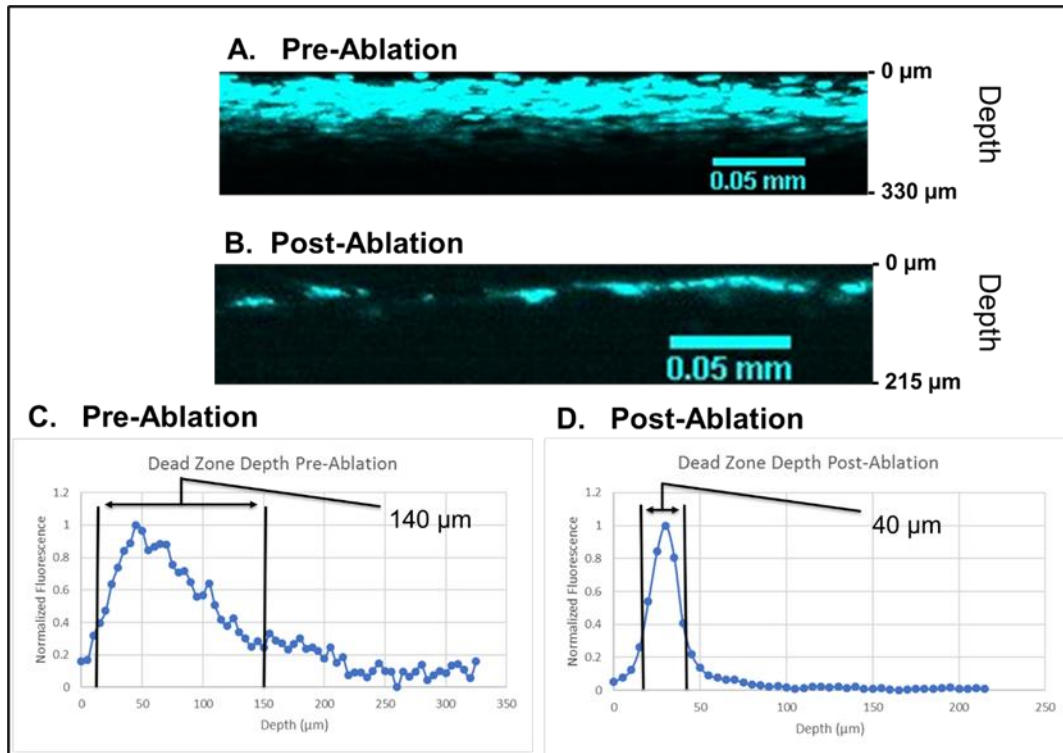
### B.4.1 Photoablation can reduce the necrosis layer of brain slices

Figure B.4-1 shows the state of the preexisting dead zone by PI staining the brain slice before the ablation process. Figure B.4-1A shows the dead zone thickness is about 140  $\mu\text{m}$  due to the brain cutting procedure. After the photoablation process there is a large reduction in the depth of fluorescence. Figure B.4-1B shows the thickness of the dead zone to be about 40  $\mu\text{m}$  after the ablation process. It should be noted that the thickness image in Figure B.4-1A is a maximum projection of all dead cells from the image stack as opposed to Figure B.4-1B, which is only one plane of thickness in the X-Z dimensions. This was done due to the fact that the normal brain slice has a uniformly flat top surface and is in the same plane, while the ablated brain slice surface is not uniform and fluorescence at each depth does not represent the distance from the surface. Using optical coherence tomography, the maximum ablation depth was found to be 200  $\mu\text{m}$  from pre-ablation to post-ablation images using the ablation parameters (30 pulses, 1 Hz, 250  $\mu\text{s}$  pulse width, 0.51 J/cm<sup>2</sup> per pulse).

### B.4.2 Photoablation protocol does not cause further necrosis in brain slices

Figure B.4-2 quantifies the damage that might be induced by the photoablation procedure, i.e., the coagulation zone. To do this, the brain slice was photoablated before the being stained with PI. This takes into account both the photoablation itself, and the procedure of removing the aCSF and oxygenation during the time of photoablation. The dead zone thickness images of the PI fluorescence are shown in Figure B.4-2. The images represent a non-ablated area adjacent to the ablated area had a dead zone thickness of about 145  $\mu\text{m}$  shown in Figure B.4-2A. The dead zone

thickness after ablation was reduced to about 45  $\mu\text{m}$  shown in Figure B.4-2B. In the X-Y orientation slices (not shown), we are able to see the dead cell bodies underneath the surface.



**Figure B.4-1. PI staining before ablation to confirm complete reduction in preexisting dead zone.**

(A) A control image of the dead zone thickness before ablation. (B) An image depicting the reduction of the dead zone thickness after ablation. (C) Quantification of subfigure A by normalized fluorescence over depth. The dead zone thickness was found to be 140  $\mu\text{m}$ . (D) Quantification of subfigure B by normalized fluorescence over depth. The dead zone thickness after ablation was found to be 40  $\mu\text{m}$ .

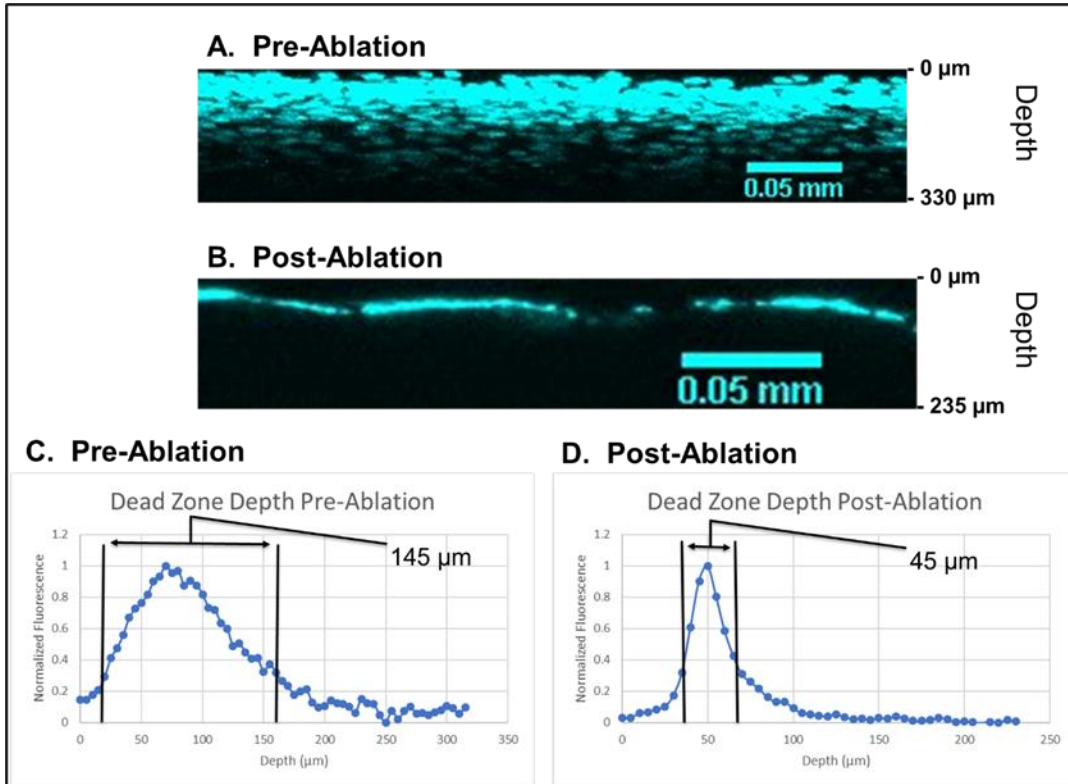


**Figure B.4-2. Staining after ablation to show laser-induced cellular damage.**

(A) A control image of the dead zone thickness that was not ablated. (B) An image depicting the reduction of the dead zone thickness after ablation. (C) Quantification of subfigure A by normalized fluorescence over depth. The dead zone thickness was found to be 145  $\mu\text{m}$ . (D) Quantification of subfigure B by normalized fluorescence over depth. The dead zone thickness after ablation was found to be 45  $\mu\text{m}$ .

## B.5 Discussion

In this study, we present the reduction of the dead zone layer to 45  $\mu\text{m}$  from 145  $\mu\text{m}$ . 145  $\mu\text{m}$  of dead tissue would result in a large reduction in the fluence rate reaching the top of the living zone due to light absorption. Our hypothesis was this reduction in optical energy reaching the living zone would impair the optical energy from inducing neural activity. If we were able to reduce our dead zone thickness, we may be able to get more optical energy to the depths that we need and induce neural signals. The reduction in fluence rate due to dead zone absorption is less than 20% using our stimulation wavelength of 1.875  $\mu\text{m}$ , which is estimated using Beer's law. This reduction should allow for more easily attainable neural activity due to INM, while keeping the neuron connections intact.

### B.5.1 Light absorption through dead zone

The use of photoablation with an erbium:YAG laser is well suited to reduce the pre-existing dead zone that is inherent in brain slice experiments. Assuming that most experimenters have adequate living zone thicknesses to perform neurophysiology research, the dead zone thickness presents a unique challenge to the neurophotonics community. Experimenters using electrical stimulation are able to penetrate the dead zone thickness with the placement of the electrode and bypassing attenuation of the electrical current. With photonic stimulation, some amount of light is absorbed by the dead zone before it can be transduced into neural signal. Our method for lessening this attenuation of light is to reduce the dead zone with photoablation. The erbium:YAG laser is well suited for photoablation of brain slices. It has a shallow penetration depth in tissue that allows for precise ablation of the brain slice with limited collateral damage to adjacent cells.

### B.5.2 Brain slice health during ablation

The photoablation protocol that was used entailed removing the brain slice from oxygenated aCSF for 2-3 minutes. This is not ideal for retaining as many healthy neurons as possible, though we showed in Figure B.4-2 that the photoablation protocol was adequate and minimally damaged larger thicknesses of neurons. This can be improved upon in the future by shortening the time period the brain slice is without oxygenated aCSF. aCSF with sucrose was used for the photoablation process for its neuroprotective properties. Using aCSF with NaCl in the cutting/photoablation process creates cellular swelling and can induce hyperactivity, both of which induce more cellular damage.

### B.5.3 Brain slice ablation reduces dead zone

There are known ways of reducing the dead zone thickness, such as cutting with newer models of vibrating microtomes. Unfortunately, this can be an expensive alternative. Since we are an optics lab and have expertise on laser-tissue interactions, we decided to use photoablation to reduce the thickness of the dead layer. We tried two different lasers, a holmium:YAG ( $\lambda=2.12 \mu\text{m}$ ) and erbium:YAG ( $\lambda=2.94 \mu\text{m}$ ), for our photoablation. The thickness of the coagulation zone was found to be about 250  $\mu\text{m}$  when using the holmium:YAG laser for ablation and the coagulation zone was found to be about 50  $\mu\text{m}$  when using the erbium:YAG laser for ablation. Since the erbium:YAG laser would create a coagulated zone of dead cells that was less than the original dead zone, we decided to use it for photoablation of brain slices. The coagulation zone can be improved upon with shorter pulses of erbium:YAG lasing by using a Q-switch. Other lasers may have been used to reduce the coagulation zone, such as an argon fluoride laser ( $\lambda=193 \text{ nm}$ ) that generate less heat at the tissue.

#### B.5.4 Future Directions

The future directions of this work are to prove that the reduction in the dead zone thickness has enhanced the ability to create neural activity in the brain slice model with INM. This will be done by taking advantage of the thalamocortical connection with electrical recordings. We will use voltage-sensitive dyes and calcium imaging to measure induced neural activity of rat brain slice cortical layers. In future studies, we will explore the neural responses of different cortical cell types due to exposure to pulsed infrared light ( $\lambda=1.875 \mu\text{m}$ , 200  $\mu\text{m}$  fiber, 200 Hz) using electrophysiological and optical techniques. These responses will lead to a finer characterization of the parameter space for different cortical cell types and may contribute to understanding the cell populations and neural components that are important for allowing optical stimulation of neurons in the CNS.

## B.6 References

1. Perlmutter, J. S. and Mink J. W., Deep brain stimulation. *Annual Review of Neuroscience* (29), 229-257 (2006).
2. Wells J., Kao C., Konrad P., Milner T., Kim J., Mahadevan-Jansen A., and Jansen E. D., Biophysical mechanisms of transient optical stimulation of peripheral nerve. *Biophys. J.* 93, 2567–2580 (2007).
3. Shapiro, M. G., Homma, K., Villarreal, S., Richter, C., and Bezanilla, F., Infrared light excites cells by changing their electrical capacitance. *Nat. Commun.* 3, 736 (2012).
4. Albert E. S., Bec J. M., Desmadryl G., Chekroud K., Travo C., Gaboyard S., Bardin F., Marc I., Dumas M., Lenaers G., Hamel C., Muller S., and Chabbert C. TRPV4 channels mediate the infrared laser-evoked response in sensory neurons. *J. Neurophysiol.* 107(12), 3227–3234 (2012).
5. Cayce, J. M., Kao, C. C., Malphrus, J. D., Konrad, P. E., Mahadevan-Jansen, A., & Jansen, E. D. Infrared Neural Stimulation of Thalamocortical Brain Slices. *IEEE Journal of Selected Topics in Quantum Electronics*, 16(3), 565–572 (2010).
6. Cayce, J. M., Friedman, R. M., Jansen, E. D., Mahavaden-Jansen, A., & Roe, A. W. Pulsed infrared light alters neural activity in rat somatosensory cortex in vivo. *Neuroimage*, 57(1), 155–166 (2011).

7. Cayce, J. M., Bouchard, M. B., Chernov, M. M., Chen, B. R., Grosberg, L. E., Jansen, E. D., and Mahadevan-Jansen, A. Calcium imaging of infrared-stimulated activity in rodent brain. *Cell Calcium*, 55(4), 183–190 (2014).
8. Cayce, J. M., Friedman, R. M., Chen, G., Jansen, E. D., Mahadevan-Jansen, A., & Roe, A. W. Infrared neural stimulation of primary visual cortex in non-human primates. *Neuroimage*, 84, 181–190 (2014).
9. Kao, C. Q. and Coulter, D. A., Physiology and pharmacology of corticothalamic stimulation-evoked responses in rat somatosensory thalamic neurons in vitro. *J. Neurophysiol.* 77, 2661–2676 (1997).
10. Reid, K. H., Edmonds, H. L., Schurr, A., Tseng, M. T., and West, C. A., Pitfalls in the use of brain slices. *Progr. Neurobiol* 31, 1–18 (1988).
11. Burgoon, P. W., Burry, R. W., and Boulant, J. A., Neuronal thermosensitivity and survival of rat hypothalamic slices in recording chambers. *Brain Res* 777, 31-42 (1997).
12. Wells, J., Kao, C., Marlappan, K., Albea, J., Jansen, E. D., Konrad, P., and Mahadevan-Jansen, A. Optical stimulation of neural tissue in vivo. *Opt. Lett.* 30(5), 504–506 (2005).
13. Plaskin, M. and Shoham, S., Thermal neural excitation mechanism involves changes in the membrane capacitor’s dimensions. *SPIE Photonics West Proceedings.* (2017).
14. Walsh, J. T., Flotte, T. J., and Deutsch T. F. Er:YAH Laser Ablation of Tissue: Effect of Pulse Suration and Tissue Type on Thermal Damage. *Laser in Surgery and Medicine* (9). 314-326 (1989).

## Appendix C

### **Real-Time Fluorescence Imaging and Pressure Measurements**

## C.1 Purpose

While experimenting with the correct photomechanical mechanism to use in Chapter 4, we discovered an issue with repeatability during Holmium:YAG bubble collapse pressure generation. Pressure measurements from a hydrophone at the cell surface found a variability of ~50% in peak positive pressure from pulse-to-pulse, likely driven by the stochastic nature of bubble collapse. Initial experimental design assumed that pulse-to-pulse variability in peak positive pressure would be no more than 10%, which would allow us to calibrate the pulse energy prior to biological experiments to estimate pressure generation. Given the complexity of the microscope, heating bath, and Holmium:YAG fiber, we would not be able to use a hydrophone that would measure pressure at the cell surface during experiments. Our hypothesized work-around was to measure each pressure transient from a pulse during the experimental pressure exposure with a hydrophone further away and at an off angle. The measured pressure at the offsite would be given a correlation coefficient to relate it to the expected pressure at the cell surface. In theory, this could allow real-time pressure measurements and fluorescence measurements. While this photomechanical mechanism was eventually abandoned, substantial effort was made to create this real-time pressure measurement method and it will be discussed in this appendix chapter.

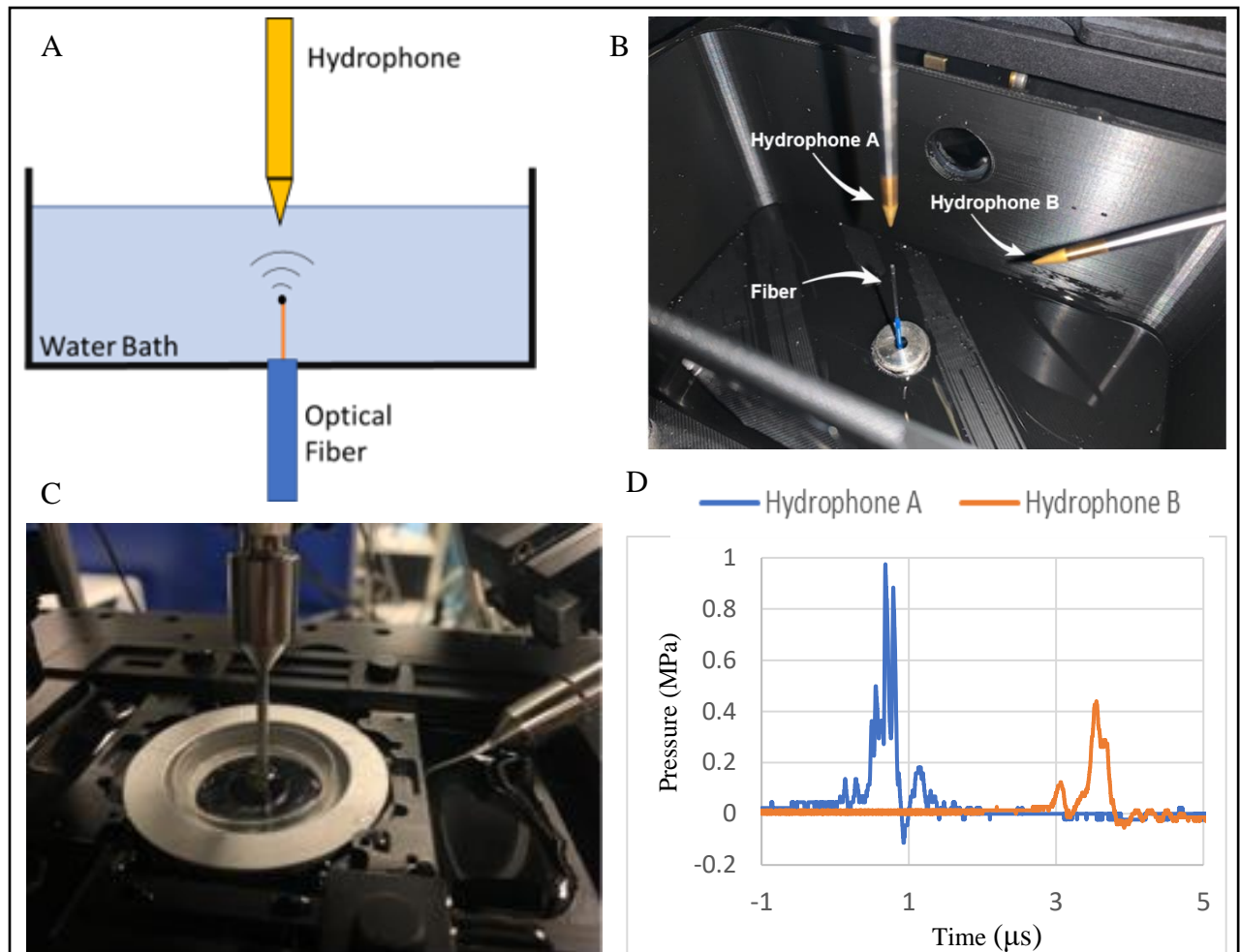


**Figure C.2-1. Positioning and calibration for real-time pressure measurements.**

(A) An illustration of the water bath with Ho:YAG laser pulse being delivered from below with a hydrophone at normal incidence. During fluorescence imaging, the hydrophone would be replaced with an optical objective. (B) An image of the two-hydrophone setup in an empty water bath which is necessary to calibrate and off-angle hydrophone (hydrophone B) to the pressures experienced by the sample (hydrophone A). (C) An image of the two-hydrophone setup in a filled water bath and imaging dish in place; replicating normal imaging conditions. (D) Hydrophone measurements taken from a single laser pulse. The blue trace is for hydrophone A and the orange trace is for hydrophone B. As hydrophone B is off-angle and further away from the pressure origin, the hydrophone B trace is both lower in magnitude and slightly delayed.

## C.2 Methods

Given the similarities of this appendix chapter to Chapter 4, only new information will be described here. Similar to the setup described in Figure 4.3-1, the experimental setup was comprised of a water bath with a submerged objective or hydrophone above and light being delivered from below. In this setup, an optical fiber transmits the light from the Holmium:YAG laser to cause bubble collapse and pressure generation (Figure C.2-1A). This setup allow for peak positive pressure and impulse to be measured at the cell surface with a hydrophone parallel to the optical fiber.

To implement real-time pressure measurements, an off-angle and shifted hydrophone (hydrophone B) was used to not impact imaging capabilities. Hydrophone B was tilted to point towards the bubble collapse point, though shifted ~3 cm away in the x-y plane and ~1 cm lower than the original hydrophone location (hydrophone A). This setup is shown in Figure C.2-1B without water in the water bath for better visualization. Figure C.2-1C is representative of the setup during hydrophones' calibrations with the addition of water, the imaging dish, and the metal dish holder.

To calibrate hydrophone B to the pressure experienced by the cells using hydrophone A, a single pressure was generated using bubble collapse in the setup. Pressures were simultaneously measured using the two hydrophones and identical hydrophone peripherals. Ten pressures were measured per batch and five batches were measured. Between each batch, the hydrophones were translated out of position and back into position to replicate the experimental procedure of swapping in a new imaging dish. A representative trace of pressure over time for each hydrophone is presented in Figure C.2-3. Hydrophone B experiences a smaller peak positive pressure and a

slightly later time due to the hydrophone being further away, but the overall shape is preserved by both hydrophones. The correcting coefficient needed to convert hydrophone B's measurement to hydrophone A's measurement by dividing the pressure measure type of hydrophone A by hydrophone B.

### C.3 Results / Discussion

The correcting coefficient needed to relate hydrophone B to hydrophone A for each pressure measurement type is shown in Table C.2-1. The variability for each type varied greatly; 35% for peak positive pressure, 57% for peak negative pressure, 2.9% for positive impulse, and 12% for negative impulse. Comparing this method to the variability in pressure measurements using one hydrophone shows a reduction in variability from 50% to 35%. This suggests that this method is a more reliable predictor of the peak positive pressure experience by cells during experiments, but it leaves much to be desired. A 35% variability in peak positive pressure using the same laser energy could impact interpretations of biological responses if the pressure was assumed to always be constant at a given laser energy. While this was not the main reason of abandoning this method of pressure generation, it would have required a larger sample size of cells at each pressure given the potential to cause variability in biological responses.

Pressure Measurement Type	Correcting Coefficient
Peak Positive	$4.19 \pm 1.45$
Peak Negative	$3.07 \pm 1.75$
Impulse Positive	$2.45 \pm 0.07$
Impulse Negative	$2.73 \pm 0.33$

**Table C.2-1. Coefficients needed to calibrate pressure measurements taken from hydrophone B.**

For each pressure measurement type, a correcting coefficient was calculated to calibrate the measurement taken from hydrophone B to hydrophone A. Errors are reported as standard deviation.

The stark contrast in the variability of the correcting coefficients to the pressure measurement types was, initially, unexpected. The lower variability in impulse measurements compared to peak pressure measurements suggest the total energy of the pressure wave is better conserved regardless of shifted hydrophone placement. The two-hydrophone calibration method described here should be an adequate method for real-time imaging and impulse measurements. I hypothesize that the pressure measurements remain highly variable due to the imperfect bubble formation at collapse. In a perfectly spherical bubble collapse, there would be a single pressure front that propagates through the medium. Regardless of where a hydrophone is at on a given radius, the measurement should be identical. Strobe imaging uncovered that there is an imperfect bubble collapse from the Holmium:YAG-based light delivery system. Imperfect bubbles, especially oval-shaped, will likely have multiple points of collapse, though clustered together. Each collapse point will produce its own pressure front. These multiple pressure fronts can interfere with one another, either constructively or destructively, at any point to increase or decrease the peak pressure. Therefore, in the described two-hydrophone setup, hydrophone A and B may be experiencing different interference patterns affect peak pressures, but total pressure over time remains conserved.